Mathematical Formulation of Tools for Assessment of Fragility and Vulnerability of Damaged Buildings

A Dissertation
Presented to
The Academic Faculty

By

Quanwang LI

In Partial Fulfillment
Of the Requirement for the Degree
Doctor of Philosophy in the
School of Civil and Environmental Engineering

Georgia Institute of Technology

May 2006

Copyright 2006 © Quanwang LI

Mathematical Formulation of Tools for Assessment of Fragility and Vulnerability of Damaged Buildings

Approved by:

Dr. Bruce R. Ellingwood, Advisor
School of Civil and Environmental Engineering
Georgia Institute of Technology

Dr. Reginald DesRoches
School of Civil and Environmental Engineering
Georgia Institute of Technology

Dr. Barry Goodno
School of Civil and Environmental Engineering
Georgia Institute of Technology

Dr. James I. Craig
School of Aerospace Engineering
Georgia Institute of Technology

Dr. Rami M. Haj-Ali,
School of Civil and Environmental Engineering
Georgia Institute of Technology

Date Approved: March 27, 2006

ACKNOWLEDGMENTS

I wish to acknowledge the great debt of gratitude I owe to Dr. Bruce R. Ellingwood for his guidance, help and encouragement during this study, and in many other facets of my stay in Georgia Tech.

I would also like to thank Dr. Barry Goodno, Dr. Rami M. Haj-Ali, Dr. Reginald DesRoches and Dr. James I. Craig for their reading of the dissertation and for offering invaluable comments.

My special thanks to my parents, my wife Xiuli and my son Yuancheng in China for supporting me in my education and in all my other endeavors. I dedicate this dissertation to them as a token of my appreciation and gratitude.

The research reported in this dissertation was supported by Sandia National Laboratory under a joint SNL/National Science Foundation Award No. A0346-15896 on decision-theoretic methods for performance-based structural engineering and by the Mid-America Earthquake Center, with additional support provided by the Georgia Institute of Technology. This support is gratefully acknowledged. The MAE Center is an NSF Engineering Research Center funded at the University of Illinois at Urbana-Champaign by Award No. EEC-9701785.

TABLE OF CONTENTS

LIST OF TABLES

LIST OF FIGURES

SUMMARY

Performance-Based (PBE) and Consequence-Based (CBE) are new approaches to seismic design, evaluation and risk assessment, in which design criteria are devised to achieve stated performance objectives, and regional losses to civil infrastructure are mitigated through selective interventions for critical components of a civil infrastructure. These new approaches give engineers more flexibility in achieving performance goals but require substantial additional computational resources to fully achieve performance goals. As a step toward making such approaches feasible, this dissertation develops a number of computationally efficient methods for performing finite element-based structural system dynamic response analysis and reliability assessment. The Enhanced Uncoupled Modal Response History Analysis (EUMRHA) procedure developed herein is an efficient response analysis procedure to make the analysis of dynamic structural response to earthquakes in the nonlinear range less time-consuming. This technique is used to investigate the potential for aftershocks to cause additional damage to steel moment frame buildings, utilizing a technique designed to enhance the efficiency of Monte Carlo simulation in estimating low-probability events. Relatively simple probabilistic tools are proposed for purposes of rapid structural evaluation and condition assessment of damaged buildings. Finally, an analysis-based inspection scheme based on an associated probability model of

connection damage is proposed for assessing the safety condition of existing buildings, and a procedure to assess the likely performance of an un-repaired building during a future earthquake is developed.

CHAPTER 1: INTRODUCTION

1.1 Background

Performance-based engineering (PBE) is a new paradigm for structural design, arising from a wish on the part of structural engineers to consider a broad spectrum of design alternatives above and beyond the narrowly defined traditional safety-related prescriptive design criteria in building codes. Structural engineers seek to achieve economical solutions to building safety and serviceability problems through engineering analysis rather than prescriptive measures, to take advantage of new building technologies and to match structural design criteria to performance expectations of building stakeholders (Ellingwood 1998). Professional interest in PBE in the United States is most strongly focused in engineering building structures for earthquake resistance. The International Code Council and the National Fire Protection Administration both are fostering performance-based engineering in building design and construction in their model codes (ICC 2003; NFPA 2002). For example, Section 104.11 of the 2003 Edition of the *International Building Code* permits alternative methods, provided that evidence is provided that the product is equivalent in terms of safety, fire resistance and durability to the intent of the Code.

Consequence-Based Engineering (CBE) is a developing systems-based methodology in the Mid-America Earthquake (MAE) center for seismic risk reduction

across regions or systems, which is aimed at quantifying the risk to societal systems and providing decision support tools to policy-makers, decision-makers and stakeholders (Abrams et al 2002). In a sense, CBE extends some of the ideas in PBE to estimating consequences and mitigating risks across an entire system of facilities rather than to individual structures. A user of CBE would assess probable hazards, synthesize damage and losses, and select interventions to minimize consequences of earthquake events. With technologies that support CBE, engineers will be able to demonstrate to their clients what consequence are likely for their systems, and how various intervention measures, such as retrofit of structures, might reduce such consequences. Because social and economic impacts of earthquakes are considered across an inventory of construction, the benefits of seismic risk-reduction measures to communities can be better assessed through this new systems approach.

PBE and CBE methodologies are distinguished from traditional prescriptive code-based design procedures by permitting alternate engineering solutions, provided that the equivalence of such solutions to the prescriptive requirements of the code can be satisfied. PBE and CBE also permit stakeholder groups to select performance objectives that include, but are not limited to, life safety and require quantitative measures of performance and satisfaction of performance goals. In proposals for both PBE and CBE, uncertainties in seismic hazards and building system response to those hazards usually are treated explicitly. Quantitative measures of performance are based on probabilities of achieving specified performance goals. In practice, however, calculating these probabilities and using them as a basis for decision-making and

design may be difficult. Among the difficulties are:

- Calculating probabilities of system response for realistic systems. Because of the inherently nonstationary nature of the random excitations in earthquakes and the analytical difficulty in modeling complex nonlinear structural behavior in realistic systems, the cost of performing nonlinear time history analysis for realistic systems is high. Efficient methods for calculating system reliabilities are very important to reduce the burden of seismic vulnerability fragility analysis, especially when evaluating vulnerability of building inventories.
- Analysis and treatment of uncertainties. Significant uncertainties arise due to the complexity in earthquake generation, attenuation and site response, and structural response. Seismic demands on building frames show great variability under different excitations of the same intensity measure. These uncertainties must be included in the decision model.
- Practically all research to date has been directed to new buildings. Structural reliability and fragility modeling has seen little application to existing buildings. In contrast with new buildings, existing buildings may have suffered damage from previous earthquakes or other hazards. The current condition of existing buildings must be evaluated by damage inspection, supported by appropriate mathematical and engineering tools. These factors challenge the seismic assessment of existing buildings.

Many of the research challenges to successful implementation of PBE and CBE in earthquake engineering center around the computational demands imposed by the

need to perform structural performance evaluations and reliability analysis of complex structural systems loaded well into the inelastic range. To support the practical application of PBE and CBE, efficient methods and tools are required in the fields of structural behavior modeling and analysis, structural seismic damage assessment, and structural reliability analysis. The research in this dissertation is aimed at developing: (1) efficient sampling techniques to reduce the effort required to perform reliability analysis of structural frames subjected to earthquake ground motions, and (2) efficient structural seismic response analysis procedures to make the analysis of structural response less time-consuming. These thrusts are introduced briefly in the following sections.

1.1.1 Sampling techniques for system reliability analysis

Performance evaluation of structural systems requires an assessment of uncertainties in structural demand and capacity, both of which are functions of numerous random variables. Often there are many random variables involved in an engineering system. To take into account the uncertainty in predicting the system performance, efficient system reliability methods such as the first-order and second-order reliability methods (Madsen et al. 1986) must be employed. The reliability methods are used almost exclusively to estimate the probability of structural failure, while the statistics of the structural responses, which are very important for PBE and CBE, are generally analyzed by sampling methods, such as direct (naïve) Monte Carlo simulation, importance sampling or Latin hypercube

sampling (Iman and Conover 1980). The efficiency of sampling technique is of most concern when structural responses are evaluated by nonlinear finite element analysis. In this thesis, the point estimate method (Rosenblueth 1975) is combined with Latin hypercube sampling to increase the sampling efficiency.

1.1.2 Efficient structural seismic response analysis

In recent years, codes for earthquake-resistant design have begun to explicitly require the consideration of nonlinear system behavior in estimating structural responses. Ideally, such performance evaluation of structural systems subjected to earthquake loading should be based on nonlinear time history analysis (NLTHA). However, the huge computational effort required by NLTHA may not justify its use in many engineering applications. As a result of the above, nonlinear static pushover analysis (NSP) has gained significance over recent years as an assessment tool. NSP can provide information on many important response characteristics (identify critical region where inelastic deformations are expected to be high, and strength irregularities in plan or elevation that might cause important changes in the inelastic dynamic response) (Krawinkler and Seneviratna 1998). However, the NSP analysis is limited in its inability to account for the progressive stiffness degradation within the structural frame and the effects of higher modes on dynamic response. To overcome the above shortcomings associated with NLTHA and NSPA, an efficient structural seismic response analysis procedure is developed herein.

With the support of the newly developed sampling and structural analysis tools,

the investigation of two important structural engineering research topics is facilitated. An introduction to these two topics is provided in the following two subsections

1.1.3 Building performance during main shock – aftershock sequences

The widespread occurrence of brittle fractures of welded beam-to-column connections in steel buildings in the Northridge Earthquake of January 17, 1994 (Bonowitz and Youssef 1995) came as a surprise to many structural engineers. These brittle connection fractures at the welded joints caused a sudden loss of strength and stiffness and resulted in significant economic losses due to the damage and disruption of building service. The poor performance of these connections raises a natural question about the level of safety of damaged buildings by seismic events. When earthquake ground motions occur in sequence, as might happen with a main event with medium-to-high intensity followed shortly thereafter by other events with comparable intensity, a structure suffering damage during the main shock may become incapable of resisting the excitation of the aftershock. There may be a question as to whether or not a damaged building may remain occupied prior to repair. Little research has been done on this topic, partially because of the burden of performing nonlinear time history analysis of sequences of earthquakes. In addition, researchers have yet to agree on differences in magnitude between a main shock and its largest aftershock (Helmstetter and Sornette 2003). Moreover, the potential for damage accumulation during successive earthquakes is related to many parameters, such as structural period (or period shift), earthquake ground motion intensities,

structural ductility and permanent deformations of the frame following a main shock (Amadio, et.al. 2003, Fragiacomo, et.al. 2004), all of which makes the analysis complex.

In this dissertation, the performance of steel buildings during earthquake main shocks and subsequent aftershocks is investigated. Using the simplified dynamic analysis method developed in this research, a structural engineer can evaluate the capacity of a damaged building to withstand the possible aftershocks.

1.1.4 Capacity assessment of damaged buildings through partial inspection.

Since the 1994 Northridge earthquake, the reliability of existing steel moment-resisting frame (SMRF) buildings with fractured beam-column connections has come into question. One concern is whether or not fractured connections should be repaired immediately prior to re-occupancy of the building. Complicating the issue is the expense of inspecting beam-column connections for fractures, ranging from $800 to $1200 per connection for typical commercial buildings[1], and their accessibility to inspection, both of which may render inspection of all the moment-resisting connections in a building uneconomical or unfeasible. As a result, the true state of damage to a frame, based on inspection, is uncertain. Therefore, the number as well as the locations of connections to inspect in order to properly assess the damage state becomes an important consideration.

[1] SAC Document http: //www.sacsteel.org / background / gates1-p1.html (assessed on 01/07/2006)

Because of the uncertainties associated with structural materials found in connections, especially the workmanship in weld joints, damaged connections tend to be widely distributed throughout building frames and may occur at locations that might not be predicted by analysis (FEMA-352). Therefore, FEMA-352 proposed random as well as analytical selection of connections to inspect. However, even in analytical selection, more than 50% of inspected connections are selected randomly, and no probability model is developed for analytical selection.

In this dissertation, an analysis-based inspection scheme and associated probability model are proposed. A procedure to assess the performance of an un-repaired building in a future earthquake is developed. This procedure accounts for the uncertainty due to incomplete inspection, and can take into account the ground motion hazard of future earthquakes. The damage in terms of repair cost estimated by the proposed procedure can be compared for two alternatives: repairing the damaged building immediately or later considering the seismic hazard level. Such information can help decide whether or not to immediately repair a damaged building.

1.2 Objective and scope

The overall goal of the proposed research is to provide a set of fragility and vulnerability assessment tools that can support structural system reliability and conditional assessment of steel frames subjected to earthquakes. This research goal will be supported through the following tasks:

- Develop mathematical tools for assessing structural damage and loss in building frames.
- Increase the feasibility and computational efficiency of structural seismic reliability analysis through efficient statistical sampling techniques and seismic response analysis tools.
- Investigate the structural performance of steel buildings subjected to main shock-aftershock sequences
- Develop an analysis-based inspection scheme and incorporate uncertainties in inspection into structural reliability assessment.
- Develop simple decision tools for assessing damage to existing buildings in term of repair cost.

1.3 Organization

Recent development in the field of structural reliability analysis are reviewed in Chapter 2, with particular reference to damage measures, damage inspection and structural damage assessment methodology. A framework for structural risk assessment is introduced.

A new sampling technique referred to as Interval Point Estimate Sampling is proposed in Chapter 3. This sampling technique combines the best features of the Latin hypercube sampling and the point estimate method. Numerical results indicate that the proposed technique is more efficient than Latin hypercube sampling for estimating probabilities of rare events and provides relatively stable and accurate

results even for highly nonlinear performance functions. The proposed sampling technique increases the sampling efficiency in structural reliability analysis.

Chapter 4 introduces an Enhanced Uncouple Modal Response History Analysis (EUMRHA) method as a substitute for nonlinear time history analysis. The proposed procedure takes into account the contributions of higher modes, as well as the effect of sudden damage to welded connections in moment-resisting steel frames during earthquake ground motion. The accuracy of the method is demonstrated by a comparison with the results of a nonlinear time history analysis. This method can be used for rapid assessment of seismic damage or damage potential and to identify buildings requiring more detailed investigation.

Chapter 5 investigates the behavior of structures subjected to earthquake ground motions characterized by one or more aftershocks within a short period following the occurrence of the principal earthquake shock. This Chapter investigates the potential for aftershocks to cause additional damage to steel moment frame buildings, and provides a probabilistic description of structural damage states prior to and following those aftershocks. Statistics of structural response and damage states for steel frame buildings subjected to main shock-aftershock sequences are calculated using the proposed EUMRHA method in Chapter 4. Simple probabilistic tools are proposed for purposes of rapid structural evaluation and condition assessment of damaged buildings.

Chapter 6 investigates patterns of connection damage in steel moment-resisting frames subjected to earthquakes, considering the uncertainties associated with

workmanship quality. Based on this observation, an analysis-based inspection scheme is proposed and its probability model is developed. It is found that inter-story drift does not appear to be a good measure of connection damage, and the number of damaged connections is used as structural damage parameter in this Chapter. As illustrated by the example, the proposed procedure can provide information that can be used to decide whether or not to repair the damaged building immediately after an earthquake and can be used as a basis for estimating the connection repair cost for a damaged building.

Chapter 7 summarizes the main conclusions and suggests areas for further research.

CHAPTER 2: REVIEW AND ASSESSMENT OF PREVIOUS WORK

Efficient methods and tools have been developed in the fields of structural reliability analysis, modeling and analysis of structural behavior, and structural damage assessment. This progress lays the groundwork for an engineer to implement concepts of performance-based engineering (PBE) and consequence-based engineering (CBE) in structural design and condition assessment (Buzzurro and Cornell 1994, Cornell 1994 and 1996, Song and Ellingwood 1999, Charles and Roeder 2002). On the other hand, many research issues remain unaddressed. For a clear understanding of the development stage of PBE / CBE, these methods and tools will be reviewed briefly in this chapter.

2.1 Structural risk assessment framework

Public safety and economic loss minimization are the most important goals of structural design. Structural design considerations include safety of the structure against collapse, limitations on damage or on deflections, or other limit states. From observation it is known that very few structures collapse, or require major repairs, so the violation of the most serious limit states is a relatively rare occurrence. On the other hand, serviceability (loss of function because of structural damage) issues are

not uncommon.

Risk assessment performed in support of CBE requires an assessment of the consequences of specific challenges to a system in addition to their probabilities of occurrence. These consequences are expressed most commonly in terms of damage and economic loss. Accordingly, the structural performance (SP) subjected to certain seismic hazard intensities (intensity measure, IM, numerically) identified by the analyst must be "mapped" to specific damage states (damage measure, DM, numerically), and, in turn, to losses. The framework of structural seismic risk assessment can be expressed as (Krawinkler 2002):

$$P[Loss] = \Sigma\Sigma\Sigma P[Loss \mid DM] \cdot P[DM \mid SP] \cdot P[SP \mid IM] \cdot P[IM] \qquad (2.1)$$

As shown in the above equation, loss assessment requires an integrated approach for dealing with seismic hazard (the fourth term), structural response (the third term), the relation between structural response and damage (the second term) and between damage and cost (the first term). In this study, the second term is emphasized, and the framework for its analysis for an existing structure will be described in Section 2.3.

The assessment of the third and fourth terms in Equation (2.1) can be achieved by a seismic demand analysis. The structural response can be seen as a function of a vector of load (especially seismic load in seismic analysis) and resistance variables $\underline{X} = (X_1, X_2, \ldots, X_n)$. The limit state function is defined, mathematically, as

$$Z = g(X_1, X_2, \ldots\ldots X_n) \qquad (2.2)$$

The structural fragility $F_R(x)$ is defined as the probability of achieving a specified limit state (LS) conditioned on the occurrence of a specific seismic hazard intensity,

IM = y.

$$F_R(y) = P[\text{LS} \mid \text{IM} = y] \tag{2.3}$$

In earthquake risk assessment of buildings, the maximum inter-story drift ratio θ_{max} during an earthquake is often used as a indicator of SP, and the LS is often defined as the state where θ_{max} exceeds a specific limit θ_{limit} ($\theta_{max} > \theta_{limit}$). A commonly used seismic hazard intensity measure is the spectral acceleration at the structure's fundamental period.

Various uncertainties must be taken into account when performing a fragility analysis. Uncertainties are categorized generally as inherent randomness (aleatory uncertainty) associated with the natural variability in nature and knowledge-based (epistemic uncertainty) due to imperfect modeling related to the assumptions and simplifications in engineering analysis, statistical uncertainty due to small sample size, and measurement errors.

The fragility can be determined from a model of the system, in which the uncertain variables are treated as random variables that are interrelated through fundamental principles of engineering science and mechanics. For most building structural systems, the structural fragility in Equation (2.3) cannot be determined in closed form, and the numerical integration required by classical reliability analysis (Melchers, 1999) is difficult to perform analytically. Those difficulties have led to the use of simulation methods such as: Monte Carlo simulation augmented with importance sampling (Melchers 1989, Turner 1991), directional simulation (Ditlevsen et.al. 1990), and Latin Hypercube sampling (Iman and Conover 1980). Therefore,

Equation (2.3) will be calculated by sampling rather than n-fold integration, as seen below:

$$F_R(y) = \int \ldots \int_{LS|IM=y} f_x(x)dx = \sum_{i=1}^{N} w_i P[LS(X_i) \mid IM = y] \qquad (2.4)$$

where N is the number of samples and w_i is the weighting factor (probability concentration factor) associated with sample *i*. For naïve Monte Carlo Simulation, w_i = 1 / N and different sampling techniques usually give rise to different w_i. Accordingly, the estimates of $F_R(y)$ from Equation (2.4) will vary from simulation to simulation. Variance reduction techniques have been proposed to reduce this sample-to-sample variability, including importance sampling, directional simulation, and Latin Hypercube sampling. A new variance reduction technique will be proposed in Chapter 3.

The uncertainties associated with earthquakes usually are taken into account using an ensemble of ground-motion records developed naturally or generated synthetically. Those records contain a range of frequency contents, durations and amplitudes. Performing nonlinear time history analysis (NLTHA) with the sampled structural model, the probability distribution of SP can be estimated, and the structural fragility as shown in Equation (2.3) can be assessed further.

A challenge in performing seismic risk analysis lies in its large computation effort. As mentioned above, the assessment of the fragility of a structure subjected to earthquake ground motions requires consideration of nonlinear structural behavior, and ideally the evaluation of seismic demand and structural performance should be based on NLTHA. However, NLTHA is time-consuming, so the static nonlinear

pushover analysis is often used as an alternative. Its advantages and shortcomings will be described in the next section.

2.2 Modeling behavior of steel frames subjected to earthquake ground motions

2.2.1 Model of beam-to-column connection

In a moment-resisting frame, the lateral stiffness is provided by the flexural rigidities of the beams, columns and connections. For welded steel moment frames (WSMF), the simple bilinear model, shown in Figure 2.1(a), has been commonly used in nonlinear analysis of steel structures. This model is not suitable for modeling the behavior of degraded connections. A hysteretic model proposed by Gross (1998) incorporates the effects of fracture of the weld connecting the beam and column flanges and subsequent nonlinear response of the connection region. The features of this model are shown in Figure 2.1(b). The primary response is characterized by a bilinear envelope with a yield capacity specified by M_y and post-yield stiffness k_2. The moment at the weld cracking is denoted by M_{cr} which is specified as a fraction of the yield moment. At the onset of weld fracture, the primary envelope is replaced by a new degraded bilinear representation with reduced stiffness (specified as $\beta_2 k_1$), reduced capacity ($\beta_1 M_y$) and modified post-yield slope ($\beta_3 k_2$). Unloading from the new envelope results in a degraded stiffness expressed as a function of the new reduced stiffness, $\beta_4(\beta_2 k_1)$. The unloading path reaches the initial stiffness path on the negative side unless the degree of inelasticity is sufficient for the unloading path to

(a) Bilinear hysteretic model

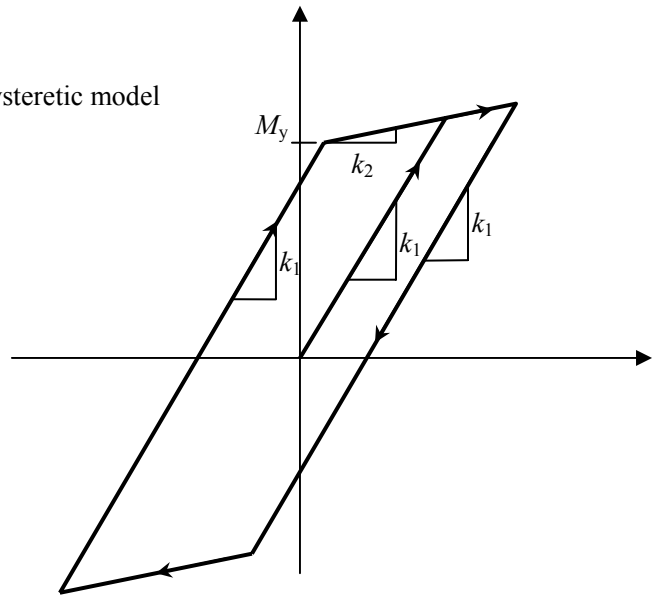

(b) Hysteretic model for weld fracture

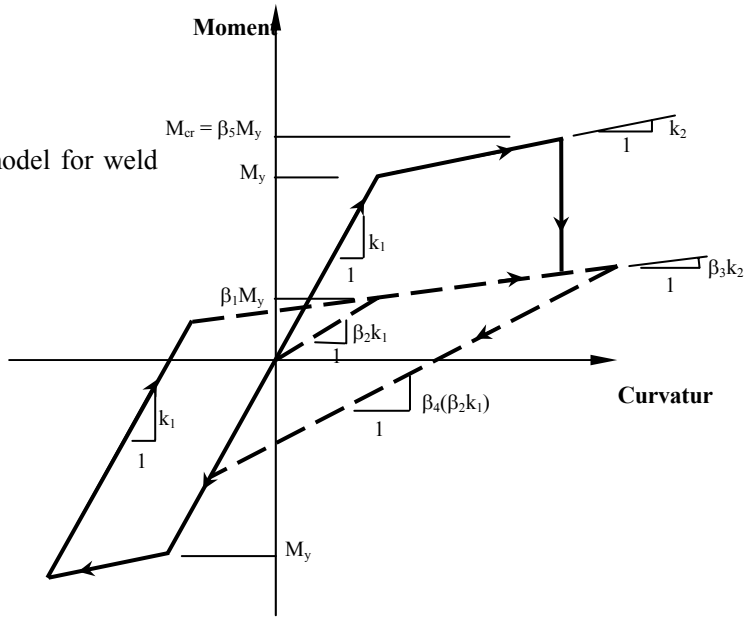

Figure 2.1. Two commonly used connection models

reach the post-yield stiffness path directly. Since weld failures occur at the beam bottom flange only, the hysteretic loops on the other side retain the original stiffness and capacity, as shown in Figure 2.1(b).

The hysteresis parameters that describe connection behavior (k_1, k_2 for the bilinear model; k_1, β_1, β_2, β_3, β_4, β_5 for the degraded model) are random. The hysteretic behavior of connections and frames can vary significantly for different sizes of beams and columns, and welding quality. As a result, the parameters needed to specify the hysteretic behavior must be characterized by probability distributions. Among the six parameters, an analysis of variation (Song and Ellingwood, 1999) showed that β_1 and β_5 are the two most important parameters in determining the structural response. Probability distributions of β_1 and β_5 are assigned so as to model the different qualities of workmanship, as described in detail in Chapter 6.

2.2.2 Static nonlinear pushover analysis

Seismic reliability analysis requires consideration of nonlinear (material and geometric) structural behavior. Several failure modes are of interest when performing reliability assessment of steel frames. Current structural engineering practice for evaluating building seismic resistance often utilizes a non-linear static pushover analysis, in which the building is subjected to monotonically increasing lateral forces with invariant distribution of forces over the building height (Krawinkler and Seneviratna 1998). A typical load-deformation relationship from static nonlinear

pushover analysis (using the OpenSees platform[2]) involving a three-story steel moment-resisting frame with gravity and lateral loads is presented in Figure 2.2. The maximum load is reached well into the nonlinear range; beyond that point, the P-delta effects become dominant, and the frame must unload to maintain equilibrium.

Static nonlinear pushover analysis has been used widely as an efficient and easy-to-use alternative to dynamic time-history analysis (FEMA 273, 1997). It is capable of providing important structural response information. Indeed, a pushover analysis can be employed to identify critical regions, where inelastic deformations are expected to be high, and strength irregularities in plan or elevation that might cause important changes in the inelastic dynamic response characteristics (Krawinkler and Seneviratna 1998). In addition, the pushover analysis is capable of predicting the sequence of yielding and deformation distribution over the frame height.

However, the static pushover analysis has some limitations in its ability to estimate seismic dynamic structural responses (Krawinkler and Seneviratna 1998,). For example, the deformation predictions can be highly inaccurate if higher modes are important or if the structure is pushed highly into its nonlinear post-yield range. Moreover, a static pushover analysis reflects the effects of material properties only, and can not reflect important characteristics of earthquake ground motions, such as amplitude, frequency content, strong-motion duration, and damping. In summary, a static pushover analysis fails to model many important features of dynamic nonlinear response, and thus cannot substitute for the latter in providing the most accurate tool

[2] Most of the analyses herein were performed using OpenSees, an open source FE platform under development at the University of California.

for structural analysis and assessment.

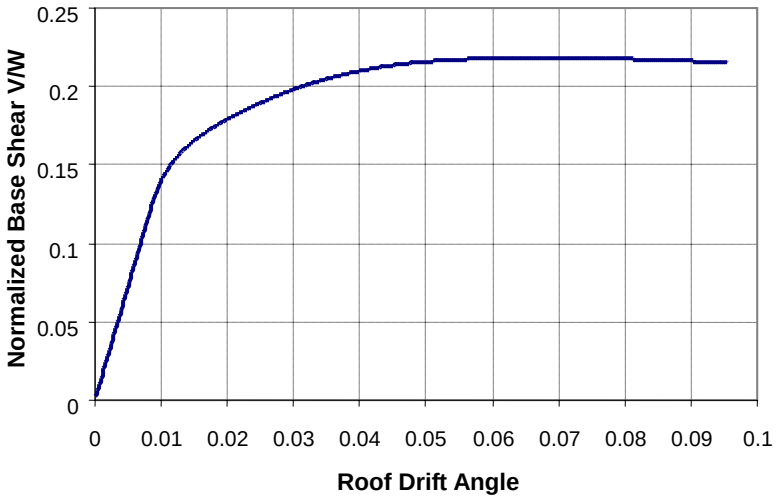

Figure 2.2 Typical nonlinear static pushover curve

On the other hand, the large computational effort involved in nonlinear dynamic analysis makes it impractical in some applications. One example is in rapid assessment of buildings immediately following an earthquake, where a decision maker must choose quickly among the alternatives of allowing continued occupancy or requiring that the building be vacated until repair/rehabilitation can be completed. Another is in sampling-based system reliability analysis. To overcome these shortcomings, an efficient dynamic analysis method that might substitute for a static pushover analysis in such situations will be proposed in Chapter 4. This method takes

into account the effect of higher modes and the degradation of the structural system, as well as the characteristics of earthquake ground motions.

2.3 Damage measure and its estimation

The requirements for acceptable building performance include safety against collapse or other life-threatening damage, limitations on deflection, and a number of other criteria, depending on the nature of the building. Each of these conditions of building performance is associated with conditions of structural behavior that are termed “limit states.” Limit states must be identified for condition assessment and reliability analysis purposes. Structural limit states for earthquake engineering have proved difficult to define and are often identified through damage indices.

2.3.1 Damage index

A damage index describes the damage (or consequences of damage) to a structure, nonstructural component, or building contents. It is often a dimensionless quantity based on inelastic response and is correlated with true structural damage.

Damage categorizations in recent proposals for performance-based engineering tend to be based on maximum inter-story drift, e.g. FEMA-273 (1997) / 351 (2000), which then is related to building performance levels – Continued Operation (CO), Immediate Occupancy (IO), Life Safety (LS), and Collapse Prevention (CP). Those categorizations and their relation to drift are based almost entirely on engineering judgment. In the SAC Steel Program (which was funded by FEMA to address design

issues related to brittle behavior of welded steel frame structures that surfaced in the January 17, 1994 Northridge earthquake), the maximum inter-story drift ratio was taken as an indicator of damage degree. Other damage indices are related to both inter-story drift and dissipated hysteretic energy (Park and Ang's index, 1985a), structural vibration parameters (DiPasquale and Cakmak, 1989), or other structural response characteristics.

Park and Ang's damage index consists of a simple linear combination of normalized deformation and energy absorption:

$$D = \frac{\delta_m}{\delta_u} + \beta \frac{\int dE}{F_y \delta_u} \tag{2.5}$$

where δ_m = maximum positive or negative plastic displacement; δ_u = plastic displacement capacity under monotonic loading; β = model parameter; F_y = calculated yield strength; and dE = incremental dissipated hysteretic energy. The advantages of this damage index are its simplicity and the fact that it has been calibrated against observed damage obtained from cyclic loading tests of components and scaled structural models (Park and Ang 1985b, Kunnath et al. 1990).

One problem with this index is the determination of β. Park and Ang (1985) estimated β from regression analysis of laboratory tests of structural members. The resulting value of β was very small (generally less than 0.05), implying that the cyclic energy dissipation term made a negligible contribution to the overall damage. A later regression analysis performed by Kunnath et al (1990) based on laboratory tests resulted in a more substantial energy term in most cases and suggested a default value of β to be 0.1. It was also recommended that β not exceed 0.5. The uncertainty in

the choice of β is undesirable.

A second problem is that equation (2.5) describes the damage state of a single member rather than a system. One way to estimate system damage is by a summation that weighs the local damage index by the local energy absorptions (Park and Ang 1985). The damage index of a structure is thus:

$$D = \frac{\sum D_i E_i}{\sum E_i} \tag{2.6}$$

where D_i is the local damage index at location i, and E_i is the energy dissapated at location i. Since the locations having high damage indices are also the locations that absorb large amounts of energy, this system puts a higher weighting on the more heavily damaged members. In a simpler form, Equation (2.6) is often written as (Park and Ang 1985):

$$D = \frac{\sum D_i^{\,2}}{\sum D_i} \tag{2.7}$$

Although Equations (2.6) and (2.7) have been used in previous research (e.g. Singhal and Kiremidjian 1996), neither has been verified in terms of ability to predict global damage from local damage.

For purposes of performance and risk assessment, structural damage must be assessed from nonlinear dynamic response quantities that are readily calculated. In Park and Ang's damage index, calculating the hysteretic energy input during earthquake for different members and then for the system using Equation (2.6) or (2.7) is far more difficult than calculating the system displacement. Furthermore, β is relatively small, indicating that the first (deformation-related) term in Equation (2.5)

is dominant. Limit states based on maximum absolute or relative displacement are already well accepted in the earthquake literature and are familiar to the earthquake engineering community. They appear to be as accurate for predicting damage as more complex methods. Inter-story drift best characterizes the architectural (and generally nonstructural) damage and its value correlates well with observed architectural damage after severe earthquake (Gunturi and Shah, 1992). Therefore, a damage index based on inter-story displacements will be used in the subsequent analysis of undamaged steel frames subjected to strong ground motion.

However, it has been observed that for damaged buildings suffering widespread bottom-beam-flange fractures, the structural response subjected to earthquakes in terms of inter-story drift is not dramatically different than that for the entirely undamaged building (Luco 2002), suggesting that that it may not be a good indicator of structural damage for a damaged building subjected to ground motions due to aftershocks.

In Chapter 6, several damage indices are investigated including the maximum inter-story drift ratio, the maximum floor acceleration, the dissapated energy during an earthquake and the number of damaged beam-column connections.

2.3.2 Damage estimation methodologies for undamaged buildings

Consistent with the specification of seismic hazard by the U.S Geological Survey (USGS), the earthquake intensity measure will be assumed to be described by the

spectral acceleration, S_a, at the fundamental period of the structure (Cornell 1996). Cornell et.al (2002) suggested that the probability of S_a exceeding a critical value s_a during a period of time, $H(s_a)$, is well-approximated over a limited range by the power-law relationship:

$$H(s_a) = P\ [S_a > s_a \text{ during a period of time }] = k_0 s_a^{-k_1} \tag{2.8}$$

where k_0 and k_1 are obtained by fitting the function to the seismic hazard near the return period of interest in design, thus serving to characterize the seismic threat at a given site of interest.

As described earlier, the maximum inter-story drift is often selected as the response parameter to represent the structural damage state for an undamaged building. Cornell, et.al (2002) have shown that the median relationship between seismic intensity (represented by S_a) and the maximum inter-story drift ratio (θ_{max}) can be represented approximately by the form:

$$\hat{\theta}_{max} = a(S_a)^b \tag{2.9}$$

in which a and b can be determined by a regression analysis of nonlinear dynamic responses to ensembles of earthquake ground motion. θ_{max} is distributed lognormally about Eq (2.9), with the standard deviation of $\sigma_{\ln(\theta)|S_a}$ (e.g. Shome and Cornell 1999). It follows that the conditional probability that the maximum inter-story drift exceeds x is:

$$P[\theta_{max} > x \mid S_a = y] = 1 - \Phi\left(\ln[x/ay^b]/\sigma_{\ln(\theta)|S_a}\right) \tag{2.10}$$

When the seismic hazard and structural response are convolved as suggested by Cornell (1996), one obtains a point estimate of limit state probability:

$$P[\theta_{\max} > x] = k_0 (x/a)^{-k_1/b} \cdot \exp\left(\frac{1}{2} k_1^2 \left(\frac{\sigma_{\ln(\theta)|S_a}}{b}\right)^2\right) \tag{2.11}$$

If the response parameter is assumed independent of the seismic hazard, then if a different earthquake hazard is later expected, no new simulations of the structural response are required.

Taking the above analysis one step further, given the probability distribution of structural response, as expressed in equation (2.10), the probabilistic damage distribution might be written as:

$$H_D(d) = \int P[D > d \mid \theta_{\max}] \cdot dP[\theta_{\max}] \tag{2.12}$$

where H_D is the hazard function of damage. However, to complete the probability calculation in Eq (2.12), it is necessary to establish a relationship between damage states and structural response. As in FEMA 273 / 356, damage state *D* is discrete with states of [CO, IO, LS, CP] from the smallest to largest. Because the structural response θ is continuous, it has to be mapped to discrete damage states. This mapping process, which is essential for decision-making regarding damage and loss assessment, presents a research challenge at the present time.

2.3.3 Damage inspection and post-earthquake capacity assessment

For seismic damage assessment of existing buildings, in-service inspection is necessary to understand the building's current condition. Motivated by the widespread and unanticipated damage to welded steel moment resisting frame (WSMF) connections, the FEMA / SAC Joint Venture (SAC Joint Venture 1995) had investigated damage inspection and rehabilitation strategies. Because of the apparent

weak correlation between analytical predictions and observed damages, a random selection process was recommended to identify the connections to be inspected.

Based on the random selection process, Luco and Cornell (2002) proposed a method for estimating the damage state by partial inspection. Suppose that an existing building contains m_t connections; m_i of them are inspected at random, and n_i connections are found to be damaged. Therefore, the estimated total number of damaged connections n_t is:

$$n_t = p(m_t - m_i) + n_i \tag{2.13}$$

where p is the damage ratio of un-inspected connections, which is described by a beta distribution:

$$f_P(p) = \frac{(m_i + 1)!}{n_i!(m_i - n_i)!} p^{n_i} (1-p)^{m_i - n_i} \tag{2.14}$$

The mean and variance of p are:

$$\mu_p = \frac{n_i + 1}{m_i + 2} \tag{2.15}$$

$$\sigma_p^2 = \frac{(n_i + 1)(m_i - n_i + 1)}{(m_i + 2)^2 (m_i + 3)} = \frac{\mu_p (1 - \mu_p)}{m_i + 3} \tag{2.16}$$

As seen from Equation (2.16), the uncertainty in damage ratio (p) caused by un-inspected damage decreases with an increase in the number of connections inspected.

It is assumed in Equation (2.14) that partial inspection can be modeled by random sampling from independent Bernoulli trials. In reality, the forces in the structure are correlated by the law of structural mechanics, so the probability of that an individual connection is damaged varies from connection to connection. The engineer might

have prior knowledge as to which part of the structure is likely to be damaged (i.e. soft story); furthermore, preliminary damage assessment may also provide such information. Thus, the assessment of damage state will be improved if this prior knowledge can be used to provide a guideline for partial inspection.

Deterministic selection and analytically based section both attempt to use some of the information gained from the characteristics of structural response to ground motion. Deterministic selection puts some limitations on the number and locations at particular floors or column lines. The analytically based selection allows up to 60% of the locations to be determined on the basis of rational analysis (FEMA-352). Understanding the laws of structural mechanics, the deterministic selection and analytically based selection both are aimed at making the sampling more reasonable. It seems apparent that analytically based selection should yield more effective inspection than random selection. However, the uncertainty in estimated damage state and impact on structural reliability remains unaddressed.

Until recently, little research has been done on the topic of damage assessment of existing buildings. It is difficult to model the probabilities of specific damage states using the results of partial inspection, and to model the structural behavior for specific damage states. The purpose of damage assessment of an existing building should be to evaluate its expected performance during a service period in the future, so that policy makers may decide to take no action to upgrade its current condition, to require rehabilitation before permitting continued occupancy, or to require that the structure be replaced. Assuming the difficulties mentioned above can be addressed, the

framework of damage assessment of existing structures can be expressed as:

$$P[DM \mid D_{Insp}] = \Sigma P[DM \mid D_{Act}] \cdot P[D_{Act} \mid P_{Insp}] \quad (2.17)$$

where D_{Insp} represents the damage state of the existing building by partial inspection, and D_{Act} is the actual damage state of the existing building. The term $P[DM \mid D_{Act}]$ requires a structural response and fragility assessment, with the damage state D_{Act} correctly modeled.

$$P[DM \mid D_{Act}] = \Sigma\Sigma P[DM \mid LS] \cdot P[LS \mid D_{Act}, IM] \cdot P[IM] \quad (2.18)$$

To evaluate the term $P[D_{Act} \mid P_{Insp}]$, the relationship between the inspected damage and actual damage must be established. In Chapter 6, an analysis-based inspection scheme is proposed and methods to evaluate Equations (2.17) and (2.18) are presented in detail.

2.4 Critical appraisal of the state-of-the-art

The review in the previous sections has identified a number of research issues that must be addressed to allow consequence-based engineering to achieve its full potential as a decision tool.

1. Efficient methods for system reliability analysis

Monte Carlo (MC) simulation is commonly used to simulate the uncertainties in structural response to earthquake excitation. The numerical burden of the MC method motivates the use of variance reduction techniques such as importance sampling and adaptive sampling. However, the most productive sampling region may not be available or reliable enough to prevent gross errors of sampling at the “wrong”

location. Latin Hypercube Sampling (LHS) is a frequent choice for fragility assessment, but because it utilizes relatively small samples (e.g., the number of ground motion records in simulating dynamic response of frames is usually less than 30), LHS can not generate rare events, which are often critical for structural failure. All simulation methods proposed to date have some deficiencies when applied to reliability assessment based on nonlinear dynamic analysis.

2. Efficient structural seismic response analysis procedure

Currently, seismic codes have begun to explicitly require the identification of sources of inelasticity in structural response. Ideally, such performance evaluation of structural systems subjected to earthquake should be based on nonlinear time history analysis (NLTHA). However, the large computation effort required by NLTHA does not justify its use in ordinary engineering application. Nonlinear static pushover (NSP) analysis has been widely used as a tool for assessment and design verification. However, it exhibits a number of limitations, as described earlier in this Chapter. An efficient structural seismic response analysis procedure, which is less time-consuming than NLTHA and overcomes NSP's limitations, is needed to perform the extensive parametric studies required for development of practical design and condition assessment procedures.

3. Damage inspection and seismic assessment of existing structures

Seismic risk mitigation must consider existing as well as new construction. Probabilistic seismic damage analysis methods can be extended to damage assessment of existing structures. To achieve that goal, inspections of building damage must be

performed to obtain a clear knowledge of the current condition of existing structures. It is burdensome and impractical to perform a complete inspection, so the damage state has to be estimated by partial inspection, which introduces uncertainties and bias. These uncertainties and biases impact the reliability assessment in an unknown manner. An efficient damage inspection scheme and associated probability model must be developed.

The remaining Chapters address the above challenges in sequence.

CHAPTER 3: INTERVAL POINT ESTIMATE SAMPLING TECHNIQUE

3.1 Introduction

In view of the complexity of realistic structural systems and the large uncertainties in both ground excitation and structural response, a general closed-form mathematical solution to the problem of estimating structural system reliability is not feasible, and a simulation method must be used to evaluate the reliability. As noted in the previous chapter, nonlinear time history analysis is time-consuming and imposes a significant computational burden. Reducing the required simulation times while minimizing or controlling the variance in the statistical estimates obtained from simulation at the same time is a significant research challenge.

In the context of structural reliability analysis, all simulation methods can be viewed as techniques for numerical integration of the joint probability distribution of the random variables over the domain that represents structural failure (Equation (2.4)). In naive (brute-force) Monte Carlo (MC) analysis, samples of the random variables are generated according to the joint probability density function of the random variables. Each randomly generated sample is used to evaluate the system performance and results in one estimated response of the system. The generated samples collectively can then be used to assess the statistics of the system response or

to estimate the probability that the system exceeds a specified limit and a specific damage state occurs. Although the naive MC method is simple to use, it is computationally intensive. The samples are generated completely randomly, and there is no assurance that an individual sample point will be generated from the particular subset of the sample space that is of specific interest to building performance assessment. As a result, the majority of sample points are non-informative in terms of structural reliability assessment, and important subsets with low probability but high consequence are likely to be missed if the number of simulations is insufficient. Moreover, the estimated statistics or probabilities obtained from repetitions of the Monte Carlo experiment vary from repetition to repetition of the experiment; for structural reliability assessment, this variation can be significant. Importance Sampling, directional simulation and Latin Hypercube Sampling (LHS) (Iman and Conover 1980) are variance reduction techniques that provide a way to address this problem.

As described in more detail below, LHS sampling with n samples has the advantage of forcing the inclusion in the simulation of n mutually exclusive and collectively exhaustive subsets, each with probability $1/n$ of occurrence. This procedure produces estimates with smaller variance than those from naïve Monte Carlo simulation, thus the outcomes from repetitions of the analysis are more stable than naive MC simulation. However, LHS sampling and MC simulation are basically both equal-probability sampling techniques, where all random samples have the same probability. Therefore, to include a rare event in sampling, e.g., one with a probability

of 1/1000 or less, one would require, on average, at least 1000 samples.

The Point Estimate (PE) Method, which was first proposed by Rosenblueth (1981), is a different probability simulation technique, which may enhance the efficiency of the MC simulation. In this chapter, a new sampling technique is proposed for reliability assessment which combines the advantages of the LHS technique and PE method. The proposed technique will be described in detail in the following sections, followed by several examples.

3.2 Latin Hypercube Sampling

The response of an engineered structural system, Z, can be described by a function of a vector of load and resistance variables $\mathbf{X} = [x_1, x_2, \ldots\ldots, x_n]$,

$$Z = h(\mathbf{X}) \tag{3.1}$$

The mathematical expectation of Z^k or the k^{th} moments of Z, $E(Z^k)$, is defined as:

$$E(Z^k) = \int_{\Omega} \left(h(\mathbf{X})\right)^k f_{\mathbf{X}}(\mathbf{X}) d\mathbf{X} \tag{3.2}$$

in which represents the domain of $\mathbf{X}$, and $f_{\mathbf{X}}(\mathbf{X})$ is the joint probability density function of $\mathbf{X}$. The parameter Z depends on the decision of interest; Z could be a displacement, rotation, or force. For the purpose of structural reliability analysis, Z is interpreted as the margin of safety or serviceability (limit state function). By convention, when $Z > 0$, the structure is safe (or serviceable); when $Z = 0$, structure is at the limit state; when $Z < 0$, the structure fails. The probability of failure P_f is given by the integral

$$P_f = \int_{\Omega} I(\mathbf{X}) f_{\mathbf{X}}(\mathbf{X}) d\mathbf{X} \tag{3.3a}$$

in which $I(\mathbf{X})$ is the indicator function, defined as:

$$I(\mathbf{X}) = \begin{cases} 0, & Z \geq 0 \\ 1, & Z < 0 \end{cases} \tag{3.3b}$$

Note that the probability of failure can be interpreted as the mathematical expectation,

$$P_f = E[I(X)] \tag{3.3c}$$

An estimate of P_f in equation (3.2) and (3.3) can be estimated as,

$$P_f = \frac{1}{N}\sum_{i=1}^{N} I_i \tag{3.3d}$$

in which N is the number of samples using the simple simulation technique.

In the LHS technique, for practical applications with independent random variables, the generation of Latin Hypercube samples of size s is carried out as follows. The domain of each random variable is divided into s mutually exclusive and collectively exhaustive intervals, and each interval covers the cumulative probability of $1/s$. One value is selected randomly or deterministically (the mean or median of each interval) in each interval so that the probability distribution of a random variable is represented by s discrete values, each with the probability concentration of $1/s$. A value is randomly selected from the s values of each of n random variables to form the first Latin Hypercube sample. The remaining s-1 values of each random variable are used to form the second Latin Hypercube sample. That is, a value is randomly selected from the remaining s-1 values of each of s random variables to form the second Latin Hypercube sample. This process is repeated until s Latin Hypercube samples are obtained.

There are two sources of variability in the statistic estimated by this procedure:

one is associated with the changing of sampled values from sample to sample; the other is associated with the randomness in the permutation. In the following paragraph, two LHS techniques are described:

·LHS1: the sampled values of each random variable are deterministic (mean or median of each interval), and their permutations are random. This is the customary LHS procedure (Imam and Conover, 1980).

·LHS2: the sampled values of each random variable are random within each interval (according to the local characteristics of the PDF), and their permutations are also random.

The variance associated LHS1 is produced by the randomness in the permutation only, so it is smaller than the variance in the estimator from LHS2. However, if the number of samples is determined, the scope of each random variable is restricted too. As a result, the estimator obtained from LHS1 may be biased. For reliability problems, moreover, the number of samples must be large enough to cover the extremes of the distributions, within which the failure domain generally lies. To ensure proper coverage of the low-probability events while keeping the variance in the estimator small, the proposed sampling technique will modify the LHS1 procedure by the Point Estimate method.

3.3 Point Estimate Method

The point estimate method originally was developed to evaluate approximately the moments of Z based on the first few statistical moments of $\mathbf{X}$ (Rosenblueth 1981)

such as the means, standard deviations and skewness coefficients. The method basically replaces the original (continuous) probability density function of each random variable by a set of sampled values and their probability masses (concentrations) determined from the moments of the random variables. The sampled values and their denoted probability concentrations are obtained by solving a set of nonlinear equations. These equations are written as:

$$\sum_{i=1}^{n} w_i x_i^j = E[X^j] \qquad \text{j} = 0, 1, \ldots\ldots, (2n\text{-}1) \tag{3.4}$$

Equation (3.4) shows that by using n samples and their denoted probability concentrations, the first $(2n - 1)$ order moments of X are satisfied. The expected value of any function of only one random variable X can be determined by:

$$E[h(X)] = \sum_{i=1}^{n} w_i h(x_i) \tag{3.5}$$

The samples in the domain of higher density are assigned larger probability concentrations, while the samples at lower density domain have smaller probability concentrations. Therefore, the PE method can cover a broader range of the random vector than LHS1 with an equal number of samples. A comparison of LHS1 and PE is illustrated in figure 3.1.

In structural reliability analysis, the function $h(\mathbf{X})$ that describes the structural behavior is a function of construction material parameters (e.g. Young's modulus and material yielding strength etc.), but is not expressed explicitly. Calculation of $h(\mathbf{X})$ is so complicated and time-consuming that very few samples are selected according to the pre-knowledge on $h(\mathbf{X})$ rather than the probability distribution of $\mathbf{X}$. In such cases,

(a) LHS1

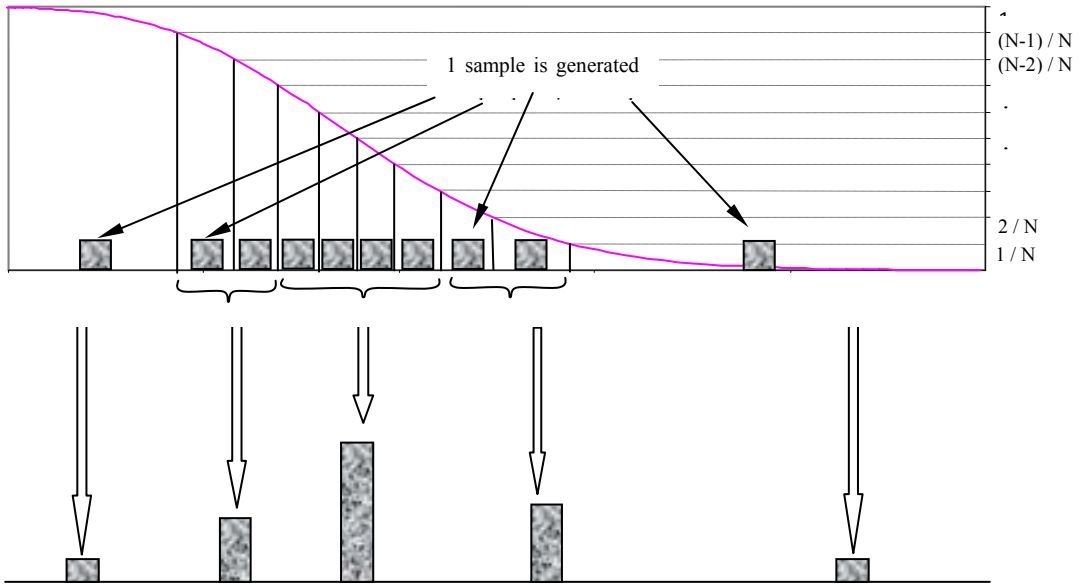

(b) PE

Figure 3.1 Illustrative comparison of LHS1 and PE

the rule of PE will be applied in this way. Assuming x_1, x_2, to x_n are n pre-selected samples and $E[\mathbf{X}^n]$ is the n^{th} moment of $\mathbf{X}$, the probability contribution $p_i = P[\mathbf{X} = x_i]$ is calculated by solving:

$$\begin{bmatrix} 1 & 1 & 1 & \cdots\cdots & 1 \\ x_1 & x_2 & x_3 & \cdots\cdots & x_n \\ x_1^{\,2} & x_2^{\,2} & x_3^{\,2} & \cdots\cdots & x_n^{\,2} \\ \vdots & \vdots & \vdots & \vdots & \vdots \\ x_1^{\,n} & x_2^{\,n} & x_3^{\,n} & \cdots\cdots & x_n^{\,n} \end{bmatrix} \cdot \begin{bmatrix} p_1 \\ p_2 \\ p_3 \\ \vdots \\ p_n \end{bmatrix} = \begin{bmatrix} 1 \\ E[X] \\ E[X^2] \\ \vdots \\ E[X^n] \end{bmatrix} \tag{3.6}$$

Then, the expected value of $h(\mathbf{X})$ is:

$$E[h(X)] = \sum_{i=1}^{n} p_i h(x_i) \tag{3.7}$$

where $h(\mathbf{X})$ could be any structural response function.

The PE method has some simulation to regression analysis. In regression analysis,

$h(\mathbf{X})$ is assumed to be a polynomial function of $\mathbf{X}$.

$$h(X) = a_0 + a_1 X + a_2 X^2 + ...a_{n-1} X^{n-1} \tag{3.8}$$

with parameters a_0 to a_{n-1} calculated by solving:

$$\begin{bmatrix} 1 & x_1 & x_1^2 & \cdots\cdots & x_1^{n-1} \\ 1 & x_2 & x_2^2 & \cdots\cdots & x_2^{n-1} \\ \vdots & \vdots & \vdots & \vdots & \vdots \\ \vdots & \vdots & \vdots & \vdots & \vdots \\ 1 & x_n & x_n^2 & \cdots\cdots & x_n^{n-1} \end{bmatrix} \cdot \begin{bmatrix} a_0 \\ a_1 \\ \vdots \\ \vdots \\ a_{n-1} \end{bmatrix} = \begin{bmatrix} h(x_1) \\ h(x_2) \\ \vdots \\ \vdots \\ h(x_n) \end{bmatrix} \tag{3.9}$$

According to Eq (3.8), the expected value of $h(\mathbf{X})$ is:

$$E[h(X)] = a_0 + a_1 E[X] + a_2 E[X^2] + ...a_{n-1} E[X^{n-1}] \tag{3.10}$$

Comparing Eq. (3.7) and (3.10), it is found that the PE sampling and regression analysis are identical. However, PE sampling is more convenient because the probability concentration factors p_i are not related to $h(\mathbf{X})$. They remain unchanged for different limit state functions $h(\mathbf{X})$. In regression analysis, the parameters a_0 to a_{n-1} must be solved again if the limit state function $h(\mathbf{X})$ changes.

3.4 Interval Point Estimate Sampling

A deficiency of the PE method is that the number of samples becomes very large in problems where there are many random variables. For example, the number of samples would be 5^{10} = 9,765,625 when there are 10 random variables represented by 5 probability points/masses for each random variable. Moreover, the LHS1 technique may provide an estimator with a smaller variance than that obtained from LHS2, but it is biased because the samples within each pre-defined interval are selected deterministically. The method described in the following paragraphs, denoted

interval point estimate sampling, is aimed at overcoming these deficiencies by increasing the samples in the higher and lower tail regions of the probability distributions with the PE method. This allows the samples in those regions to be randomized in order to capture the tail behavior more accurately without unduly increasing the total number of samples. The procedure is described by the following steps:

1) Transform the random variables x_i (i = 1, 2, ……, n) to be standard normal variates, u, allowing the samples to be generated in the standard normal space. One difficulty in the PE method is to calculate the sampling values x_i and probability concentration factors w_i in Equation (3.4). If x_i and w_i are calculated in standard normal space, they can be used later for any type of probability distribution.
2) Obtain $\Phi^{-1}(j/s)$, j = 1, 2……(s-1), so that $\Phi^{-1}(j/s)$ divides the standard normal distribution into s mutually exclusive and equally probable intervals.
3) For all intervals except the first and nth, the sampled value is the median of each interval, $u_j = \Phi^{-1}\left((j-0.5)/s\right)$, j = 2, 3……(s-1). For intervals 1 and n (the upper and lower tail regions), s^* sampled values are used to simulate the probability distribution. The sampled values for the lower tail interval u_{tk}, k = 1, 2,…., s^* and their denoted probability concentrations p_{tk} are obtained by solving:

$$\begin{aligned} p_{t1} + p_{t2} + ... + p_{ts^*} &= 1/s \\ p_{t1}u_{t1} + p_{t2}u_{t2} + ... + p_{ts^*}u_{ts^*} &= E[U]\Big|_{-\infty}^{\Phi^{-1}(1/s)} \\ &\vdots \\ p_{t1}u_{t1}^{\,2s^*-1} + p_{t2}u_{t2}^{\,2s^*-1} + ... + p_{ts^*}u_{ts^*}^{\,2s^*-1} &= E[U^{2s^*-1}]\Big|_{-\infty}^{\Phi^{-1}(1/s)} \end{aligned} \tag{3.11}$$

The right side of equations $E[U^{2s^*-1}]\Big|_{-\infty}^{\Phi^{-1}(1/s)}$ refers to the $(2s^* - 1)^{th}$ moment of the random variable in the lower tail interval, which can be obtained from:

$$\begin{aligned} E[U^o]\Big|_{-\infty}^{a} &= \Phi(a) \\ E[U^1]\Big|_{-\infty}^{a} &= \frac{-e^{-a^2/2}}{\sqrt{2\pi}} \\ E[U^k]\Big|_{-\infty}^{a} &= \int_{-\infty}^{a} x^k \frac{e^{-x^2/2}}{\sqrt{2\pi}}\,dx = (k-1)E[U^{k-2}]\Big|_{-\infty}^{a} - \frac{a^{k-1}e^{-a^2/2}}{\sqrt{2\pi}} \end{aligned} \tag{3.12}$$

In a similar way, the sampled values and denoted probability concentration for the upper tail interval can be obtained.

4) After all random variables are discretized, these intervals are combined in the same way as in LHS1 to form the sampling space.

If a sample is drawn from only intervals 2…n-1, the probability concentration for that sample is 1/*s*. When one lower or upper tail interval of a random variable, which has s^* sampled values ($x_{k,t1}$, $x_{k,t2}$,…,$x_{k,ts*}$), is combined with middle intervals (1 sampled value each interval) of other random variable, s^* samples will be generated. They are:

$$(x_{1,?}, x_{2,?} \ldots, x_{(k\text{-}1),?}\ \mathbf{x_{k,ti}}, x_{(k+1),?}, \ldots, x_{n,?}), \quad i = 1, 2, \ldots, s^* \tag{3.13}$$

in which $x_{1,?}$ to $x_{n,?}$ refers to the LHS sample from random variables X_1 to X_n to form the complete sample. The probability concentrations for the s^* samples are p_{ti},

which are obtained from equation (3.11).

When n_t lower or upper tail intervals are combined with (n-n_t) middle intervals to form s^* samples, the sampled values in the tail intervals are combined as in LHS1, to form s^* combinations. Including (n-n_t) sampled values of the middle intervals of other random variables, s^* samples are generated. Their probability concentrations are:

$$(s \times s^*)^{n_t - 1} \prod_{j=1}^{n_t} p_{j,ti}\,, \qquad i = 1, 2, \ldots, s^* \tag{3.14}$$

where $p_{j,ti}$ refers to the probability concentration corresponding to the sampled value of x_{ti} of the jth random variable.

5) The samples are transformed from standard normal space to their original space. The mean and variance of any function of random variables can be obtained by:

$$E[h(\mathbf{X})] = \sum_{S} p_i h(\mathbf{X}_i) \tag{3.15a}$$

$$\mathrm{Var}[h(\mathbf{X})] = \sum_{S}^{*} p_i h^2(\mathbf{X}_i) - E^2[h(\mathbf{X})] \tag{3.15b}$$

in which "S" refers to the sample space. The sampled values that form one sample and that sample's probability concentration are given in step (4). The number of samples "i" depends on the combination of intervals.

$$i = s - k + ks^* \tag{3.16}$$

in which k refers to the number of combinations consisting tail intervals. It can be seen that $1 < k \leq s$.

In the following section, the proposed method will be illustrated for three simple problems involving transformations of random variables and two problems involving

the analysis of structural reliability of frames. The first of the simple problems has a closed-form solution, so the approximate solutions can be verified independently. In these problems, both the variance in the estimate and any bias introduced by the sampling procedure are of interest. If the bias can be estimated, it can be removed as part of the simulation.

3.5 Illustration of the proposed method

Example 1: Polynomial function of two random normal variables.

Consider a simple transformation of random variables, with random variable Z defined by

$$Z = X_1^4 + X_2^4 + X_1^2 X_2^2 \tag{3.17}$$

where X_1 and X_2 are independent normally distributed random variables, both having mean of zero and standard deviation of one. Using the well-known result for standard normal variables that $E[X^m] = \begin{cases} 2^{m/2}\pi^{-1/2}\Gamma((m+1)/2); & m \text{ is even} \\ 0; & m \text{ is odd} \end{cases}$, it can be shown that the exact value of $E[Z]$ is 7.

If we use the LHS1 technique with 108 samples, the estimator of the mean of Z is 6.5 with standard deviation in this estimator, to be 0.18 [The experiment must be repeated on the order of 1,000 times to obtain the sampling distribution and statistics of the estimator of interest.]. If we use the LHS2 technique with 108 samples, the estimator is unbiased, but the standard deviation in the estimator increases significantly to 0.79. If we use naïve MC simulation, the standard deviation increases further to 0.87. The proposed method is used with the number of intervals

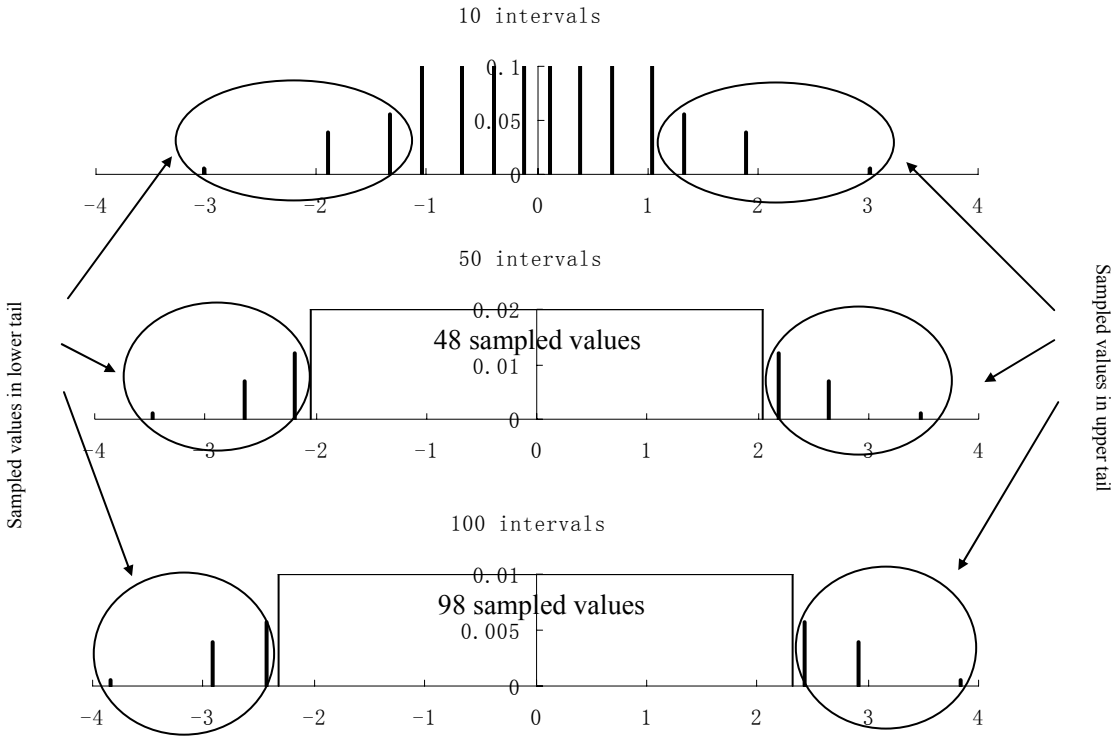

Figure 3.2 Illustration of sampled values with 10, 50 and 100 intervals

equal to 10, 50, and 100, respectively; the upper and lower tail intervals are sampled with three values each. The sampled values and their probability concentrations are shown in Figure 3.2. The estimated mean and coefficient of variation (c.o.v.) obtained from the proposed method are compared to the results from LHS1, LHS2 and naïve MC simulation in Figure 3.3. The efficiencies of the three variance reduction techniques can be seen by comparing their results with naïve MC simulation. LHS1 and the proposed method are very efficient in reducing the variance of the estimator, while the reduction in variance by LHS2 is not significant. The bias caused by LHS1

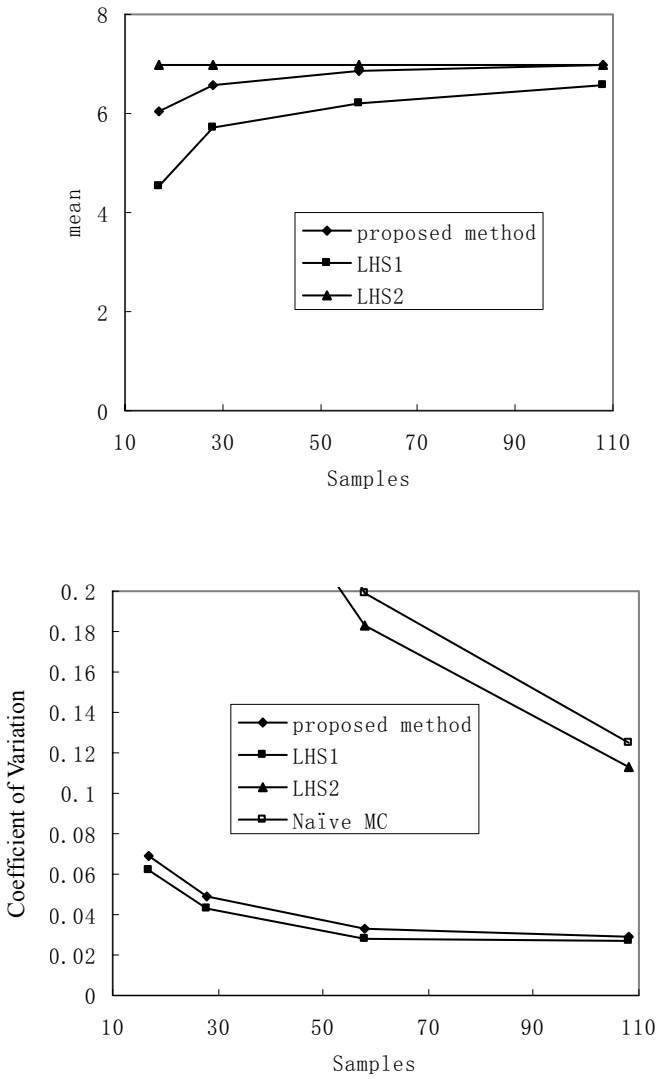

Figure 3.3 Comparison of mean and c.o.v of different simulation methods for example 1

is reduced significantly at the price of the slightly increase in the variance of the estimator.

Example 2: Nonlinear function with two exponential random variables

The function Z now is defined as in eq (3.17), but X_1 and X_2 are independent and exponentially distributed with the parameter λ = 1.0. Equation (3.17) becomes highly nonlinear in the u-space:

$$Z = \left(\ln\left[\Phi(-U_1)\right]\right)^4 + \left(\ln\left[\Phi(-U_2)\right]\right)^4 + \left(\ln\left[\Phi(-U_1)\right]\right)^2 \times \left(\ln\left[\Phi(-U_2)\right]\right)^2 \qquad (3.18)$$

where U_1 and U_2 are independent and normally distributed with means of zero and standard deviations of unity. The exact value of E[Z] is 52.9. Now, E[Z] was estimated by the proposed method, using 10, 20 and 100 intervals to model U_1 and U_2; the tail intervals are sampled with 3 values. The convergence of the estimates is shown in figure 3.4. The effect of variance reduction by LHS1 and the proposed

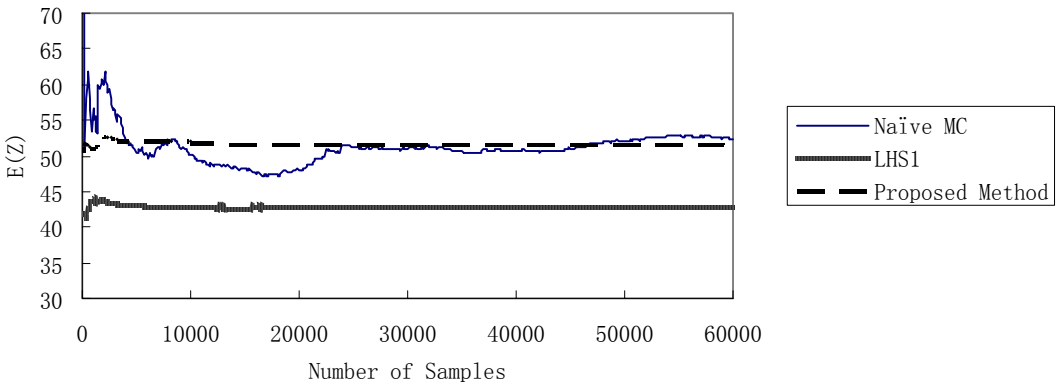

Figure 3.4 Comparison of convergence of different sampling techniques

method is evident by comparing with naïve MC simulation. It is also found that the bias introduced by the proposed method is negligible, while the bias of LHS1 is significant.

The estimated mean of Z and the c.o.v. of this estimator are presented in Figure 3.5. The results from LHS1, LHS2 and naïve MC are also presented in the same figure for comparison. It can be seen that the bias associated with the proposed method is much less than LHS1. When the proposed method uses 10 intervals, the variance is slightly larger than that for LHS1. The variance decreases as the number of intervals increases, and becomes almost equal to that of LHS1 when 100 intervals are used. As shown in figure 3.5, the c.o.v. in the estimate from the proposed method at 100 intervals is less than that of LHS1 because LHS1 underestimates the mean of Z.

Figure 3.6 shows that the variance associated with the proposed method is larger than that of LHS1 especially when the number of intervals is small. As the number of intervals increases, the variances of the two estimation methods become comparable. In general, estimates from the proposed method have larger variances than those obtained from LHS1. Instead of using only one sampled value in the tail interval, the proposed method uses several sampled values denoted with different probability concentrations. Unless only one tail interval is included in a sample, this introduces extra-randomness into the sampling process. For example, suppose two tail intervals are included in a combination. Each tail interval has 3 sample values, with probability of $p_{t1} = 0.056$, $p_{t2} = 0.038$, $p_{t3} = 0.006$ (this is the case of 10 intervals). There are 6 combinations to form 3 samples, and each combination has a different probability

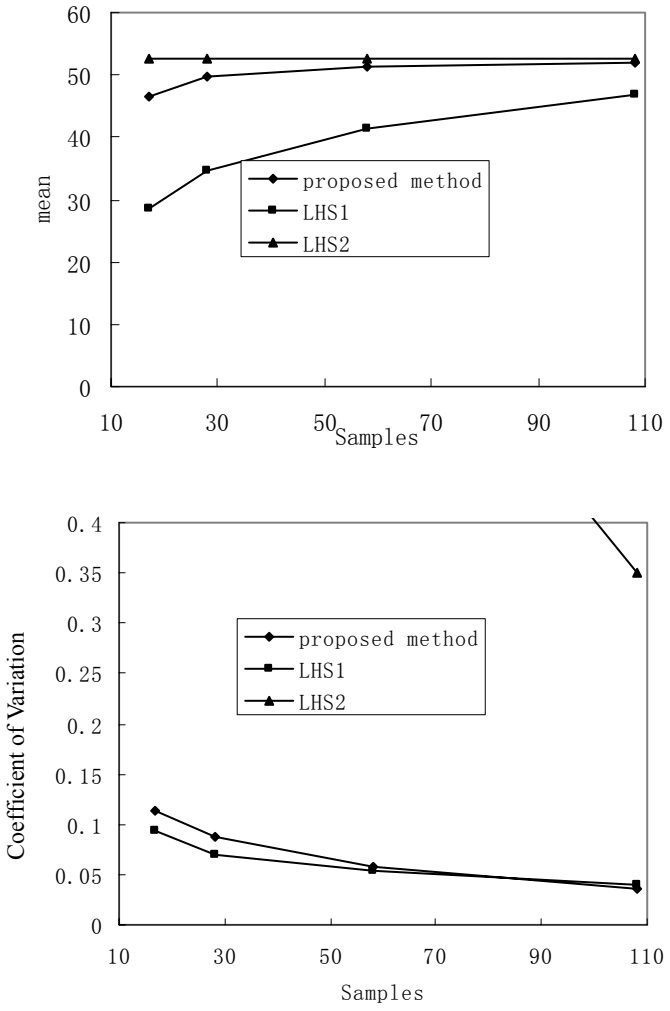

Figure 3.5 Comparison of mean and c.o.v of different methods for example 2

concentration. For example, for the (1, 2, 3) – (1, 2, 3) combination, the probability concentrations, according to equation (3.14), are 0.094, 0.043, 0.001, respectively, and the probability for the interval combination is 0.138. Similarly, for the (1, 2, 3) – (3, 2, 1) combination, the probability concentration is 0.010, 0.043, 0.010, respectively, and the probability for the interval combination is 0.063. In contract with the proposed method, each interval combination in LHS has a deterministic probability concentration, which equals 1/(number of intervals). The variance associated with the probability concentration of interval combinations causes the proposed method to have larger variance than LHS1. Therefore, to decrease the variance, the proposed method must use a larger number of intervals compared with the number of random variables.

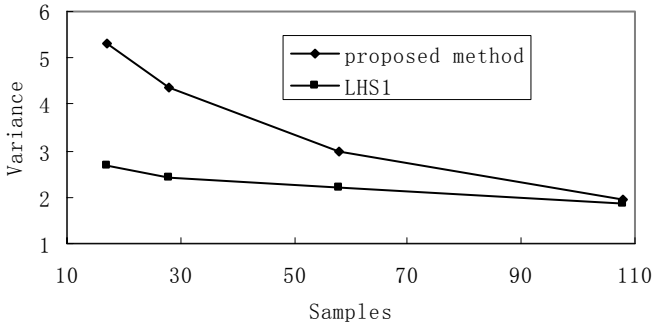

Figure 3.6 Comparison of variance of the proposed method and LHS1 for example 2

Example 3: Nonlinear limit state function with five random variables

In the proposed method, the variance in the estimator is related to the number of random variables. In this example, the number of random variable increases to 5, and the function is:

$$Z = \sum_{i=1}^{5} X_i^{\,4} + \prod_{i=1}^{5} X_i \tag{3.19}$$

where X_1 to X_5 are statistically independent and exponentially distributed, each with parameter λ =1.0.

The mean of Z is estimated by the proposed method, and the results are compared with LHS1 and LHS2, as shown in figure 3.7. The mean is estimated accurately by the proposed method when 50 intervals are used. The estimate of the mean from LHS1 is much lower than the actual mean and thus is highly biased, even though the number of samples is 120. The c.o.v. of the proposed method is very close to that of LHS1 although the variance of the proposed method is larger than LHS1.

Example 4: Failure probability of a simple frame structure

To test the feasibility of the proposed method in structural reliability analysis, the failure probability of the simple plane portal frame (Madsen, et al 1986) shown in figure 3.8 was calculated. The moment-curvature relationship for beams and columns in this frame is assumed to be elastic-perfectly plastic.

Accordingly, the structural system failure state is defined by the following three limit state functions:

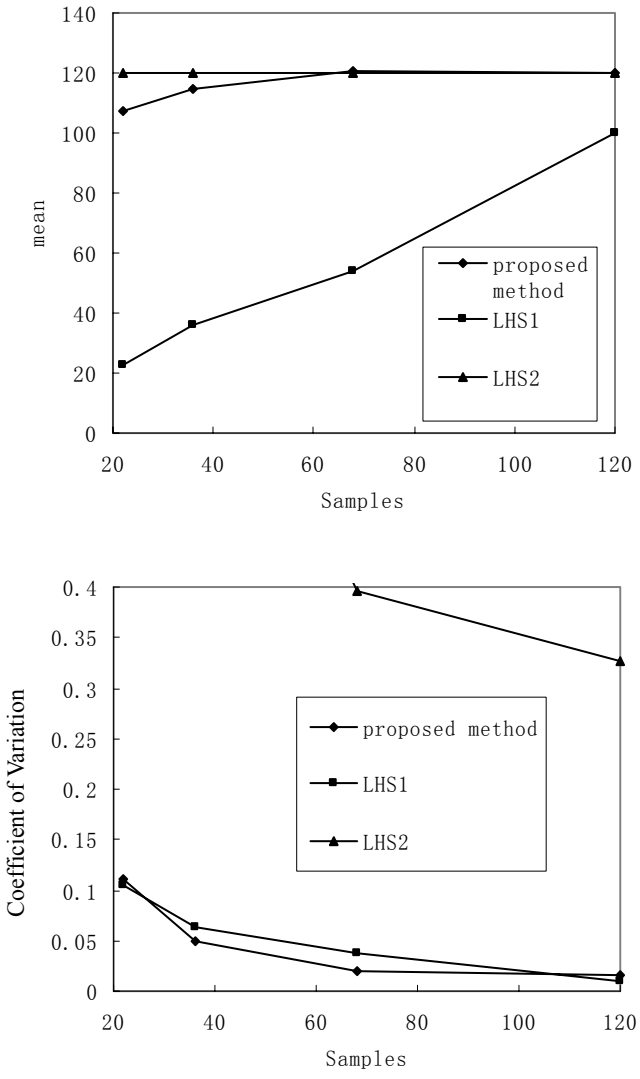

Figure 3.7 Comparison of means and coefficients of variation for example 3

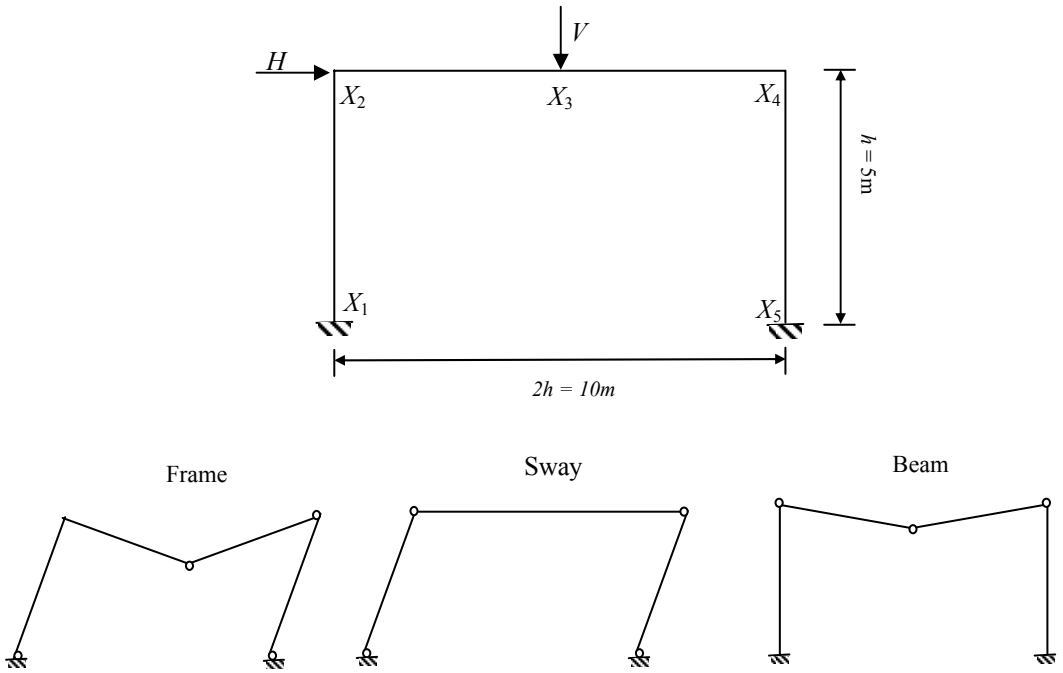

Figure 3.8 Plane frame structure and its three plastic failure mechanisms

$$\begin{cases} g_1(X) = X_1 + X_2 + X_4 + X_5 - h \cdot X_6 \\ g_2(X) = X_1 + 2X_3 + 2X_4 + X_5 - h \cdot X_6 - h \cdot X_7 \\ g_3(X) = X_2 + 2X_3 + X_4 - h \cdot X_7 \end{cases} \tag{3.20}$$

where h = 5.0. The plastic moment capacities X_i are assumed to be log-normally distributed independent variables with the following mean values and standard deviations:

$E[X_i] = 134.9$, $SD[X_i] = 13.49$ for $i = 1, 2, 3, 4, 5$;

$E[X_6] = 50$, $SD[X_6] = 15$; $E[X_7] = 40$, $SD[X_7] = 12$.

The exact probability of failure is: $P_f = P\left(\bigcup_{i=1}^{3} F_i\right) = 4.85 \times 10^{-3}$ using the branch and bound method (Madsen, et al 1986).

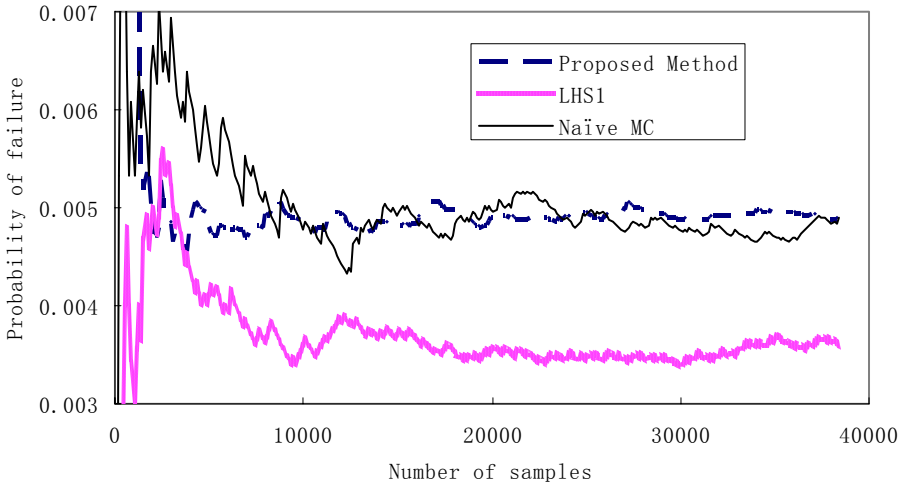

Figure 3.9 Convergence of system reliability solutions

The probability of failure is estimated by the proposed method using 100 intervals for each of the seven variables, and the tail intervals are sampled by 3 values. The convergence of the solution with increasing number of samples is compared to the results obtained by LHS1 and naive Monte Carlo (MC) in figure 3.9. It can be seen that faster convergence and small bias are achieved with the proposed method. The comparison of variance based on 128 samples is presented in table 3.1. The reduction in SD[P_f] when using the proposed method is evident from table 3.1.

Table 3.1 Comparison of different reliability analysis methods for example 4

Proposed Method		LHS1		LHS2		MC	
P_f (10^{-3})	c.o.v.	P_f (10^{-3})	c.o.v.	P_f (10^{-3})	c.o.v.	P_f (10^{-3})	c.o.v.
4.89	0.618	3.61	1.221	5.57	0.930	4.88	1.432

note: P_f is calculated with 38,400 samples by naïve MC simulation

Example 5: Reliability of structure with small probability of failure

This example compares the quality of estimates from the proposed method to estimates obtained from importance sampling, a common variance reduction technique in structural reliability analysis (Engelund and Rackwitz 1993). The limit state function is defined by:

$$g = X_1 X_2 - PL \tag{3.21}$$

where P and L are deterministic parameters with values of 14.614 and 10.0 respectively. X_1 and X_2 are normally distributed variables with means of 78064.4 and 0.0104, and standard deviations of 11709.7 and 0.00156 respectively. Such a limit state might describe the strength of a structural member, where X_1 = critical stress (yielding, buckling) and X_2 is a section property (area, section modulus). The "exact" failure probability P_f = 1.451 * 10^{-6} has been determined by conditional integration (Engelund and Rackwitz, 1993). This example serves to illustrate the ability to handle low-probability reliability estimation problems.

From the limit state function, it can be seen that the failure domain lies in the

lower tail of X_1 and X_2, so only the lower tail interval need be sampled. The domain of each random variable is separated into 100 intervals, and 5, instead of 3, values are sampled in the lower tail interval to widen the scope of sampling because the probability of failure is very small. In the standard normal space, the values are {-4.094, -3.606, -2.978, -2.566, -2.454} and the associated probability concentrations are {0.000494, 0.00113, 0.00181, 0.00224. 0.00433}.

The probability of failure is estimated to be $1.76 * 10^{-6}$ by the proposed method, 21% higher than the "exact" P_f, and the c.o.v. in the estimate is 0.64 (based on 525 samples). For comparison, the failure probability estimated by importance sampling is about 30% lower than the "exact" P_f, , and the c.o.v. is around 0.2 when the number of samples is 500. Considering the difficulties of calculating the optional position for importance sampling distribution when using that method, the accuracy of the proposed method is acceptable.

If the failure domain can be identified as falling in the lower tail region defined by the two random variables, the sampling points can be restricted in that "importance" domain. So if five sampled values are used for each random variable, and five samples are formed, the probability concentrations given in equation (3.14), in which $s = 100$, $s^* = 5$, $n_t = 2$, $p_{j,ti}$ are the probability concentrations of sampled values. When the proposed method is improved this way, the probability of failure is estimated to be $1.41 * 10^{-6}$, and the c.o.v. is 1.11. Since only 5 samples are used, the c.o.v. should decrease to $1.11/\sqrt{500/5} = 0.111$ when the total number of samples are 500. The advantage compared with importance sampling is demonstrated.

3.6 Summary

A new sampling technique suitable for structural system reliability analysis is proposed in this Chapter. This sampling technique is based on features of the Latin hypercube sampling technique, with the upper and lower intervals sampled by the Point Estimate method. The aim is to achieve more stable estimates of statistical moments and failure probabilities than is possible from naïve Monte Carlo simulation based on small samples. Furthermore, the proposed method widens the sampling scope and reduces the bias introduced by LHS1 significantly. Numerical results indicate that the proposed sampling technique is more efficient in covering the probability space than Latin hypercube sampling and provides relatively stable and accurate results even for highly nonlinear performance functions and low-probability events.

CHAPTER 4: ENHANCED UNCOUPLED MODEL RESPONSE HISTORY ANALYSIS (EUMRHA) FOR INELASTIC SYSTEMS

4.1 Introduction

The assessment of structural damage or damage potential in building frames subjected to earthquake ground motion requires consideration of nonlinear structural behavior. Ideally, this damage assessment should be based on nonlinear time history analysis (NLTHA). However, the large computational effort involved in NLTHA makes it difficult to justify its use in many applications. One example is in rapid assessment of buildings immediately following an earthquake, where a decision maker must choose quickly between allowing continued occupancy or requiring that the building be vacated until repair/rehabilitation can be completed. A second is in rapid screening of buildings to identify those that should receive a more detailed examination for purposes of rehabilitation (perhaps using nonlinear time-history analysis, inspection, or a combination of measures).

Current structural engineering practice for evaluating building seismic resistance often utilizes a non-linear static pushover analysis, in which the building is subjected to monotonically increasing lateral forces with invariant distribution of forces over the building height. As mentioned in Section 2.2, estimates from this procedure are

reasonably accurate provided that the structural response is first-mode dominated (Gupta and Krawinkler 2000). However, a static nonlinear pushover analysis cannot account for the progressive changes in the fundamental mode shape that occur as a result of stiffness degradation from nonlinear action; nor can it account for higher-mode contributions. To overcome these limitations, an adaptive pushover procedure that attempts to follow the time-variant distribution of inertia forces closely has been proposed (Bracci et al. 1997; Elnashai 2001). However, the adaptive pushover analysis provides a picture of behavior that is only slightly improved over its conventional counterparts (Antoniou et al. 2004) because it does not account for the frequency characteristics of expected ground motion.

A modal pushover analysis (MPA) and uncoupled modal response history analysis (UMRHA), as extended to nonlinear structures (Chopra and Goel 2002), allow the contributions of the higher modes and frequency characteristics of the excitation to be reflected in the assessment. As implemented by Chopra and Goel, the pushover curves representing the various modes of vibration were idealized and transformed into bilinear curves describing the forces of equivalent single degree of freedom (SDOF) systems, and the structural response parameters were determined for each mode separately. The total response was then determined by combining the peak modal responses using the square root of sum of squares (SRSS) rule. Typically, two or three modes were found to be sufficient to achieve accurate results (Chatpan and Chopra 2002). This method explicitly considers the influence of higher modes and the frequency characteristics of the expected earthquake through its reliance on nonlinear

dynamic responses of a set of SDOF systems. However, it does not account for structural damage and the resulting modification of the modal parameters, which might affect the response characteristics of a given structure significantly. In a structural steel frame, in particular, the beam-to-column connections are susceptible to damage. Such damages are likely to be concentrated at several specific stories because of customary structural design and construction practices. When connection damage occurs, the modal parameters may change suddenly. Failure to account for such changes may lead to large errors in structural response and damage prediction.

The principal objective of this Chapter is to enhance the UMRHA and MPA procedures outlined above by allowing for the modification in the lateral force distribution to reflect the displaced shape of a SMRF following connection damage. The procedure is illustrated using the 9-story and 20-story steel frames designed in the SAC project for Los Angeles CA using the pre-Northridge Uniform Building Code (1994). This frame was selected as being representative of many existing buildings to which the procedure might be applied. Errors in the procedure relative to the use of nonlinear time history analysis are documented and its use in damage assessment and post-earthquake capacity evaluation is described.

4.2 UMRHA for inelastic systems

The differential equations governing the response of a multistory building to horizontal earthquake ground motion $\ddot{u}_g(t)$ are as follows:

$$\mathbf{m}\ddot{\mathbf{u}} + \mathbf{c}\dot{\mathbf{u}} + \mathbf{k}\mathbf{u} = -\mathbf{m}\boldsymbol{\iota}\ddot{u}_g(t) \tag{4.1}$$

where **u** is the vector of *N* lateral floor displacements relative to the ground, and **m**, **c**, and **k** are the mass, classical damping, and lateral stiffness matrices of the system; each element of the influence vector $\boldsymbol{\iota}$ is equal to unity. The right-hand side of Equation (4.1) can be interpreted as the effective earthquake force:

$$\mathbf{p}_{\text{eff}}(t) = -\mathbf{m}\boldsymbol{\iota}\ddot{u}_g(t) \tag{4.2}$$

For elastic systems, the floor displacements **u** can be expressed as:

$$\mathbf{u}(t) = \sum_{n=1}^{N} \phi_n q_n(t) \tag{4.3}$$

where ϕ_n is the *n*th natural vibration mode of the structure, and $q_n(t)$ is the modal co-ordinate due to the *n*th mode effective earthquake force $\mathbf{p}_{\text{eff},n}(t)$. However, when the structure yields and responds in the inelastic range, ϕ_n no longer remains constant. The floor displacement **u** for inelastic systems is:

$$\mathbf{u}(t) = \sum_{n=1}^{N} \int_{r=0}^{t} \phi_n(r) \cdot d[q_n(r)] \tag{4.4}$$

Compared with $q_n(t)$, the variation of ϕ_n with time can be neglected, so the time derivatives of **u** can be approximated as:

$$\dot{\mathbf{u}}(t) = \sum_{n=1}^{N} \phi_n(t) \cdot \dot{q}_n(t) \tag{4.5a}$$

$$\ddot{\mathbf{u}}(t) = \sum_{n=1}^{N} \phi_n(t) \cdot \ddot{q}_n(t) \tag{4.5b}$$

For inelastic systems, the relations between lateral forces $\mathbf{f}_s$ at the *N* floor levels and the lateral displacements **u** are not single-valued, but depend on the history of the displacements:

$$\mathbf{f}_s = \mathbf{f}_s(\mathbf{u}, \text{sign}(\dot{\mathbf{u}})) \tag{4.6}$$

Substituting (4.4), (4.5a), (4.5b) and (4.6) into Equation (4.1), we have:

$$\mathbf{m}\sum_{n=1}^{N}\phi_n(t)\cdot\ddot{q}_n(t)+\mathbf{c}\sum_{n=1}^{N}\phi_n(t)\cdot\dot{q}_n(t)+\mathbf{f}_s(\mathbf{u},\text{sign}(\dot{\mathbf{u}}))=-\mathbf{m}\iota\ddot{u}_g(t) \tag{4.7}$$

By pre-multiplying $\phi_n^{\ T}(t)$ and using the mass- and classical damping-orthogonality property of modes, Equation (4.7) is transformed to:

$$\ddot{q}_n+2\zeta_n\omega_n\dot{q}_n+\frac{\phi_n^{\ T}(t)\mathbf{f}_s(q,\text{sign}(\dot{q}))}{M_n}=-\Gamma_n(t)\ddot{u}_g(t)\text{ , }n=1,2,\ldots\ldots,N \tag{4.8}$$

in which:

$$\Gamma_n(t)=\frac{L_n}{M_n},\quad L_n=\phi_n^T(t)\mathbf{m}\iota\text{ },\quad M_n=\phi_n^T(t)\mathbf{m}\phi_n(t) \tag{4.9}$$

Equation (4.8) shows that the resisting force depends on all modal co-ordinates $q_n(t)$, implying that the modal co-ordinates are coupled because of yielding of the structure. However, in extending the modal analysis procedure to inelastic building frame systems in which connection behavior was modeled as bilinear, it was confirmed numerically that the modes are weakly coupled (Chopra and Goel, 2002; Chopra and Goel, 2003). Therefore, Equation (4.8) can be solved approximately as a single degree of freedom (SDOF) vibration problem. The solution q_n is given by:

$$q_n(t)=\Gamma_n(t)D_n(t) \tag{4.10}$$

If the change of Γ_n with time is neglected compared with that of D_n, then:

$$\dot{q}_n=\Gamma_n(t)\dot{D}_n\quad\text{ and }\quad\ddot{q}_n=\Gamma_n(t)\ddot{D}_n \tag{4.10a}$$

When Equation (4.10a) is substituted into equation (4.9), we find that $D_n(t)$ is governed by:

$$\ddot{D}_n+2\zeta_n\omega_n\dot{D}_n+\frac{F_{sn}}{L_n}=-\ddot{u}_g(t) \tag{4.11}$$

and

$$F_{sn} = \phi_n^T(t)\mathbf{f}_s(D, \text{sign}(\dot{D})) \tag{4.12}$$

Equation (4.11) may be interpreted (loosely) as the governing equation for the *n*th-'mode' inelastic SDOF system, a SDOF system with (1) the same elastic vibration properties (natural frequency ω_n and damping ratio ζ_n of the *n*th-mode of the corresponding MDOF system); and (2) the $\frac{F_{sn}}{L_n}$ vs D_n relation between resisting force $\frac{F_{sn}}{L_n}$ and modal co-ordinate D_n defined by Equation (4.11). Equation (4.11) shows that the UMRHA concept for elastic systems can be extended to inelastic systems by introducing the *n*th-'mode' inelastic SDOF system. The accuracy of this approximation is examined subsequently in this chapter.

4.3 Properties of the *n*th-mode inelastic SDOF system

The relation between $\frac{F_{sn}}{L_n}$ and D_n in Equation (4.11) must be determined before a solution can be obtained. Because Equation (4.11) governing $D_n(t)$ is based on Equation (4.4) for floor displacements, the relationship between lateral forces $\mathbf{f}_s$ and D_n in equation (4.12) can be determined by a non-linear static pushover analysis of the structure as the structure undergoes displacements described by equation (4.4) with increasing D_n. It is obvious that an invariant distribution of lateral forces cannot make the structure undergo such a displacement once the structure yields. Equation (4.4) shows that the change in lateral force distribution should be consistent with the change in the mode shape. When a strong column weak beam steel frame is subjected

to either static lateral force or an earthquake accelerogram, it often is found that the demands on the connections relative to their capacities across the structural bays at a given story are similar. Thus, during the nonlinear static pushover analysis the beam-to-column connections in one particular story are damaged almost simultaneously, causing the vibration modes to change abruptly. Figure 4.1 shows the change in the first vibration mode of the 9-story building at Los Angles in the SAC project, with the beam-to-column connection model incorporating the beam bottom flange fracture as shown in Figure 2.1b (Gross, 1998).

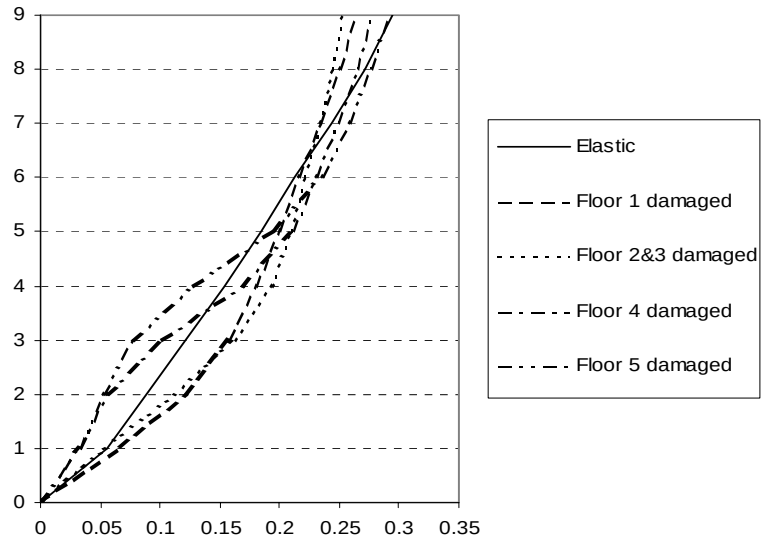

Figure 4.1 Change in first vibration mode when damage occurs

The structure is pushed with a lateral force distribution proportional to the first vibration mode shape and the base shear V_{b1} is plotted against roof displacement u_{r1} as shown in Figure 4.2a. In practice, the distribution of lateral forces is proportional to the elastic vibration mode shape until the structure yields (point 1 in Figure 4.2a), and the lateral force distribution of the *n*th mode during the pushover ($\mathbf{s}_n$) is:

$$\mathbf{s}_n = \Gamma_n \mathbf{m} \phi_n \tag{4.13}$$

Subsequently, it changes abruptly when additional damage occurs (from point 2 to 3; from point 4 to 5; from point 6 to point 7 in Figure 4.2a), but remains unchanged between points where additional damage occurs. The points of discontinuity in Figure 4.2 correspond to damage at specific floor levels. The relation between V_{b1} and $\mathbf{u}_{r1}$ in the elastic range is converted to the restoring force ($\frac{F_{s1}}{L_1}$) vs displacement (D_1) relationship of a SDOF system with unit mass by:

$$F_{s1} = \omega_1^2 D_1, \qquad D_1 = \frac{\mathbf{u}_{r1}}{\Gamma_1 \phi_{r1}} \tag{4.14}$$

in which $\omega_1 = 2\pi/T_1$ = natural frequency in the first mode, T_1 = fundamental period, Γ_1 is the first mode participation factor prior to structural yielding and ϕ_{r1} is the roof displacement term in the first elastic vibration mode. In the inelastic range, the restoring force is reduced in proportion to the peak elastic demand, while the displacement D_1 is obtained, the displacements at point 2 and point 3 are:

$$D_{1,(2)} = D_{1,(1)} + \frac{\mathbf{u}_{r1,(2)} - \mathbf{u}_{r1,(1)}}{\Gamma_{1,(2)} \phi_{r1,(2)}}; \quad D_{1,(3)} = D_{1,(1)} + \frac{\mathbf{u}_{r1,(3)} - \mathbf{u}_{r1,(1)}}{\Gamma_{1,(2)} \phi_{r1,(2)}} \tag{4.15}$$

where $D_{1,(1)}$ and $D_{1,(2)}$ are the displacements of the equivalent SDOF system at points 1 and 2 respectively, $\mathbf{u}_{r1,(1)}$ and $\mathbf{u}_{r1,(2)}$ are the roof displacements at points

1 and 2 in the pushover curve, and $\phi_{r1,(2)}$ and $\Gamma_{1,(2)}$ are the first vibration mode and its participation factor at point 2. The relationship at other stages can be obtained in a similar way. This leads to a relation between V_{b1} and u_{r1} that is converted to the $\frac{F_{sn}}{L_n}$ vs D_n relation and is idealized as the multi-linear curve shown in Figure 4.2(b).

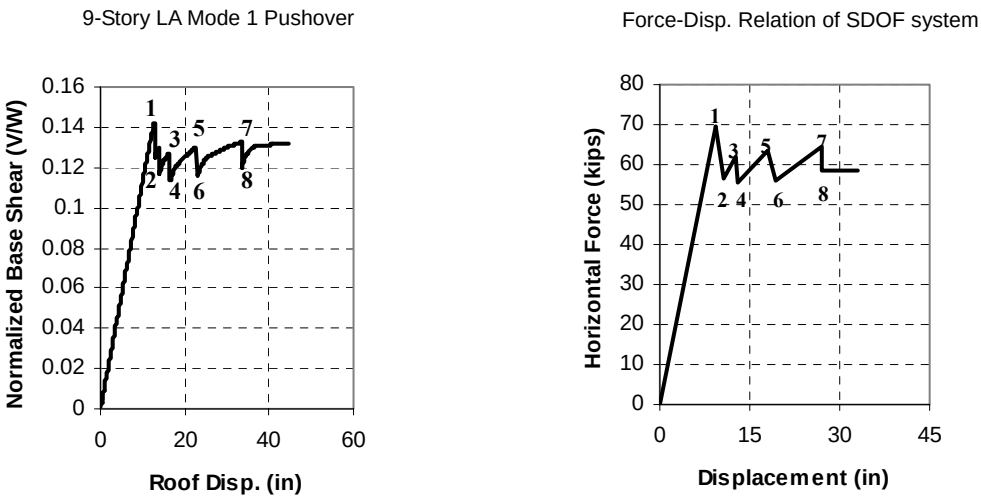

Figure 4.2. Properties of the first 'mode' inelastic SDOF system from the pushover curve

An equivalent SDOF system with behavior being equivalent to the first mode of the damaged steel frame can be modeled by the system illustrated in Figure 4.3(a). In this case, the unit mass is supported by four rigid bars, and the lateral stiffness is provided by the four rotational springs designed to mimic the force discontinuities in

Figure 4.2(a) arising from connection failures in the frame. The moment-rotation relations of the four rotational springs are shown in Figure 4.3(b). Enforcing static equilibrium at each of the eight points in Figure 4.2(b) yields the set of Equations (4.16) that must be solved to define their stiffness parameters. Next, a time history analysis is performed for the equivalent SDOF system subjected to ground motion, and the displacement response history $D_1(t)$ is obtained.

$$\begin{cases} (K_1+K_2+K_3+K_4)\theta_1 = F_1 h \\ 0.4K_1\theta_1 + (K_2+K_3+K_4)\theta_2 = F_2 h \\ (K_2'+K_3+K_4)(\theta_3-\theta_2) = (F_3-F_2)h \\ 0.4K_1\theta_1 + 0.4K_2\theta_2 + (K_3+K_4)\theta_4 = F_4 h \\ (K_3'+K_4)(\theta_5-\theta_4) = (F_5-F_4)h \\ 0.4K_1\theta_1 + 0.4K_2\theta_2 + +0.4K_3\theta_4 + K_4\theta_6 = F_6 h \\ K_4'(\theta_7-\theta_6) = (F_7-F_6)h \\ 0.4K_1\theta_1 + 0.4K_2\theta_2 + +0.4K_3\theta_4 + 0.4K_4\theta_6 + M_d = F_8 h \end{cases} \tag{4.16}$$

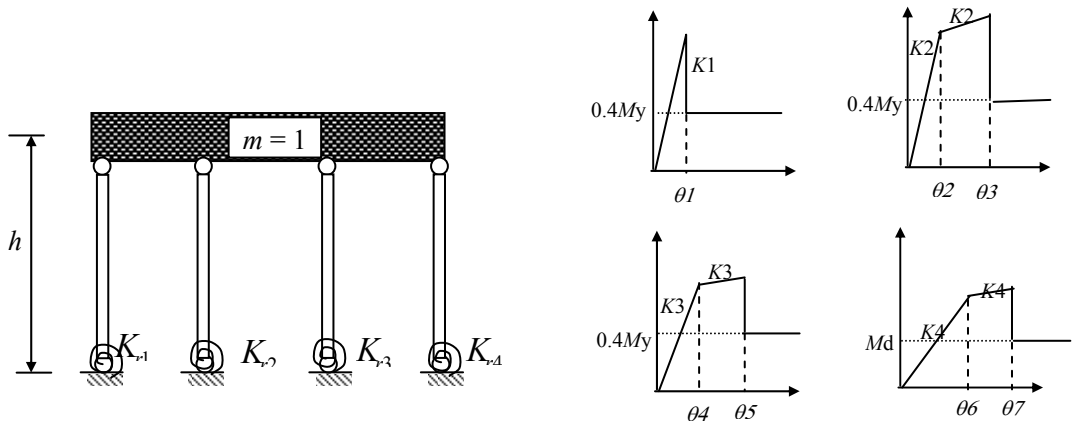

(a) Equivalent SDOF system

(b) Moment–rotation relationship of springs

Figure 4.3. Equivalent SDOF system and the rotational spring properties

The procedure is repeated for higher modes, yielding $D_2(t)$, $D_3(t)$,……, to $D_N(t)$.

4.4 Peak structural responses

The peak structural responses within the frame are obtained by combining peak modal responses according to the square-root-of-sum-of-squares (SRSS) rule. When the structure responds in the inelastic range, we can see from Equation (4.4) that the floor displacements subjected to the *n*th mode effective earthquake forces $\mathbf{p}_{\text{eff,n}}(t)$ depend on the entire history of loading. These displacements are no longer proportional to the *n*th vibration mode shape. The nonlinear static pushover analysis described above yields the database of the distribution of floor displacements with the increasing of $\mathbf{u}_{rn}$, from which the 'assumed' mode shape ϕ_n' and its participation factor Γ_n' can be calculated.

The time history analysis of the SDOF system results in $D_n(t)$ with the maximum value of D_{n0}, which corresponds to the maximum roof displacement $\mathbf{u}_{rn0}$ with the value of $\mathbf{u}_{rn,(k)} + \Gamma_{n,(k)}\phi_{rn,(k)}(D_{no} - D_k)$ and ($D_{n,(k)}<D_{no}<D_{n,(k-1)}$). From the database of floor displacements, the floor displacement distribution $\mathbf{u}_n$ with the maximum roof displacement $\mathbf{u}_{rn0}$ is identified. Then, the 'assumed' mode shape ϕ_n' when the structure reaches its maximum deformation is obtained by:

$$\phi_n' = \frac{\mathbf{u}_n}{\mathbf{u}_n^T \mathbf{m} \mathbf{u}_n} \tag{4.17}$$

To calculate the 'assumed' modal participation factor Γ_n', Equation (4.10) is substituted into Equation (4.4). The maximum *n*th mode floor displacement occurs at time $t_{\max}$, and $D_n(t_{\max})=D_{n0}$, so:

$$\mathbf{u}_{n,\max} = \mathbf{u}_n(t_{\max}) = \int_{r=0}^{t_{\max}} \phi_n(r)\Gamma_n(r) \cdot d[D_n(r)] \tag{4.18}$$

Since the mode shape is already known,

$$\mathbf{u}_n(t_{\max}) = \phi'_n \int_{r=0}^{t_{\max}} \Gamma_n(r) \cdot d[D_n(r)] = \Gamma'_n \phi'_n D_{n,o} \tag{4.19}$$

According to Figure 4.2(b), the integration in Equation (4.19) can be approximated by:

$$\int_{r=0}^{t_{\max}} \Gamma_n(r) \cdot d[D_n(r)] = \Gamma_{n,(0)} D_{n,(1)} + \Gamma_{n,(2)}(D_{n,(3)} - D_{n,(1)}) + \ldots + \Gamma_{n,(2i)}(D_{n0} - D_{n,(2i-1)})$$

$$\text{with} \quad D_{n,(2i)} < D_{no} < D_{n,(2i+1)} \tag{4.20}$$

Therefore:

$$\Gamma'_n = \frac{\Gamma_{n,(0)} D_{n,(1)} + \Gamma_{n,(2)}(D_{n,(3)} - D_{n,(1)}) + \ldots + \Gamma_{n,(2i)}(D_{n0} - D_{n,(2i-1)})}{D_{n0}} \tag{4.21}$$

Finally, given the 'assumed' vibration modes and their participation factors, the maximum roof displacement and maximum inter-story drift ratio at each story during the earthquake are obtained by:

$$\max(\mathbf{u}_r) = \left(\sum_{n=1}^{N} (\Gamma'_n \phi'_n D_{n0})^2 \right)^{1/2} \tag{4.22a}$$

$$\max(\Delta_i) = \left(\sum_{n=1}^{N} \left[\Gamma'_n (\phi'_{n,i} - \phi'_{n,i-1}) D_{n0} \right]^2 \right)^{1/2} \tag{4.22b}$$

4.5 Results and approximation errors

Modal pushover analysis by Chopra and Goel (2004) indicated that the 9-story and 20-story SAC buildings for Boston buildings remained elastic for all "modes" under demands that would be imparted by the SAC ground motions with hazard level of even 2%/50yr. On the other hand, for the Seattle and Los Angeles buildings, the demands from several ground motions force the structures well beyond their elastic

limit in the first two modes but not in the third "mode". Therefore, this method can be simplified by assuming that all modes remain linearly elastic except the first two "modes," thus reducing the computational effort.

For linearly elastic systems, the number of modes required to achieve reasonable accuracy can be calculated through the modal contribution factor $\bar{r}_n$ (Chopra, 2001), which is defined as:

$$\bar{r}_n = \frac{r_n^{st}}{r^{st}} \tag{4.23}$$

in which r_n^{st} denotes the *n*th modal response and r^{st} is the static response due to external forces. If only the first J modes are included, the error in the static response is

$$e_J = 1 - \sum_{n=1}^{J} \bar{r}_n \tag{4.24}$$

However, for inelastic systems, $\sum_{n=1}^{N} r_n^{st} \neq r^{st}$ and the modal contribution factor loses its meaning.

To determine the number of modes that must be included when the system responds inelastically, we begin by observing, as described above, that the third and higher mode responses can be assumed to remain linearly elastic. We then examine the difference in response if the first and second "modal" responses are assumed to be linearly elastic as well. Treating the structure as elastic in the modal pushover procedure leads to a different estimated demand for two reasons. First, the floor displacement distribution at a given roof displacement differs depending on whether the structure is treated as elastic or inelastic. Second, the roof displacement, obtained by THA of an equivalent SDOF system, differs depending on whether the

force-displacement relation of the SDOF system is determined from the nonlinear modal pushover procedure described above or from the pushover curve of the assumed elastic structure.

To examine the implication of the first source of difference, the results of modal pushover analysis (according to the method presented earlier in this Chapter) of the 9-story building at Los Angles subjected to SAC natural ground motions la01 – la30 (la01 – la20 are 10%/50 year ground motions and la21 – la30 are 2%/50 year ground motions. Only natural ground motions from the SAC project were utilized in this dissertation; hence the difference in sample size for the 10%/50yr and 2%/50yr ensembles) are compared with the results assuming that the first and second "modes" of the building remain linearly elastic. The mean floor displacements are presented in Figure 4.4. For the mode 1 analysis, for the same roof displacement, the displacements of all other floors are smaller if the building is assumed to be elastic; the inter-story drifts are underestimated by the elastic analysis in the lower stories, while they are overestimated in the upper stories. For the mode 2 analysis, for the same roof displacement, the displacements of floors other than 7 and 8 are larger if the building is assumed to be elastic, and the inter-story drift is overestimated if the building is assumed to be elastic.

To examine the implication of the second source of difference, the roof displacements estimated by the proposed method are compared to displacements computed assuming that the first and second "modes" are linear-elastic modes. The results for each of the 30 ground motions are plotted on Figure 4.5. The mean values

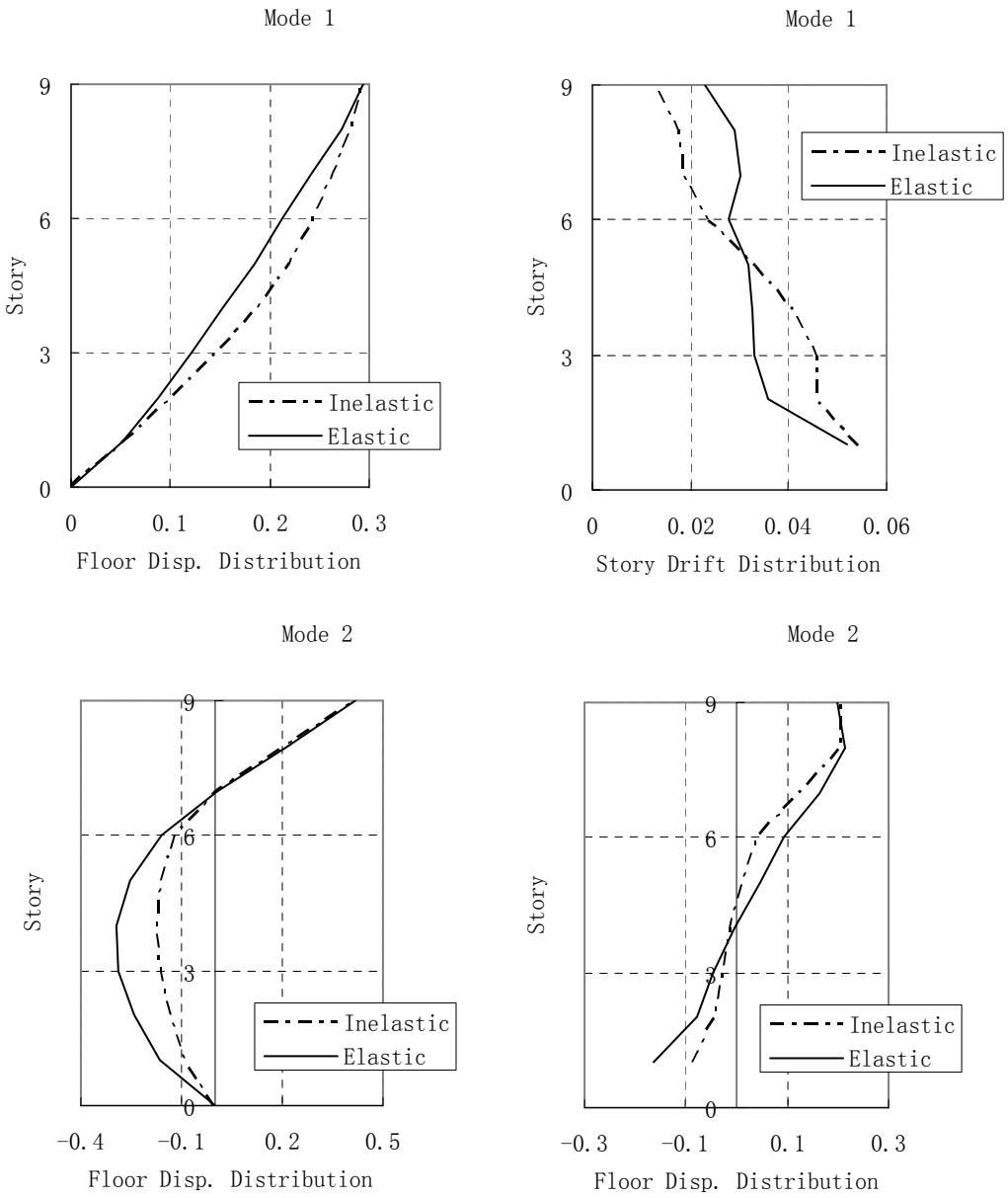

Figure 4.4. Distribution of floor displacement and story drift of nine-story LA frame from nonlinear and linear pushover

of the roof displacements from the two procedures and the roof displacements beyond which the structural response becomes nonlinear are also noted. It is seen that the roof displacements by the two procedures are very close when the structural response is only slightly nonlinear for both modes. Once the structure has yielded, assuming it to be linearly elastic tends to overestimate roof displacement in most cases. The mean roof displacements by the two procedures are close for both modes. However, considering that the roof displacements should be the same when the structure reaches the yield point, the difference would be larger if only the cases where the yield point is exceeded are considered.

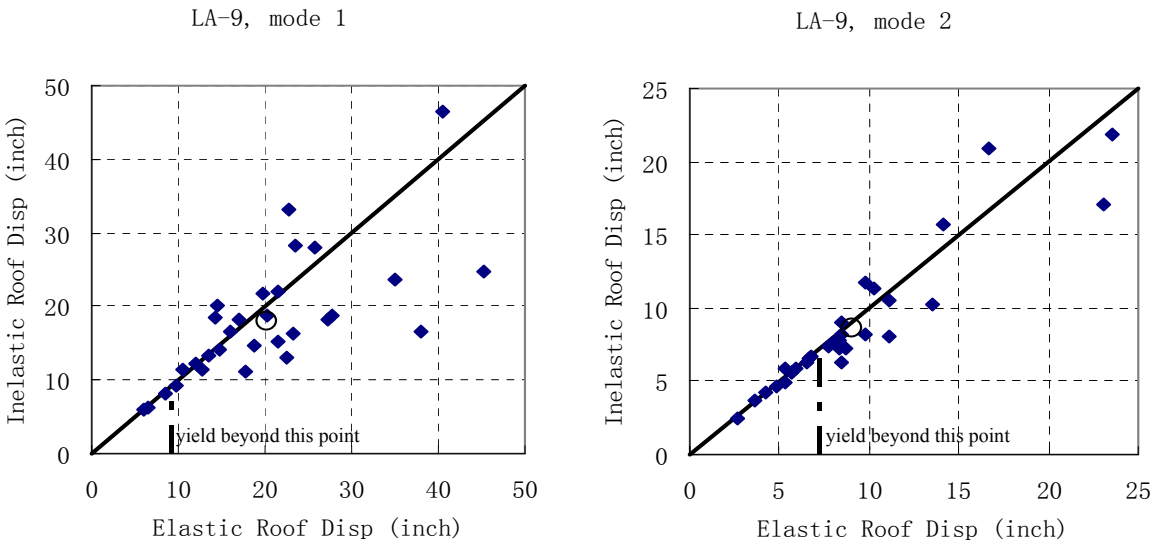

Figure 4.5. Inelastic versus elastic roof displacements for the first and second “modes” of nine-story LA frame

To summarize, the first and second "modal" structural responses tend to be overestimated if the modal behavior is assumed to be elastic. Therefore, compared with the classical UMRHA of linear elastic buildings, more modes should be included for the EUMRHA of inelastic buildings. It should be noted that the above conclusion may not hold for short-period frames, e.g. the fundamental period is smaller than about 1 second, where the structural response may be underestimated by elastic assumption. Therefore, including more modes than elastic cases sometimes achieves less error than required.

The number of modes required can be determined by tracking the accumulated error as more modes are added. In practice, it is found that if the first or second "modal" pushover analysis shows only slightly nonlinear behavior, the building can be assumed to be nonlinearly elastic to calculate the number of modes required from Equation (4.24). On the other hand, if highly nonlinear behavior is observed in the first or second "modal" pushover procedure, one additional mode should be included beyond that determined from Equation (4.24).

It is also should be noted that at least two modes must be included to estimate the inter-story drift with reasonable accuracy, even for a low-rise building. To illustrate this point, the 3-story Los Angeles frame from the SAC project is analyzed subjected to an ensemble of 20 ground motions representing the 10%/50 year hazard level (la01-la20). The inter-story drifts obtained by the proposed method with 1 mode and 2 modes are compared with the "exact" results by nonlinear time history analysis in Figure 4.6. It can be seen that if only the first mode is included, the story drift is

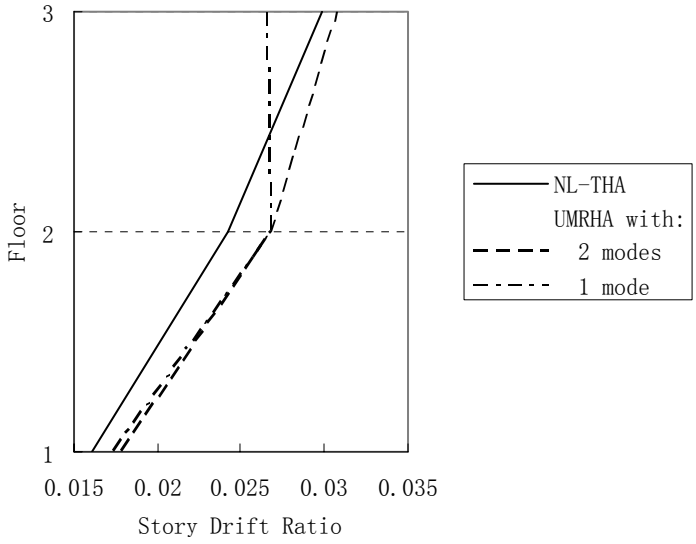

Figure 4.6. Mean story drift ratio determined by UMRHA with 1 and 2 modes, and compared with that by nonlinear THA

overestimated at the first and second stories and underestimated at the top story. If two modes are included, only the top story drift increases significantly, making the height-wise distribution of inter-story drifts consistent with the exact distribution.

4.6 EUMRHA analysis of 9 and 20-story steel moment frames

To verify the efficiency of the enhanced method, a series of analyses were conducted of the 9- and 20- story steel moment frames that were designed for Los Angeles, CA as part of the SAC Project (1995). Figures 4.7(a) and 4.7(b) show the floor plans and elevations for these buildings. The moment frames are located on the building perimeters; the remaining frames were designed only for gravity loads. Both

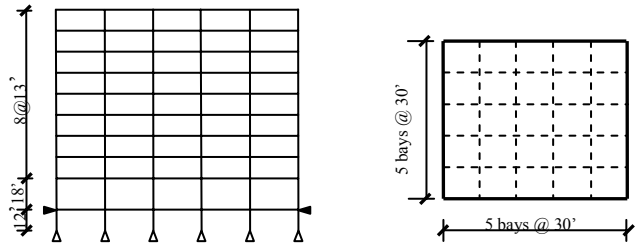

(a) SAC 9-story building at Los Angeles, CA

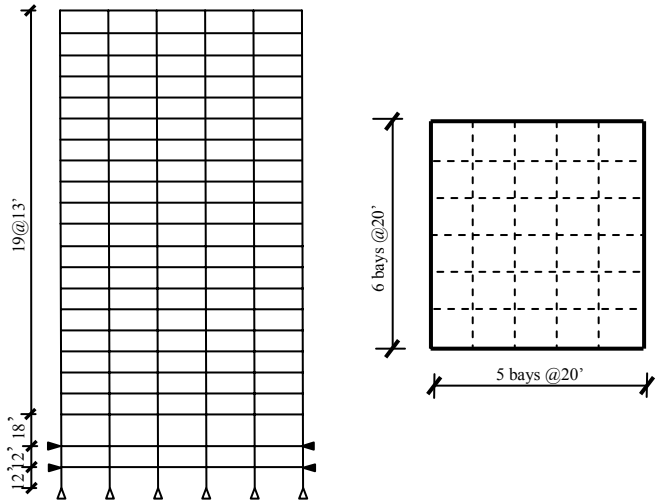

(b) SAC 20-story building at Los Angeles, CA

Figure. 4.7 Floor plan and elevation view of 9- and 20- story frames designed for Los Angeles, CA (after FEMA-355/SAC)

frames were designed in conformance with the *1994 Uniform Building Code*. Design details and other considerations are reported elsewhere (FEMA-355, 2000).

4.6.1 Structural response of LA 9-story frame

The response of the LA 9-story building was analyzed by the proposed method and the results were compared with the "exact" results from nonlinear time history analysis performed using the OpenSees computational platform (Mazzoni and McKenna, 2003). The natural periods of vibration for the first 3 modes were calculated as 2.34s, 0.90s and 0.51s, respectively, and the structural damping ratio was assumed to be 5% in all three modes. For comparison, Chopra and Goel (2002) found the first three periods for this frame as 2.27s, 0.85s, and 0.49s, respectively. Natural ground motion ensembles with probabilities of 2% in 50 years (10 records identified as LA21-LA30) and 10% in 50 years (20 records identified as LA01-LA20) (Somerville et.al., 1997) were chosen to ensure that the steel frame responds well into the inelastic range (Somerville et al, 1997).

The first vibration mode was shown in Figure 4.1. The second and third vibration modes are shown in Figure 4.8. The force distributions $\mathbf{s}_n$ to perform 'modal' pushover analyses are based on the vibration mode shape according to Equation (4.13). Note that Γ_n and ϕ_n are subject to change following structural damage to the connections. The first 'mode' pushover curve was shown in Figure 4.2. The second and third 'mode' pushover curves are shown in Figure 4.9. These curves are idealized by multi-linear curves and are simulated by equivalent SDOF systems, as described

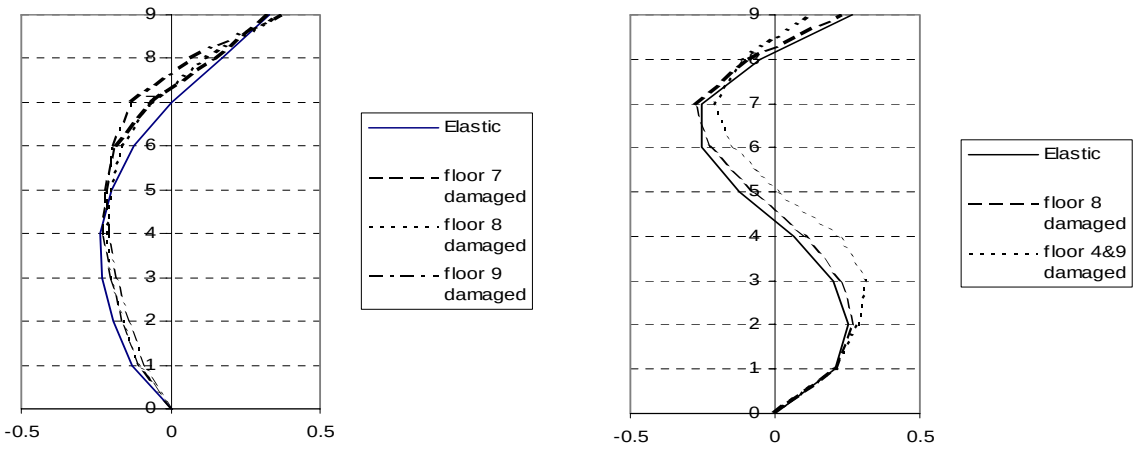

Figure 4.8. Second and third vibration modes of LA 9-story frame

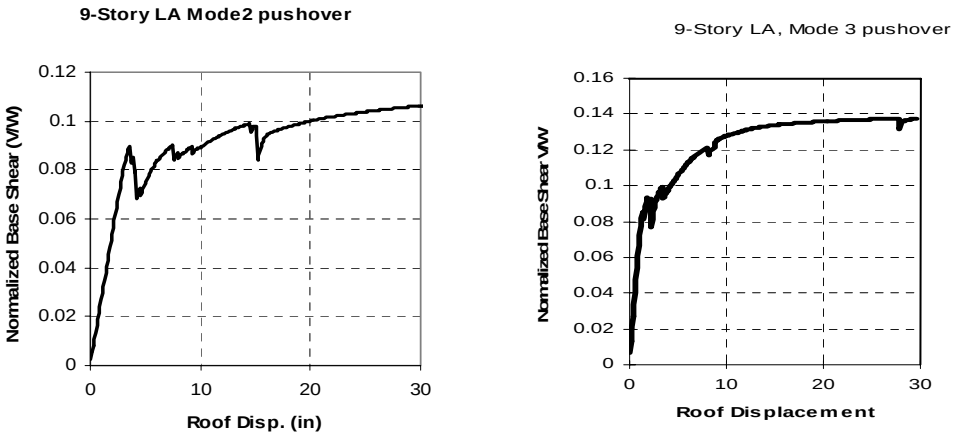

Figure 4.9. Second and third modal pushover curves for LA 9-story frame

previously.

The individual 'modal' responses of the three SDOF models subjected to a particular accelerogram (LA04 - a 10%/50 yr record for which $S_a(T_1) = 0.283g$) are illustrated in Figure 4.10, along with the combined response u_r due to three 'modes', and the 'exact' response from nonlinear time history analysis for the roof displacement u_{THA}. The peak values of floor displacements and story drifts, including one, two, and three modes, are compared with the 'exact' values obtained from OpenSees in Figure 4.11. The agreement is reasonable for the intended usage of the

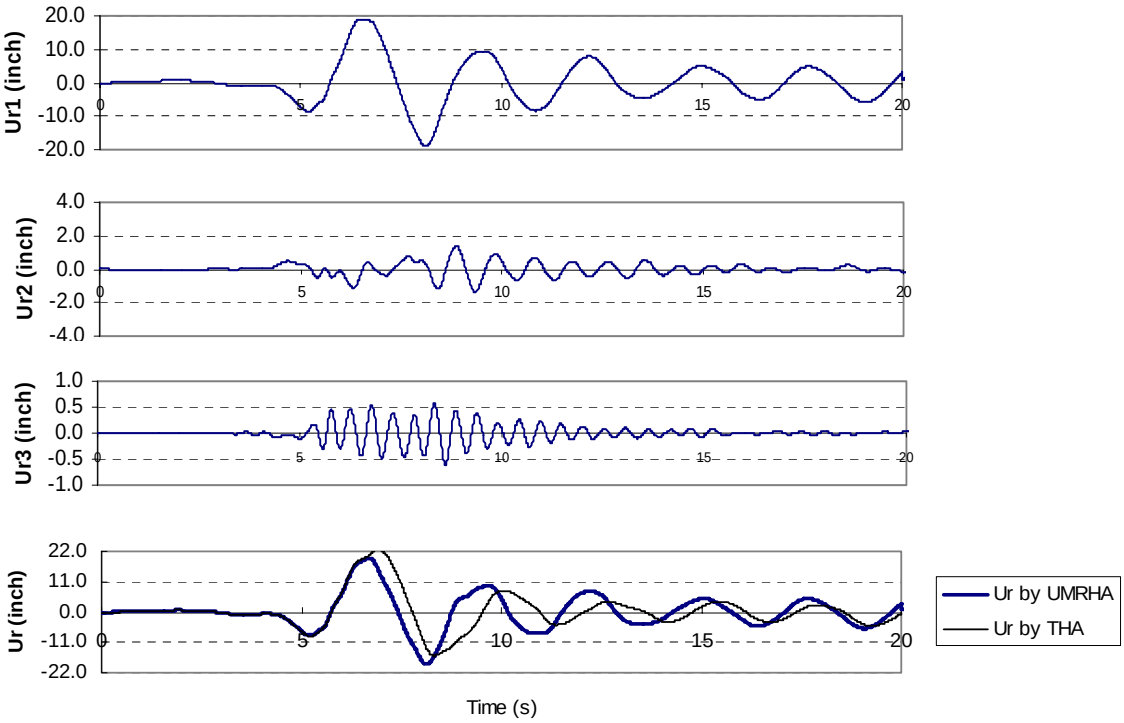

Figure 4.10. Comparison of response histories of roof displacement due to LA04

simplified model (differences are on the order of 20% or less over the height) and the errors tend to decrease as response contributions of more 'modes' are included, although the decrease is less apparent in the lower stories.

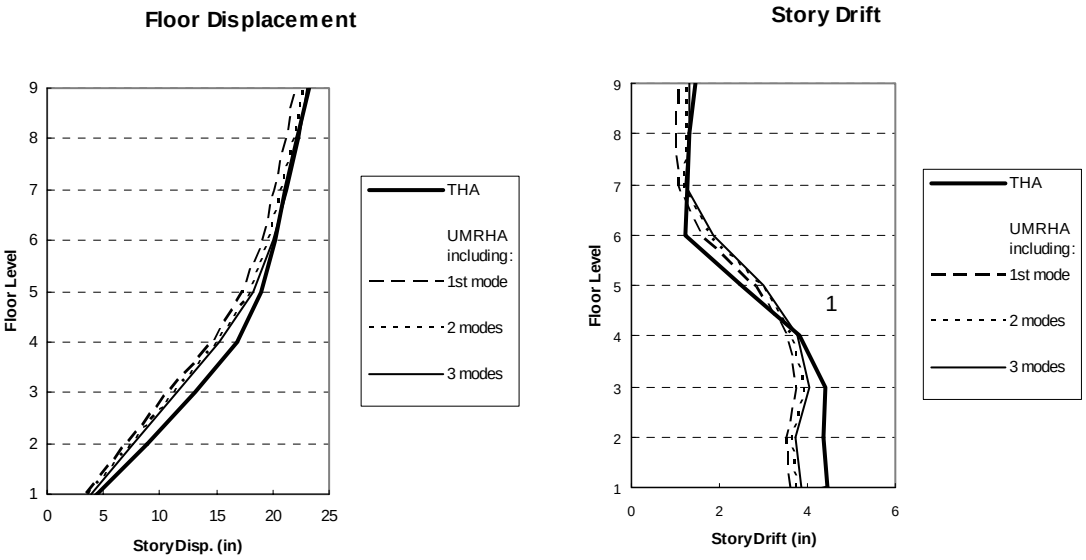

Figure 4.11. Height-wise variation of floor displacement and story drift due to LA04

To investigate how the error varies with the intensity of ground motion, the above analysis is repeated for the more intense record, LA22 (a 2%/50yr near-field record), for which $S_a = 0.404g$. The peak values of floor displacements and story drifts are compared with the 'exact' values in Figure 4.12. The errors are slightly larger than in the case of LA04, especially in the story drifts in the higher stories. This increase

occurs because damage tends to concentrate in specific stories at very large ground motions, and the modal analysis procedure becomes an increasingly poor approximation as the nonlinear action in the SMRF increases.

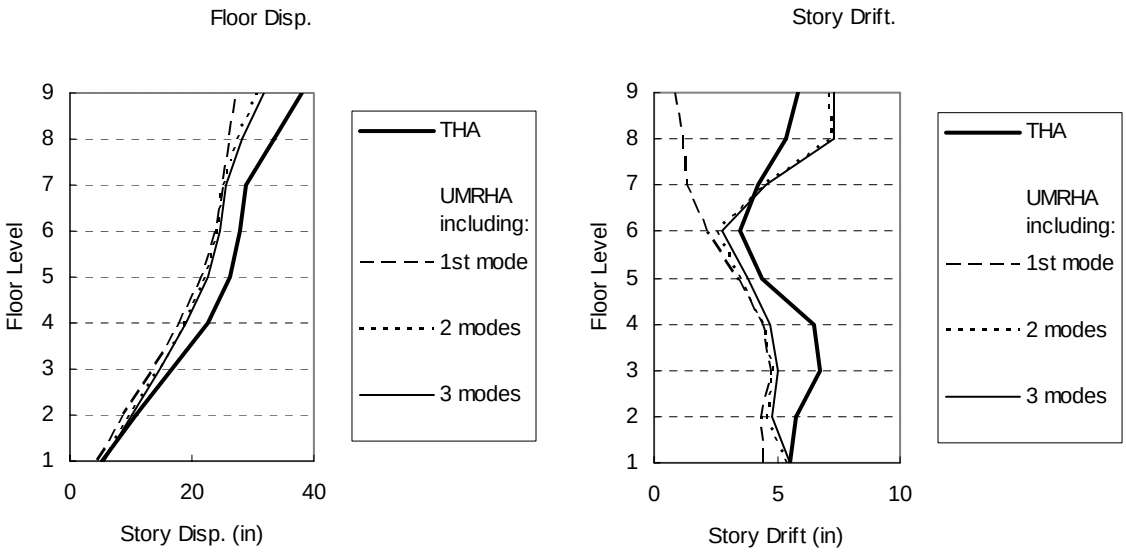

Figure 4.12. Height-wise variation of floor displacement and story drift due to LA22

The ratios of estimated maximum inter-story drift to 'exact' maximum inter-story drift were calculated using the ensembles of ground motions for 2%/50yr (LA21-LA30) and 10%/50yr (LA01-LA20). The mean and standard deviation of these ratios are presented in Figure 4.13 as a function of story height. The standard deviation is relatively constant with height, at about 19% for 10/50 ground motions

and about 27% for the 2/50 ground motions, indicating that the modeling uncertainty associated with the use of the approximate solution increases for the stronger ensemble. On the other hand, the error for the 10%/50yr ground motions tends to be larger in the middle stories, where damages are less likely to occur than in the upper and lower stories. This observation is consistent with that of Luco and Cornell (2000), who also noted that the seismic demands for the middle stories of this 9-story frame are smaller than either upper and lower stories.

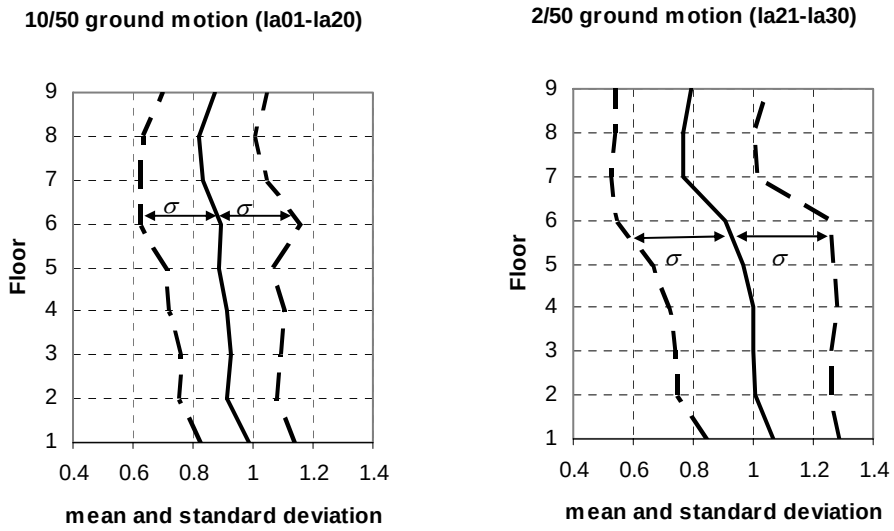

Figure 4.13. Height-wise variation of error in estimated story drifts for LA 9-story building

4.6.2 Structural response of LA 20-story building

The EUMRHA method introduced earlier in this Chapter is investigated further with an analysis of the LA 20-story frame. The first four vibration modes are shown in Figure 4.14, which also shows the changing of vibration modes when bottom flange fractures occur. It should be noted that the 3rd and 4th mode vibration remain elastic even during the 2%/50-yr ground motions la21-la30. The first and second 'mode' pushover curves are shown in Figure 4.15. These curves are idealized by multi-linear curves and are simulated by equivalent SDOF systems, as described previously.

To examine the accuracy of the EUMRHA method when applied to this frame, the maximum inter-story drift ratios calculated by EUMRHA are compared with those by NLTHA in Figure 4.16 using the ensembles of ground motions for hazard levels of 2%/50yr (LA21-LA30) and 10%/50yr (LA01-LA20). The height-wise variation of story drift ratios calculated by EUMRHA matches well with the NLTHA results for both ground motion ensembles.

The ratios of estimated maximum inter-story drift to 'exact' maximum inter-story drift were also calculated. The mean and standard deviation of these ratios are presented in Figure 4.17 as a function of story height. The standard deviation (which effectively measures uncertainty in the use of the EUMRHA, assuming that the results of the NLTHA are exact) is about 23% for 10/50 ground motions and about 31% for 2/50 ground motions. Similar with the LA 9-story frame, the accuracy decreases when the earthquake ground motions become stronger, because the strong ground motions force the structure to respond far beyond its yielding limit.

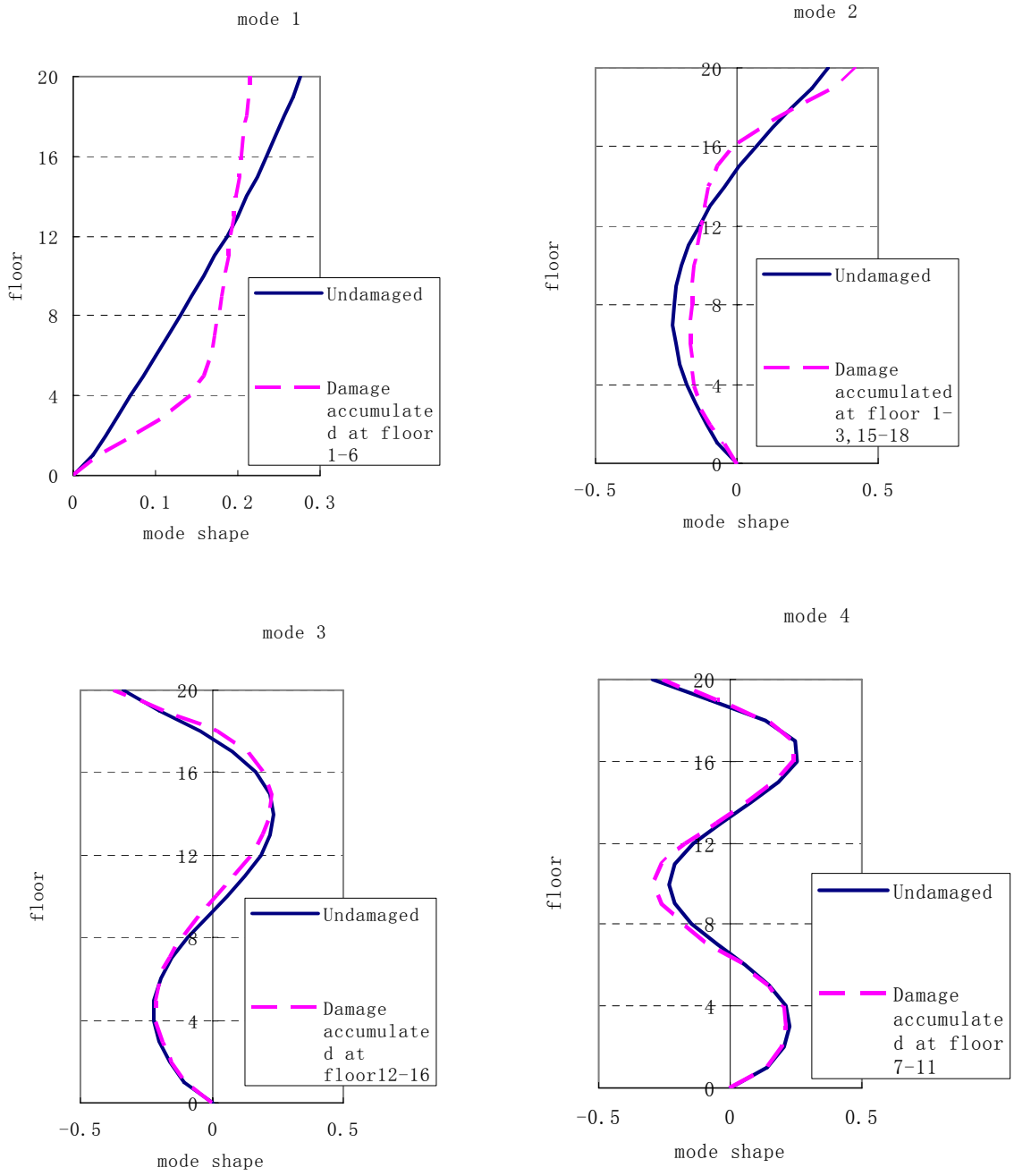

Figure 4.14 The first four vibration modes of LA 20-story frame

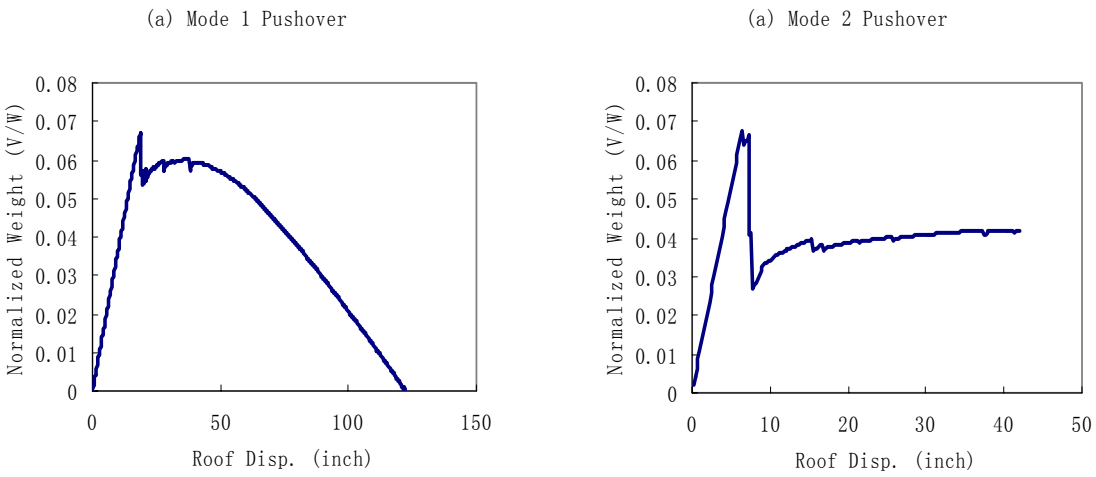

Figure 4.15 The first and second 'mode' pushover curve of LA 20-story frame

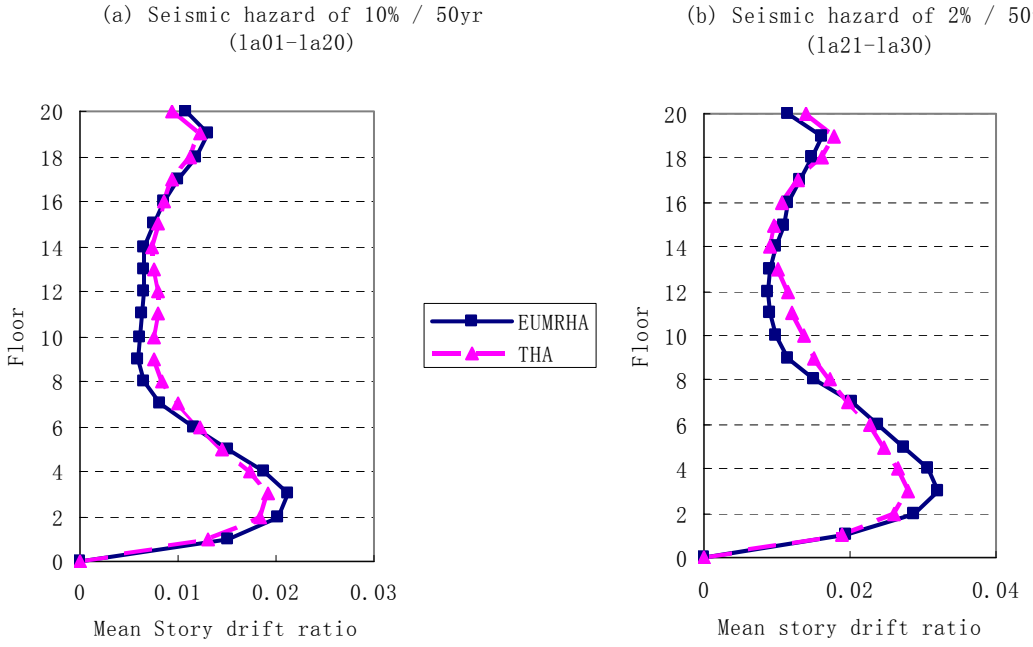

Figure 4.16 Comparison of height-wise variation of mean story drift of LA 20-story frame

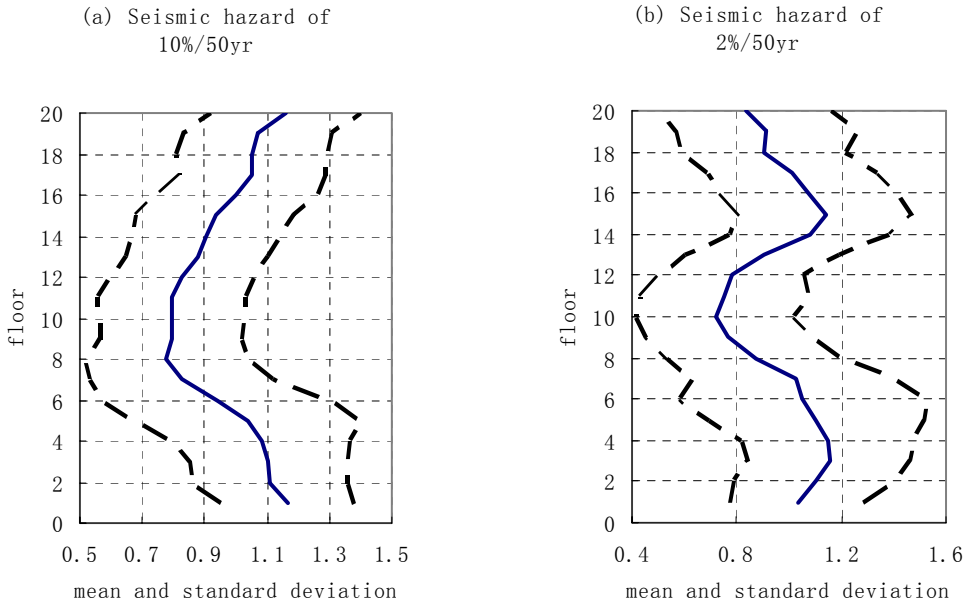

Figure 4.17. Height-wise variation of error in estimated story drifts for LA 20-story frame

4.7 Summary

This Chapter extended the UMRHA procedure to evaluate the potential for damage to connections in steel frames by considering how such damage might change "mode" shapes and vibration characteristics of the sequence of equivalent nonlinear SDOF systems required in the UMRHA assessment. Comparing the structural response of LA 9-story and LA 20-story SAC steel frame calculated by the enhanced method with that by NLTHA, it was shown that:

1. The EUMRHA method yields reasonably accurate estimates of structural response to the ensemble of 10%/50yr ground motions. As the ground motion intensity increases, the accuracy of this method decreases.
2. The estimated height-wise variation of inter-story drift response agrees reasonably well with estimates obtained from NLTHA, suggesting that this method can predict the stories most likely to be damaged. This would be helpful for damage inspection and assessment. Damage inspection will be discussed in greater detail in Chapter 6.
3. The advantages of the EUMRHA with regard to computational efficiency are substantial. For example, in the seismic response analysis of the 9-story frame subjected to one earthquake ground motion, the NLTHA took approximately 100 minutes to complete, while enhanced method required only less than 10 minutes to complete the same analysis (the finite element program is run by a desktop with Pentium 4 CPU 1.80GHz). This advantage is attractive for performing rapid assessments immediately following an earthquake, where a decision must be made quickly whether or not to evacuate the damaged building. It also is useful in simulation-based reliability assessment and in performing parametric studies required to support the development of performance-based seismic engineering.

In summary, the enhanced method is highly efficient and sufficiently accurate in calculating seismic structural responses for the purposes at hand. In the following chapter, the EUMRHA will be used to analyze the structural response of frames

subjected main shock-aftershock sequences, an analysis which is difficult to perform by NLTHA because of the calculation demands.

CHAPTER 5: PERFORMANCE EVALUATION OF STEEL FRAMES UNDER SEQUENCES OF GROUND MOTIONS

Earthquake events often consist of a sequence of foreshocks, a main shock and several aftershocks. The main shock in most cases imparts the largest amount of energy and causes the most damage. Aftershocks, however, have also been known to cause considerable damage and may be detrimental to structures that have been weakened by the main shock and have not been repaired or rehabilitated. Current damage estimation methods consider the effect of only the main shock on frame performance. In structural safety evaluation, it is important to consider the possibility that a series of aftershocks may occur and to assess this damage potential. In this Chapter, the contribution of aftershocks to structural damage is considered in the damage estimation method.

5.1 Introduction

Sequences of seismic events characterized by a principal earthquake with medium-to-high intensity, followed by aftershocks with comparable intensity, have been observed in many instances, including in Italy (Friuli 1976, Umbria-Marche 1997), Greece (1986, 1988), Turkey (1992), and Mexico (1993, 1994, 1995). In such

cases, a structure that is damaged by the main shock may be incapable of resisting the excitation of a strong aftershock, increasing the risk of major damage or building collapse. If the earthquake is moderate and severe damage is not apparent, there may be a question as to whether or not a damaged building may remain occupied prior to repair.

Only limited research has been done on this topic (Lee and Foutch, 2004; Fragiacomo, et al, 2004; Luco, et al, 2004). The burden of performing the necessary nonlinear time history analysis to assess damage under a sequence of earthquakes is substantial, especially when residual deformations in the frame following the occurrence of the first (main) shock must be taken into account. Researchers have yet to agree on the differences in characteristics (e.g., intensity or magnitude, frequency content, duration) between a main shock and major aftershocks (Helmstetter and Sornette 2003). Moreover, the damage accumulation during successive earthquakes is related to many factors, including structural period (or period shift), frequency characteristics of the earthquake ground motions, structural ductility, and permanent deformations of the frame following a main shock (Amadio et al, 2003; Fragiacomo, et al, 2004). Finally, the stochastic nature of the main shock and aftershock ground motions must be taken into account for the analysis of damage accumulation to be useful as a risk assessment tool.

The Enhanced Uncoupled Modal Response History Analysis (EUMRHA) proposed in Chapter 4 was shown to be efficient and accurate for the analysis of structural response of steel moment frames to earthquake ground motion. In this

Chapter, the EUMRHA tool is used to analyze the seismic behavior of the 9-story and 20-story steel moment frames designed by the pre-Northridge code for Los Angeles, CA, considered in previous sections. These frames were subjected to sequences of earthquake main shocks and aftershocks. We begin by characterizing the relationship between the main shock and aftershock in terms of their respective intensities. Next, the EUMRHA method is used to calculate the stochastic structural responses and damage patterns of the 9-story and 20-story steel moment frames subjected to ensembles of main shock-aftershock sequences. Finally, simple probabilistic tools are presented for post-earthquake structural evaluation and condition assessment.

5.2 Properties of aftershocks

In order to evaluate structural behavior under main shock-aftershock sequences, the distribution of aftershock intensities must be modeled. Moreover, a procedure must be developed to obtain the aftershock ground motion ensembles for use in stochastic analysis of seismic demands on the frames. In the previously cited paper by Lee and Foutch (2004), main shock-aftershock sequences were modeled by considering a set of back-to-back identical accelerograms, a conservative (albeit unlikely) occurrence. A more realistic procedure to model the main shock-aftershock sequences will be taken herein.

Previous studies have shown that the characteristics of aftershocks depend on the main shock, but that these characteristics differ from region to region (Bath 1965, Utsu 1961, Drakopoulos 1971). The distribution of magnitudes of aftershocks was

assumed by these authors to take the form of the Gutenberg/Richter formula:

$$N_a(M_a) = \alpha \exp(-\beta M_a) \tag{5.1}$$

where $N_a(M_a)$ is the number of aftershocks with magnitudes greater than or equal to M_a, and α and β are constants greater than zero that are related to the main shock magnitude. These constants can be determined from a regression analysis of data on historical seismicity. Since the steel buildings in this study are located at Los Angeles, CA, characteristics of main shock-aftershock sequences in southern California are of particular interest.

Sunasaka and Kiremidjian (1993) studied 11 main shock-aftershock sequences with aftershock magnitudes greater than or equal to 3.0 for earthquakes that occurred from 1940 to 1992 near Eureka, CA. Their conclusions on the magnitudes of aftershocks will be used in this study. Consistent with Eq. 5.1, the probability density function (PDF) of aftershock magnitudes is:

$$f_{M_a}(m_a) = \frac{\beta e^{-\beta m_a}}{e^{-\beta M_{\min}} - e^{-\beta M_{\max}}} \tag{5.2}$$

where M_a is the (random) magnitude of the aftershock and m_a is its state variable, $M_{\min}$ is the minimum aftershock magnitude considered ($M_{\min}$ = 3.0 in Sunasaka and Kiremidjian's study), and $M_{\max}$ is the maximum magnitude of aftershock considered. If it is assumed that the magnitude of aftershocks cannot exceed the magnitude of the main shock (Sunasaka and Kiremidjian, 1993), then $M_{max} = M_m$, where M_m is the magnitude of the main shock. Therefore, the probability density function describing the magnitudes of aftershocks is:

$$f_M(m_a) = \frac{\beta e^{-\beta m_a}}{e^{-3\beta} - e^{-\beta m_m}} \tag{5.3}$$

Sunasaka and Kiremidjian (1993) studied the relationship between β and M_m, and the relationship between the number of aftershocks with magnitude greater than 3, $N_a(3.0)$, and M_m. Both relationships were obtained by regression analysis. In the first instance, the mean of β is,

$$E(\beta) = \exp(1.113 - 0.135M_m) \tag{5.4}$$

in which the conditional standard deviation of the logarithm of β on M_m is 0.41. In the second instance, the mean of $N_a(3.0)$ in Eq. 5.1 becomes,

$$E(N_a(3.0)) = \exp(-0.647 + 0.684M_m) \tag{5.5}$$

in which the conditional standard deviation of the logarithm of N_a regressed on M_m is 0.79.

It has been observed (Fragiacomo, et al, 2004) that the first aftershock causes greater damage to buildings than do later aftershocks of similar magnitude. This observation also is consistent with the analysis by Lee and Foutch (2004), who found that the repetition of "identical" earthquake ground motions causes only slightly more damage to a steel frame than one occurrence of the same earthquake ground motion. Therefore, it will be assumed that for damage assessment purposes, the aftershock sequence can be modeled with a single aftershock; however, in this dissertation, the magnitude of that aftershock is described probabilistically as the *maximum* of a series of $N_a(M_m)$ aftershocks.

Given that the main shock magnitude is M_m, the probability distribution of the maximum magnitude of a sequence of aftershocks can be obtained by Monte Carlo

simulation from Eqs (5.3), (5.4) and (5.5). First, the values of N_a and β are sampled from lognormal distributions (with mean values given in Eqs (5.4) and (5.5) and the conditional logarithmic standard deviations 0.41 and 0.79 respectively). Second, N_a samples of M_a are generated according to the PDF in Eq (5.3). Finally, the maximum value of M_a is selected from these N_a samples; this maximum value is denoted $M_{a,max}$. Repeating this process a sufficient number of times leads to the cumulative distribution function (CDF) of (M_m - $M_{a,max}$) (conditioned on M_m); this conditional distribution is illustrated in Figure 5.1 for main shock magnitudes of 7.0 and 6.8. (The reason for selecting these particular magnitudes will be explained in the next section, where the ground motion ensembles are discussed).

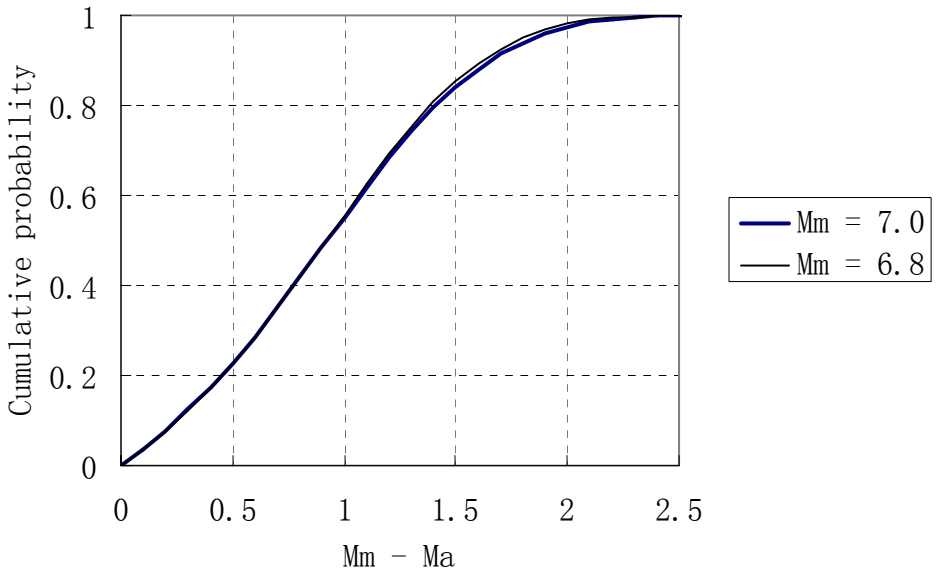

Figure 5.1. Probability distribution of magnitude difference between the main shock magnitude (M_m) and the maximum magnitude of aftershocks (M_a)

With the magnitudes of the aftershocks determined, it remains to model the main shock and aftershock ground motion ensembles for stochastic dynamic analysis. The main shock earthquake ensembles used in this study are modeled by ground motions developed in the SAC Project for Los Angeles, CA (FEMA-355, 2000), as noted with previous Chapter. A total of 30 records were selected. Records la01 to la20 (20 accelerograms identified in the SAC study as coming from earthquakes having an average magnitude of 6.8) and records la21 to la30 (10 accelerograms identified with earthquakes having an average magnitude of 7.0) correspond, respectively, to seismic hazards with 10% and 2% probability of being exceeded in 50 years (Somerville et al, 1997). Note that the accelerograms in both 2%/50yr and 10%/50yr ensembles actually represent a range of earthquake magnitudes and epicentral distances. It was found that smaller earthquakes, such as those from the 50%/50yr ensemble developed in the SAC Project, did not cause any damage to the frames analyzed in this paper, and for this reason, they were not included in this evaluation.

In the absence of ground motion records to describe main shock-aftershock sequences, it was assumed that the aftershocks also could be modeled by ensembles of the SAC-derived ground motions, appropriately scaled using the relations between M_a and M_m from the Sunakala / Kiremidjian study (1993) reflected in Figure 5.1. The mean rate of occurrence of earthquakes with magnitude equal to or greater than M is, approximately,

$$\log_{10}(\lambda_M) = a - bM \tag{5.6}$$

in which λ_M = mean annual occurrence rate and a and b are constants. Using

equation (5.6),

$$\frac{\lambda_{M_a}}{\lambda_{M_m}} = 10^{-b(M_m - M_a)} \tag{5.7}$$

A typical value for parameter *b* in the Western United States is 1.14 (Esteva, 1970). The corresponding annual mean occurrence rates of earthquakes with hazard levels of 10% /50 yr and 2% /50 yr in Los Angeles are presented in the "λ_{M_m}" column in Table 5.1.

Table 5.1 Comparison of main shocks and aftershocks (M_m - M_a = 0.2)

Main shock			Aftershock		
EQ records	Seismic hazard	λ_{M_m}	λ_{M_a}	Seismic hazard	Scale factor
la01 - la20	10% / 50yr	0.00211	0.00356	15% / 50yr	0.90
la21 – la30	2% / 50yr	0.000404	0.000683	3% / 50yr	0.91

The aftershock ensembles are based on the probability distribution of the magnitude difference between the main shock and the aftershock (Figure 5.1). For example, for main shocks associated with the 2%/50yr and 10%/50yr hazard levels, suppose that the difference between the main shock and aftershock magnitudes is 0.2. The associated occurrence rate (λ_{M_a}) and seismic hazard probability needed to scale the ground motion ensemble to account for the difference in magnitude are calculated from Eq. 5.7, as shown in the "aftershock" column in Table 5.1. The spectral ordinates at these return periods, obtained from the hazard curves at the U.S. Geological Survey

website, define the mean target spectra of the aftershocks as a function of period, as illustrated in Figure 5.2 (the smooth curves are fit by least-squares analysis). Finally, the aftershock earthquake ensembles are obtained by scaling the main shock earthquake ensembles to match the mean aftershock response spectra shown in Figure 5.2. The process is repeated to cover the range of aftershock magnitudes of interest from Figure 5.1. These scaling factors (determined at the fundamental period of the building) are presented in the last column of Table 5.1. Note that the occurrence rate and hazard probabilities in the aftershock column are used solely to scale the ensembles in order to model the aftershocks.

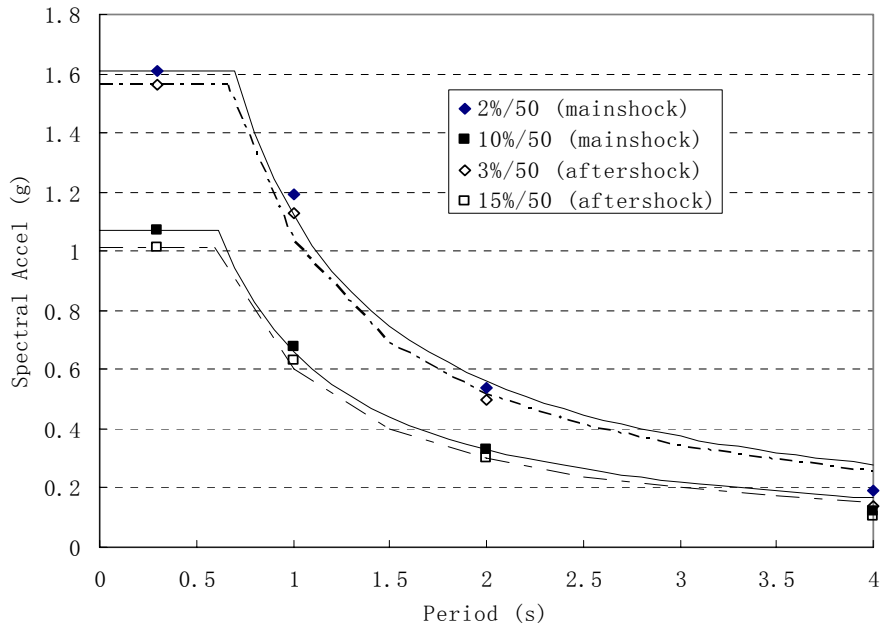

Figure 5.2. Spectral acceleration at different seismic hazards

It has been observed (Lee and Foutch 2004) that aftershocks associated with smaller earthquake intensities produced little or no additional damage. In this study, it was found that if the main shock was modeled with accelerograms corresponding to a seismic hazard of 10%/50 years (la01 - la20), aftershocks derived by scaling the main shock by a factor less than 0.68 caused no additional damage to either frame. Similarly, when the main shock corresponded to a seismic hazard of 2%/50 years (la21 - la30), aftershocks derived by scaling the main shock with a factor less than 0.60 caused no additional damage. Therefore, only aftershock ensembles that might cause additional damage are considered in the subsequent analysis. Table 5.2 summarizes the magnitude, aftershock hazard, and scaling factor for each aftershock ensemble considered in this study. Note that the designators M_m and M_a in Table 5.2 and in the sequel are used to identify the ensembles; they do not imply that the main shock or aftershock are associated specifically with earthquakes of these magnitudes.

Table 5.2 Characteristics of aftershock following main shock with hazard levels of 10%/50yr and 2%/50yr

M_m	M_a	Seismic Hazard	Scale factor
6.8 (la01-la20)	6.2	37 / 50	0.68
	6.4	23 / 50	0.80
	6.6	15 / 50	0.90
	6.8	10 /50	1.0
7.0 (la21-la30)	6.3	12/50	0.67
	6.5	7/50	0.78
	6.8	3/50	0.91
	7.0	2/50	1.0

Intuitively, the characteristics (amplitude and frequency content) of the main shock and aftershock signatures should exhibit some stochastic dependence. However, this research was unable to identify information that would relate these signatures definitively. Therefore, two extreme conditions were considered. In the first case (denoted the "replicate" case, for simplicity), the earthquake accelerograms in the main shock ensemble are simply repeated (but appropriately scaled, as in the last column of Table 5.1) to form the earthquake accelerograms for the aftershock ensemble. (This procedure also was adopted by Lee and Foutch (2004), but without scaling the main shock to obtain the aftershock.) In the second case (denoted the "randomized" case, for simplicity), the ground motions modeling the aftershock ensemble were randomized with respect to the main shock ensemble, but were appropriately scaled, as indicated in Table 5.1.

5.3 Performance of buildings subjected to main shock-aftershock sequences.

An inspection of a steel frame building following an earthquake might reveal that some of the beam-to-column connections have been damaged. One question that might be asked is: "Can the damaged building remain accessible on a temporary basis or continue to be occupied, considering the possibility of aftershocks?" To provide insight regarding this question, a series of analyses were conducted of the 9- and 20-story steel moment frames that were mentioned in Chapter 4.

The ensembles for earthquake main shock-aftershock sequences were derived as

described in Section 5.2. The time history analyses and the EUMRHA method described previously both were conducted using OpenSees. The damping ratio was assumed to be 5% in all modes considered.

5.3.1 Structural response of 9-story building subjected to "replicate" aftershocks

In this section, the main shock and aftershock were assumed to have the same frequency content. The structural responses of the 9-story frame at Los Angles were analyzed using NLTHA method and the EUMRHA method. These results were compared to verify the validity of the proposed method further.

5.3.1.1 Time history analyses of 9-story building

The difference in damage patterns produced by the main shock and the main shock-aftershock sequence, with the aftershock scaled from the main shock, is analyzed. For each analysis, the time between main shock and aftershock is 20 seconds, to allow the vibrations from the main shock to damp out prior to the beginning of the aftershock excitation. Two intensities of aftershocks are considered: one is the repetition of the main shock, and the other is derived by scaling the main shock by a factor 0.91 (see Table 5.2). For accelerogram la14 (peak acceleration = 0.59g), the aftershocks derived by multiplying 0.8 and 0.68 are also applied to the 9-story building. Figure 5.3 shows the damage pattern that the 9 story building experiences after main shock and main shock-aftershock sequences. At each beam-column joint, a half-circle having two sections is provided to indicate the

(1) After the mainshock
(fractured connections = 35/90, 39%)

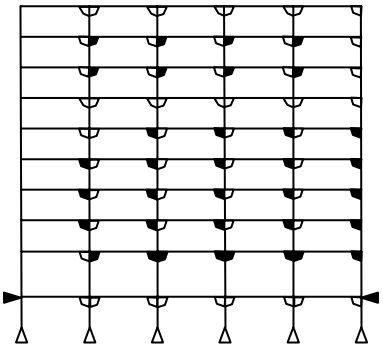

(2) After the aftershock, which has the same magnitude as mainshock
(fractured connections = 48/90, 53%)

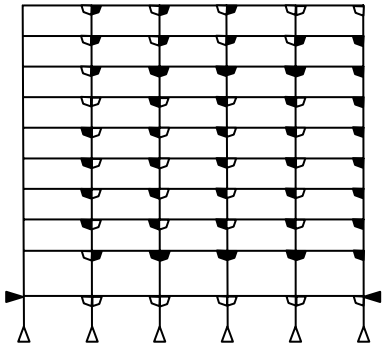

(6) After the aftershock, which is generated by 0.9 scaling of mainshock
(fractured connections = 43/90, 48%)

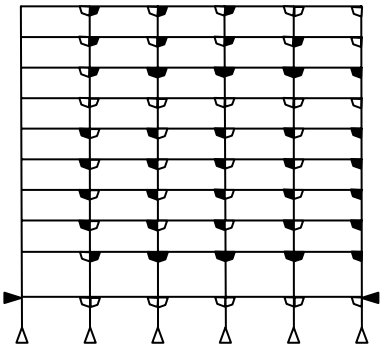

(5) After the aftershock, which is generated by 0.8 scaling of mainshock
(fractured connections = 41/90, 46%)

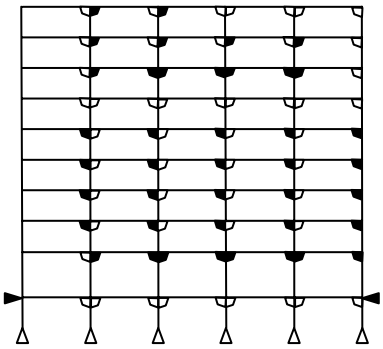

(4) After the aftershock, which is generated by 0.7 scaling of mainshock
(fractured connections = 37/90, 41%)

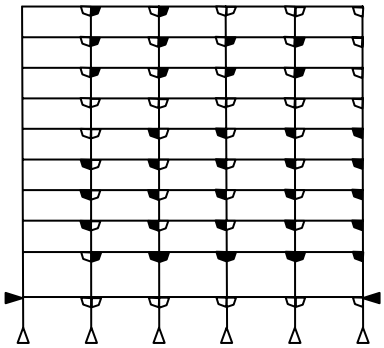

(3) After the aftershock, which is generated by 0.6 scaling of mainshock
(fractured connections = 35/90, 39%)

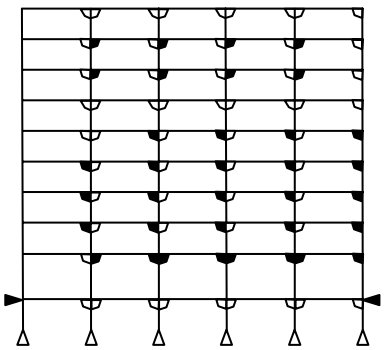

Figure 5.3 Observed damage from the main shock and main shock-aftershock sequence excitation for SAC 9-story frame at Los Angeles ("Replicate aftershock")

location of the fractured welds in the connections. (Recall that the connection moment-rotation model in Figure 2.1(b)) models damage in the bottom flange of the beam-to-column weld (Gross, 1998), which was the damage most frequently noted in the post-Northridge survey of damaged steel frames). The darkened segment indicates fracture of a bottom flange on the left- or right-hand of the joint. The main shock produces fracture in 35 out of 90 welded bottom flanges in these connections (or 39%), while the aftershock (a scaled repetition of the main shock) causes 13 more bottom flange fractures. As the aftershock's intensity becomes smaller, the number of additional bottom flange fractures also becomes smaller, and no additional damage was observed when the aftershock was derived by scaling the main shock by 0.6.

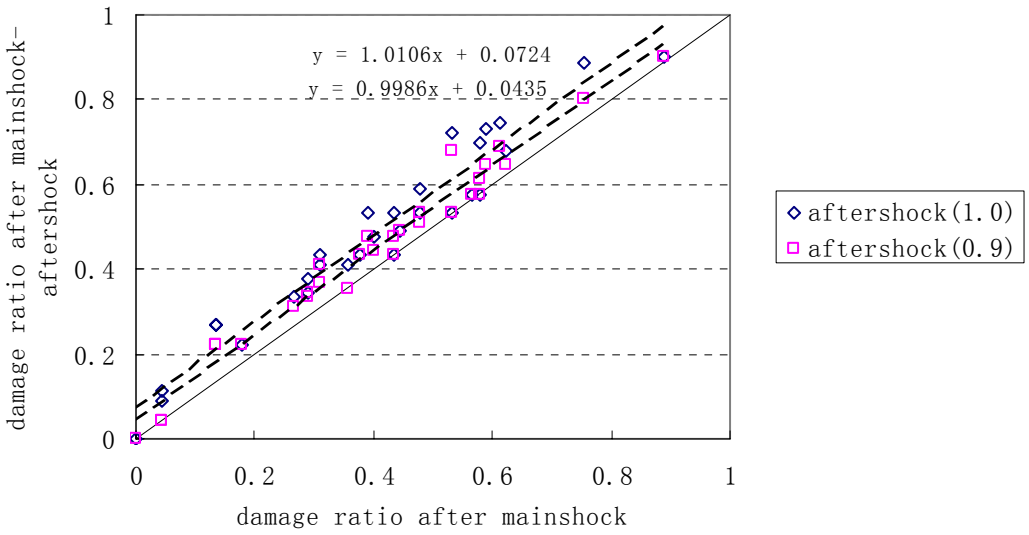

Figure 5.4 Relationship between damage ratio by main shock and by main shock-aftershock sequence (THA, "Replicate" aftershocks)

The above process was repeated for all accelerograms and scaling factors identified above. The damage ratios of beam-to-column connections (defined as the number of damaged connections divided by total number of connections) were calculated for each accelerogram and the aftershocks were derived by multiplying the main shock accelerograms by 1.0 and 0.9 respectively. The relationship between the damage ratio after the main shock and after the main shock-aftershock sequence is presented in Figure 5.4 (The scale factors used to derive the aftershock accelerograms are noted in the legend). The increase in damage ratio caused by an aftershock appears to be virtually independent of the damage ratio following the main shock; this observation was verified by regression analysis. Because the damage increment must be non-negative, the relationship between D_a and D_m (we assume that $D_m < 0.5$, since for $D_m > 0.5$, post-earthquake condition is obvious) is assumed for simplicity to be:

$$D_a = D_m + \varepsilon \tag{5.8}$$

in which ε is assumed to be a log-normal random variable. The mean and coefficient of variation (COV) of ε are presented in column "THA" of Table 5.3.

Table 5.3 Comparison of THA and EUMRHA in terms of mean and COV of the additional damage ratio ($D_a - D_m$) for the 9-story building

Scale factor to derive aftershock	THA		EUMRHA	
	Mean	COV	Mean	COV
1.0	0.075	0.693	0.090	0.689
0.9	0.044	0.727	0.046	0.707

The above relationships show that it is unlikely that the 9-story frame slightly damaged by a main shock will suffer severe additional damage or collapse if an aftershock were to occur.

The variations of inter-story drift ratio along the building height during the main shock and during the aftershock were calculated for each sequence. The mean values of these inter-story drift ratios are shown in Figure 5.5. The height-wise distribution of inter-story drift remains unchanged during the aftershock, meaning that if connections at a floor level suffer significant damage during the main shock, it is likely that those same connections will be damaged more seriously during the aftershocks. Conversely, if little or no connection damage occurs during the main shock, it is unlikely that those connections will be damaged during a subsequent aftershock.

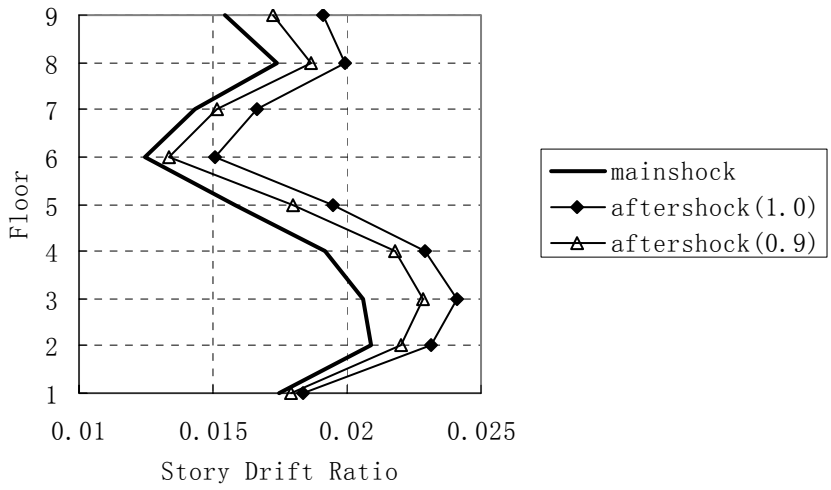

Figure 5.5 Height-wise distribution of inter-story drift ratio after main shock and main shock-aftershock sequences (THA, “Replicate” aftershocks)

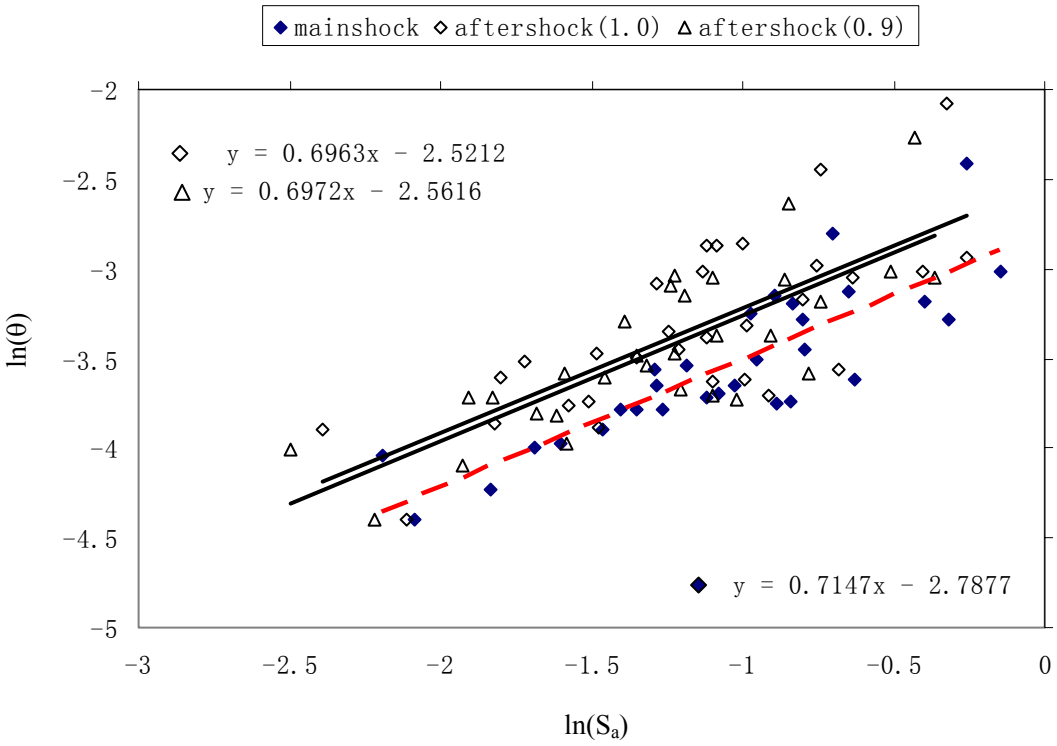

Figure 5.6 Maximum inter-story drift ratio vs spectral acceleration at the structure's fundamental period (THA, "Replicate" aftershocks)

The maximum inter-story drift ratio, θ, is commonly used as a measure of nonlinear structural system response (Gunturi and Shah, 1992; Shome and Cornell 1999) and can be related to specific damage states (e.g., FEMA 273). The θ during both the main shock and the aftershock were calculated for each sequence. Their relationship with the spectral acceleration S_a of the aftershock at the building's fundamental period in the undamaged or damaged state, as appropriate, is shown in Figure 5.6 and is presented in column "THA" of Table 5.4. It should be noted that the building was damaged in most cases following the main shock, so its fundamental

period lengthens, as presented in Table 5.5. The fundamental period of the 9-story building was lengthened by an average of 12% by the main shock with hazard level of 10%/50yr (la01-la20), and by an average of 27% by main shock with hazard level of 2%/50yr (la21-la30). This elongation of fundamental period reflects the loss of stiffness due to damage from the main shock, and leads to smaller seismic forces from the aftershock (see Figure 5.2). As a result, the maximum structural responses during aftershock were not significantly larger than those during the main shock, even when the intensities of the two ground motions were the same.

Table 5.4 Comparison of THA and EUMRHA in terms of relationship between θ and S_a during the aftershock

Scale factor to derive aftershock	THA		EUMRHA	
	Mean relationship	$\sigma_{\ln(\theta)\|S_a}$	Mean relationship	$\sigma_{\ln(\theta)\|S_a}$
1.0	$\theta = 0.0804(S_a)^{0.696}$	0.326	$\theta = 0.0710(S_a)^{0.688}$	0.314
0.9	$\theta = 0.0772(S_a)^{0.697}$	0.321	$\theta = 0.0669(S_a)^{0.660}$	0.307

Table 5.5 Fundamental period of vibration of 9-story building prior to and following ground excitations at 10%/50yr and 2%/50yr hazard levels.

T (undamaged)	T (damaged)			
	Main shock	T	Main shock	T
2.31	la01	2.79	la11	2.53
	la02	2.40	la12	2.39
	la03	2.46	la13	2.40
	la04	2.54	la14	2.41
	la05	3.10	la15	2.78
	la06	2.62	la16	2.59
	la07	2.60	la17	2.56
	la08	2.42	la18	2.51
	la09	3.05	la19	2.40
	la10	2.40	la20	2.42
	la21	2.76	la26	2.92
	la22	3.17	la27	3.05
	la23	3.091	la28	3.14
	la24	3.37	la29	2.40
	la25	3.16	la30	2.40

5.3.1.2 EUMRHA of 9-story building and comparison with THA

To investigate the structural response under main shock-aftershock sequences using time history analysis, as done in the previous section, is costly. For example, performing time history analysis of the 9-story building under 30 main shock-aftershock sequences (la01 – la30) took nearly one week (The finite element program is run by a desktop with Pentium 4 CPU 1.80GHz). Such computational demands are impractical for rapid structural performance evaluation. The EUMRHA method is much more efficient than THA. For the same task as above, the EUMRHA

computations consumed less than one hour and achieved acceptable accuracy. In this section, then, the results using EUMRHA method will be presented and compared with those using NLTHA.

The relationship between the damage ratio after the main shock and after the main shock-aftershock sequence is presented in Figure 5.7. Analyzing the date according to Eq. 5.8, the mean and COV of ε are presented in column "EUMRHA" of Table 5.3 for comparison with the results of NLTHA. The aftershock produces slightly larger increases in damage ratio using EUMRHA than using THA, so EUMRHA tends to overestimate the structural damage caused by aftershock slightly. Consistent with Figure 5.5, the increase in damage ratio caused by the aftershock indicates no dependence on damage ratio following the main shock.

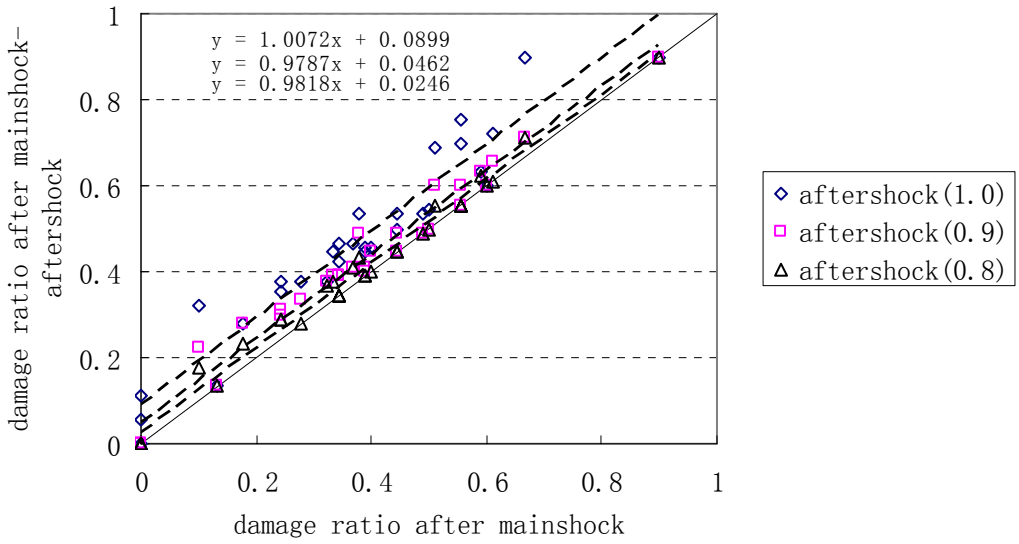

Figure 5.7 Relationship between damage ratio by main shock and by main shock-aftershock sequence (using UMRHA)

With the above relationships, if the damage ratio following the main shock D_m is assessed, the probability that the damage ratio caused by the aftershock D_a exceeds its limit can be evaluated, as will be described in a later section.

The distributions of mean inter-story drift ratio over the building height were calculated using EUMRHA and are shown in Figure 5.8. It can be seen that during the aftershock, the maximum inter-story drift usually exceeded that occurring during the main shock when the aftershocks were derived by scaling the main shock by 1.0 or 0.9. On the other hand, in many cases, the maximum inter-story drift during the aftershock was smaller than that during the main shock if the aftershocks were derived using scaling factor of 0.8 and seldom exceeded it the scaling factor was 0.7.

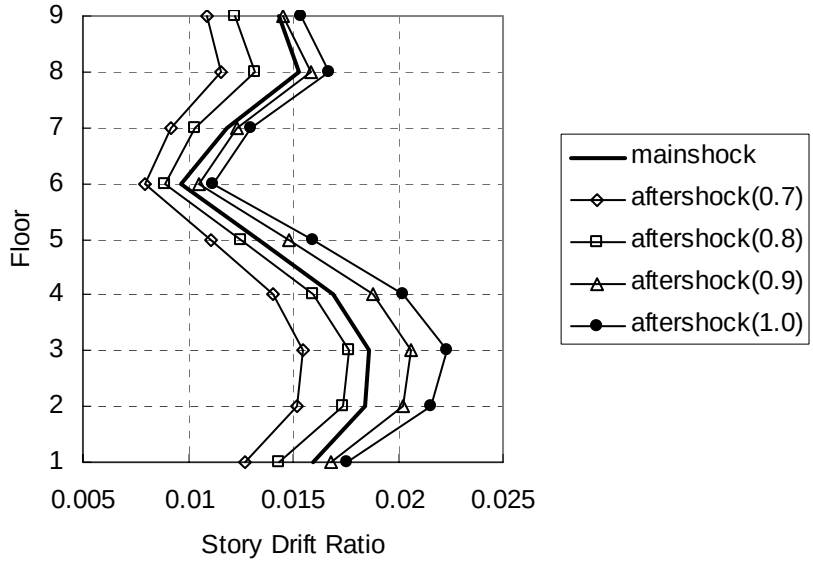

Figure 5.8 Height-wise distribution of inter-story drift ratio after main shock and main shock-aftershock sequences (using UMRHA)

Consistent with the results obtained using NLTHA, the height-wise variation of inter-story drift remained unchanged when the building was excited by an aftershock. Comparing Figure 5.8 with Figure 5.6, it is observed that the inter-story drift obtained using UMRHA is a little smaller than that obtained using THA but that the predicted increase in drift caused by aftershocks from the two analyses show good agreement.

The maximum inter-story drift ratio θ during main shock and during aftershock were also calculated using EUMRHA. Their relationship with the spectral acceleration, S_a, associated with the main shock or aftershock at the building's fundamental period is shown in Figure 5.9 and is presented in column "EUMRHA" of Table 5.4 for comparison.

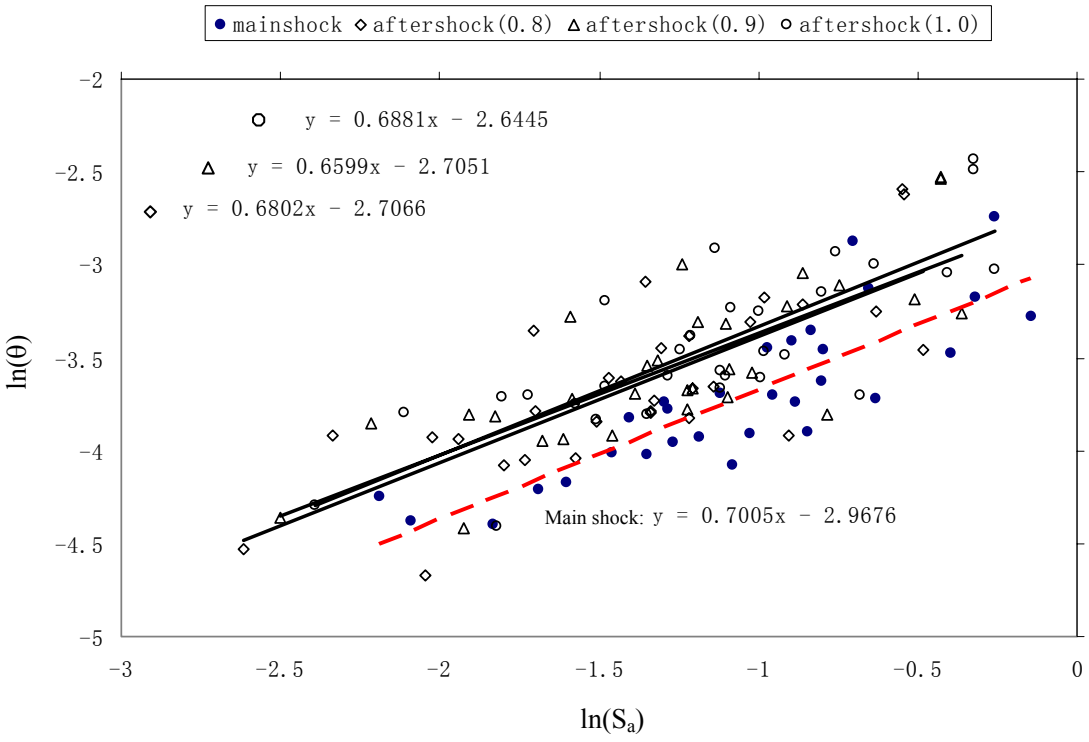

Figure 5.9 The relationship between the maximum inter-story drift ratio and spectral acceleration at the structure's fundamental period (UMRHA)

Results from the proposed EUMRHA method for structural damage and inter-story drift compare well with results from THA, supporting the use of EUMRHA in the analysis that follows in the next section. Furthermore, Figures 5.6 and 5.9 show that the relationships between θ and S_a calculated for different aftershock intensities are very close to one another. Thus, to achieve a conservative estimate of possible subsequent damage to a damaged building frame, the relationship for the aftershock having the same intensity as the main shock could be used for this purpose. Put anther way, the Lee/Foutch (2004) approach provides a conservative estimate of damage due to main shock – aftershock sequences.

5.3.2 Structural response of 9-story building subjected to "randomized" aftershocks

In the above analysis, it was assumed that the aftershock has exactly the same frequency content as the main shock. This assumption makes the energy at certain frequencies in the main shock that affects the structural response significantly work again during the aftershock. In this section, cases where the aftershock has totally different frequency content were analyzed by randomizing the aftershock records (following scaling) with respect to the main shock ensemble.

The inter-story drift ratios for the 9-story building during the main shock and aftershock were calculated using EUMRHA. The variation of the mean drifts over the building height is presented in Figure 5.10. Compared with Figure 5.8, the mean inter-story drift distributions are very close for both "replicate" and "randomized"

cases. In the "randomized" case, the variance associated with the inter-story drift is 0.339, which is slightly less than the 0.382 obtained in the "replicate" case. The same frequency content in main shock and aftershock causes the response pattern during main shock to be reinforced by the aftershock, resulting in larger scatter in inter-story drift.

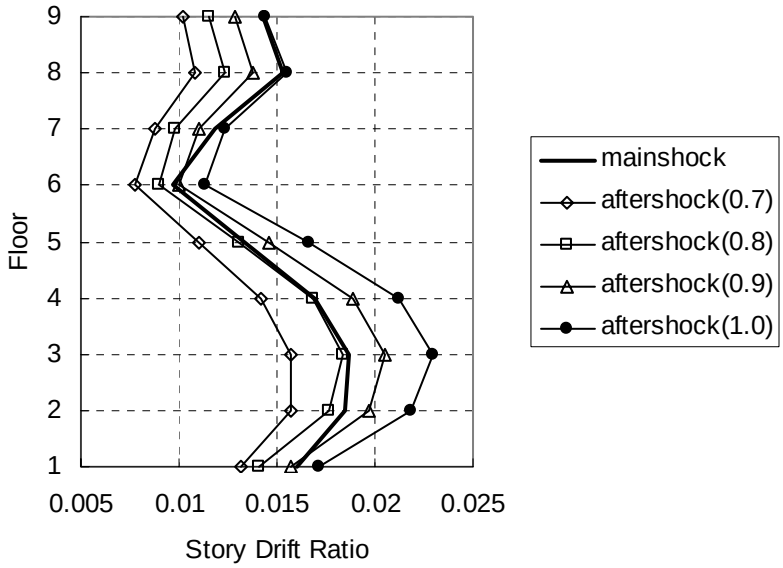

Figure 5.10 Height-wise distribution of inter-story drift ratio after main shock and main shock-aftershock sequences (randomized)

As noted in section 5.3.1, the height-wise distribution of *mean* inter-story drift remained unchanged during the aftershock in the "replicate" case. Figure 5.10 shows

that the mean remains unchanged in the "randomized" case as well. However, if we investigate the structural response under *one* specific main shock-aftershock sequence, we find that this is not the case. Figure 5.11 illustrates the distribution of inter-story drift in the 9-story frame following one particular main shock (la05) and a main shock-aftershock sequence in which the aftershock was represented by either la05 or la16, both scaled by the factor 0.9. The distribution of inter-story drift changed during the scaled la16 aftershock, as shown in Figure 5.11(a), but not under the scaled la05 aftershock, as shown in Figure 5.11(b) and 5.11(c). Comparing Figure 5.11(a) and 5.11(c), it is obvious that the pattern of inter-story drift is dominated by the characteristics of the aftershock.

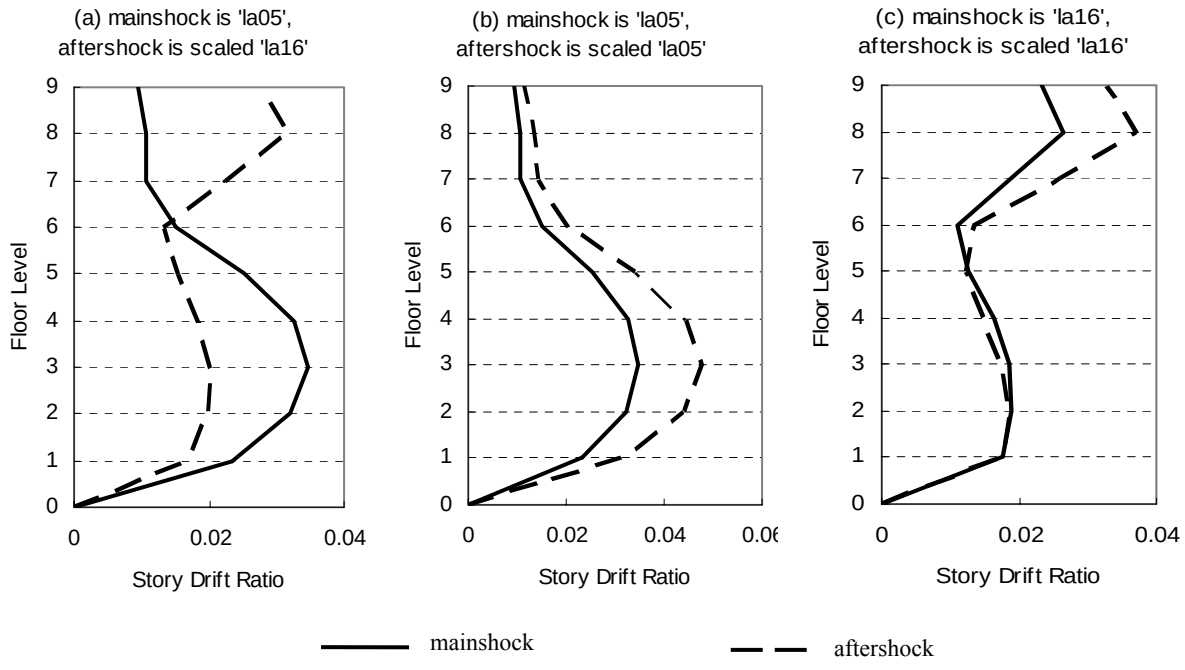

Figure 5.11 Comparison of inter-story drift distributions during main shock and during aftershock

The patterns of connection damage are presented in Figure 5.12. The main shock produces 36 fractures in 90 bottom-flange welds (abbreviated subsequently as 36/90, or 40%, as noted in Figure 12(a)). The aftershock with "replication" causes only 4 additional bottom-flange fractures (Figure 12(b)), while the aftershock with "randomization" causes 17 additional bottom-flange fractures (Figure 12(c)).

(a) damage pattern after main shock of la05 (Fractured ratio = 36 / 90)

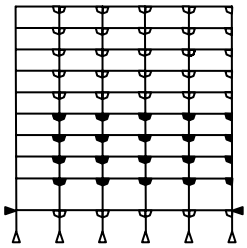

(b) damage pattern after aftershock of scaled la05 (Fractured ratio = 40 / 90)

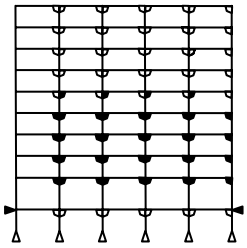

(c) damage pattern after aftershock of scaled la16 (Fractured ratio = 53 / 90)

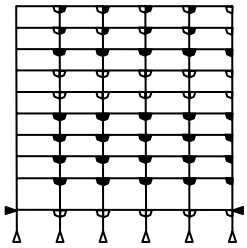

Figure 5.12 Damage pattern in 9-story frame following main shock and main shock-aftershock sequences

The frequency characteristics of record la05 lead to damage accumulation in the lower stories, while la16 leads to damage accumulation in the upper stories. The displacement spectra for these records in Figure 5.13 shows that the seismic demand from la05 strongly affects the first mode (for the 9-story building, T_1 = 2.31s and

participating mass is 84% of total mass, while for the second mode, T_2 = 0.89s with participating mass 10% of the total mass), while the demand from la16 is reflected in the higher modes and amplifies their impact on overall behavior. Conclusions from a study of responses to the remaining ground motion sequences in the two ensembles were similar. In general, it was observed that the "replication" assumption does not lead to changes in the damage pattern in the frame during the aftershocks (regardless of the residual deformations following the main shock). In other words, if connections at a floor level suffer significant damage during the main shock, it is likely that those same connections will suffer additional damage during the aftershocks. Similarly, if connections at a particular level are undamaged by the main shock, it is unlikely that those connections will be damaged during a subsequent aftershock. On the other hand, under the "randomization" assumption, the damage pattern might change during the

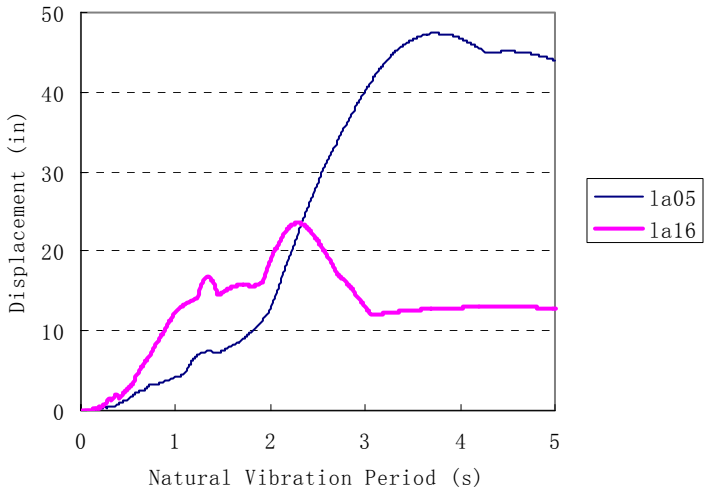

Figure 5.13 Displacement Spectra for la05 and la16

aftershocks, depending on the period shift caused by damage due to the main shock and the frequency characteristics of the aftershock ground motion.

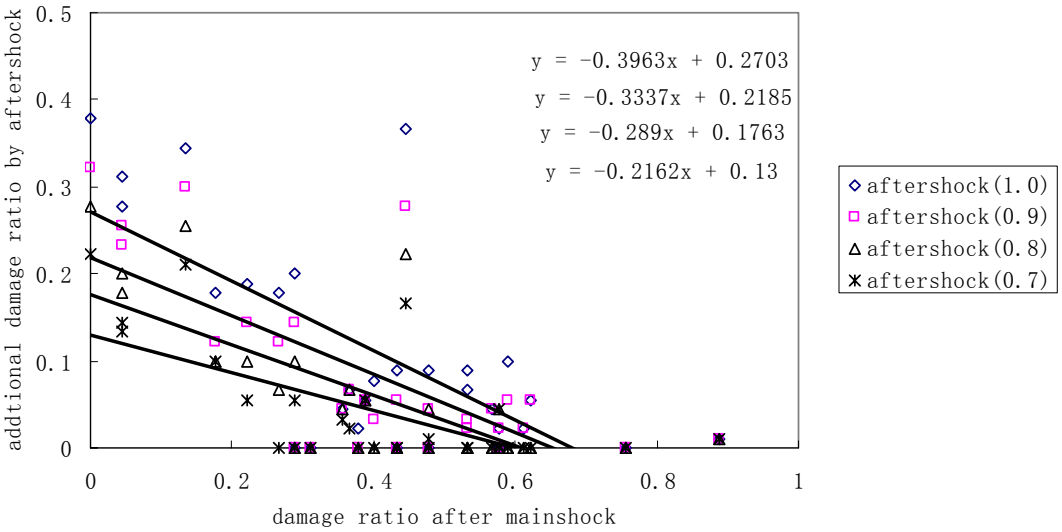

Figure 5.14 Relationship between additional damage ratio by aftershock and the additional damage ratio by main shock ("Randomized" case)

The additional structural damage ratios caused by aftershocks in the "randomized" case are presented in Figure 5.14 as a function of D_m. In contrast to Figure 5.7, the additional damage caused by the "randomized" aftershock decreases as D_m increases; moreover, when D_m exceeds approximately 0.6, the aftershock seldom causes additional damage. The relationship between D_a and D_m is presented in Table 5.6, along with the mean and COV in ε. (see Eq 5.8). The COV in the estimate of

damage increment due to the aftershock is quite large in both cases. The additional damage depends on not only D_m, but also the frequency characteristics of the aftershock. Comparing Figures 5.7 and 5.14, it can be seen that the additional damage caused by the aftershock is more pronounced when the aftershocks are randomized with respect to the main shock; in particular, the incremental damage from the aftershock is larger if the damage ratio following the main shock is smaller than approximately 0.4.

Table 5.6 Mean and COV of the additional damage ratio ($D_a - D_m$) for the 9-story building

Scale factor to derive aftershock	replication		randomization	
	Mean	COV	Mean	COV
1.0	0.090	0.689	$-0.396D_m + 0.270$	0.772
0.9	0.046	0.707	$-0.334D_m + 0.219$	0.831
0.8	0.025	0.989	$-0.289D_m + 0.176$	0.993
0.7	na	na	$-0.216D_m + 0.130$	1.155

The maximum inter-story drift ratios, θ_{max} of the 9-story building during "randomized" aftershock are presented in Figure 5.15. As was found with the "replicate" case, the relationships between θ and S_a calculated for different aftershock intensities are very close to one another, Thus, it is appropriate, although conservative,

Table 5.7 Relationship between θ and S_a during the aftershock

Building	replication		randomization	
	Mean relationship	$\sigma_{\ln(\theta)\|S_a}$	Mean relationship	$\sigma_{\ln(\theta)\|S_a}$
9-story	$\theta = 0.0710(S_a)^{0.688}$	0.314	$\theta = 0.0534(S_a)^{0.572}$	0.225
20-story	$\theta = 0.173(S_a)^{0.936}$	0.283	$\theta = 0.103(S_a)^{0.703}$	0.265

to estimate the damage from the aftershock from the relationship where the main shock and aftershock have the same intensity, which is presented in the "9-story" line in Table 5.7

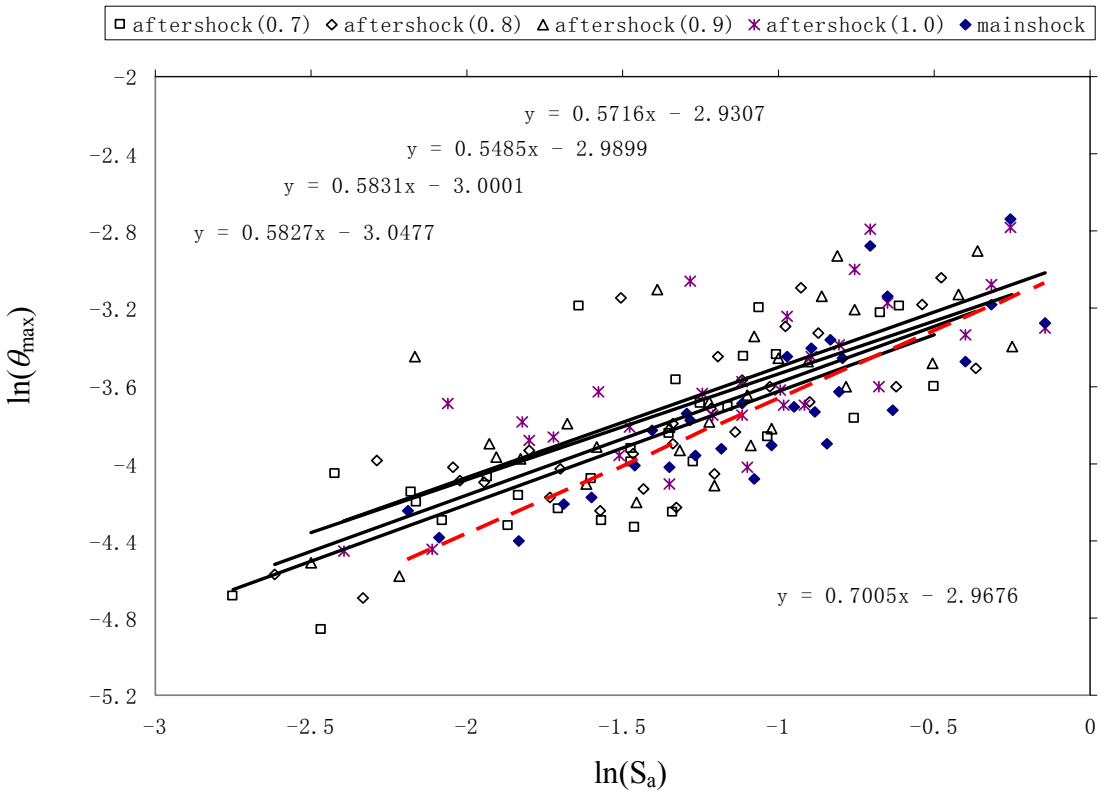

Figure 5.15. The relationship between the maximum inter-story drift ratio during aftershock and the aftershock's spectral acceleration at the damaged building's fundamental period

5.3.3 Structural response of 20-story building

The 20-story Los Angeles frame also was analyzed using EUMRHA under the main shock-aftershock sequence accelerograms. The mean inter-story drift distributions along the building height are shown in Figure 5.16. The shape of inter-story drift distribution indicates that structural damage tends to accumulate in the lower and upper stories, rather than the middle stories. Similar to the 9-story building, the shape of inter-story drift distribution remains unchanged for both "randomized" and "replicate" cases and different aftershock intensities.

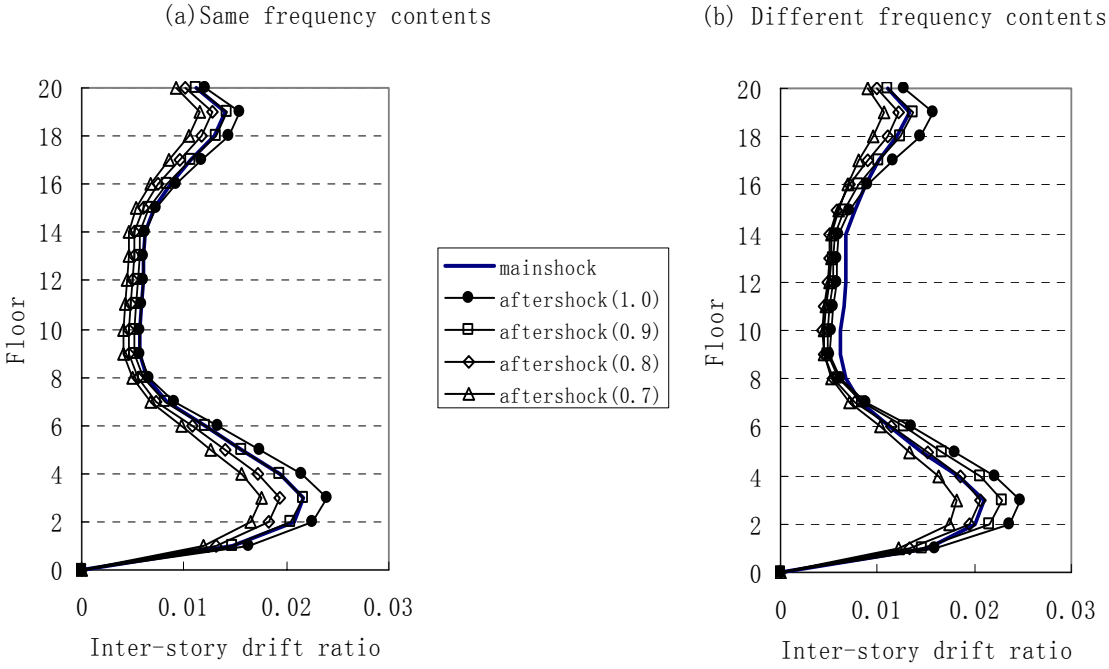

Figure 5.16 Story drift ratio of 20-story building

The damage ratios caused by main shocks and main shock-aftershock sequences were also investigated for the 20-story frame. A summary of results is presented for the replicate and randomization assumptions, respectively, in Figures 5.17(a) and 5.17(b). Note that the aftershock derived by multiplying the main shock by 0.8 causes no additional damage in any of the samples. The damage ratio caused by the main shock to the 20-story building was smaller than that in the 9-story building. Moreover, the additional damage to the 20-story building produced by the aftershock was also smaller than that in the 9-story building. Other investigators (e.g., Lee and Foutch, 2004) have observed that shorter buildings tend to perform less favorably than taller buildings when both were designed under the *1994 Uniform Building Code.* As before, the relationship between D_a and D_m can be defined by Eq 5.8; the mean and COV of ε obtained from the analysis of the 20-story frame are presented in Table 5.8.

The maximum inter-story drift ratios θ in the 20-story building from the aftershock were calculated and are presented in Figure 5.18 for "replicate" and

Table 5.8 Mean and COV of the additional damage ratio ($D_a - D_m$) for the 20-story building

Scale factor to derive aftershock	replication		Randomization	
	Mean	COV	Mean	COV
1.0	0.0302	1.06	$-0.539D_m + 0.202$	0.696
0.9	0.0228	0.91	$-0.454D_m + 0.165$	0.644

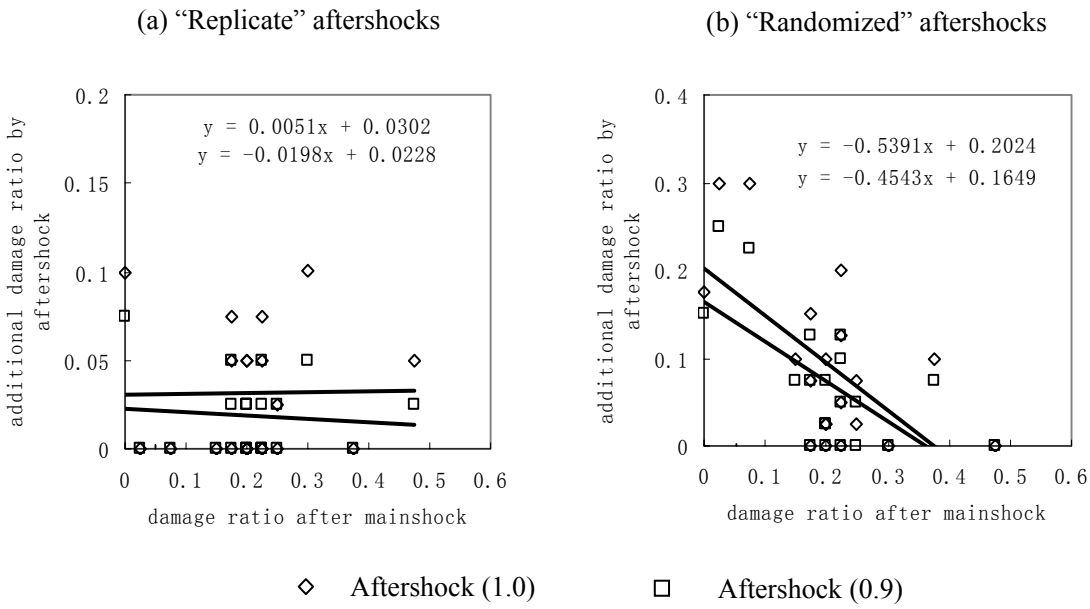

Figure 5.17 Additional damage ratio by aftershock vs damage ratio by main shock for 20-story buildings

"randomized" cases. The fundamental periods of vibration of the damaged 20-story building are listed in table 5.9. Period lengthening averaged 4% for the main shock corresponding to 10%/50yr (la01-la20), and averaged 15% for main shock with hazard level of 2%/50yr (la21-la30). Similar to what was found for the 9-story building, the relationships between θ and S_a calculated for different aftershock intensities are very close to one another for different magnitudes of aftershocks. Thus, the relationship for the aftershock having the same intensity as the main shock can be adopted for conservatism. This relationship is presented in the "20-story" line of Table 5.7.

(a) "Randomized" case

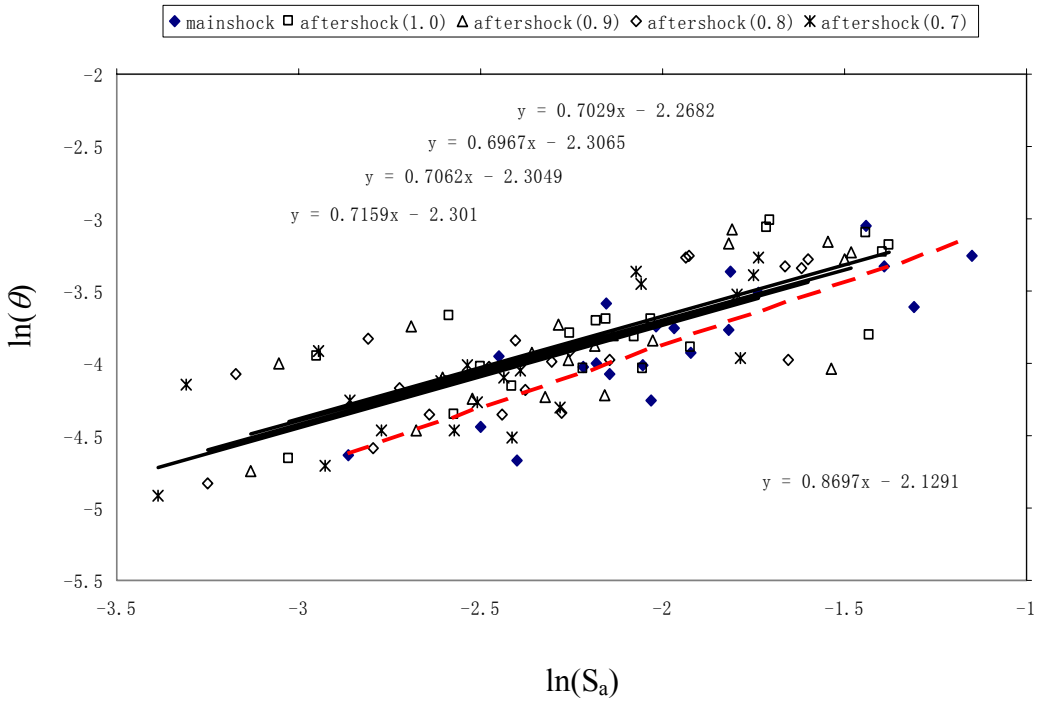

(b) "Replicate" case

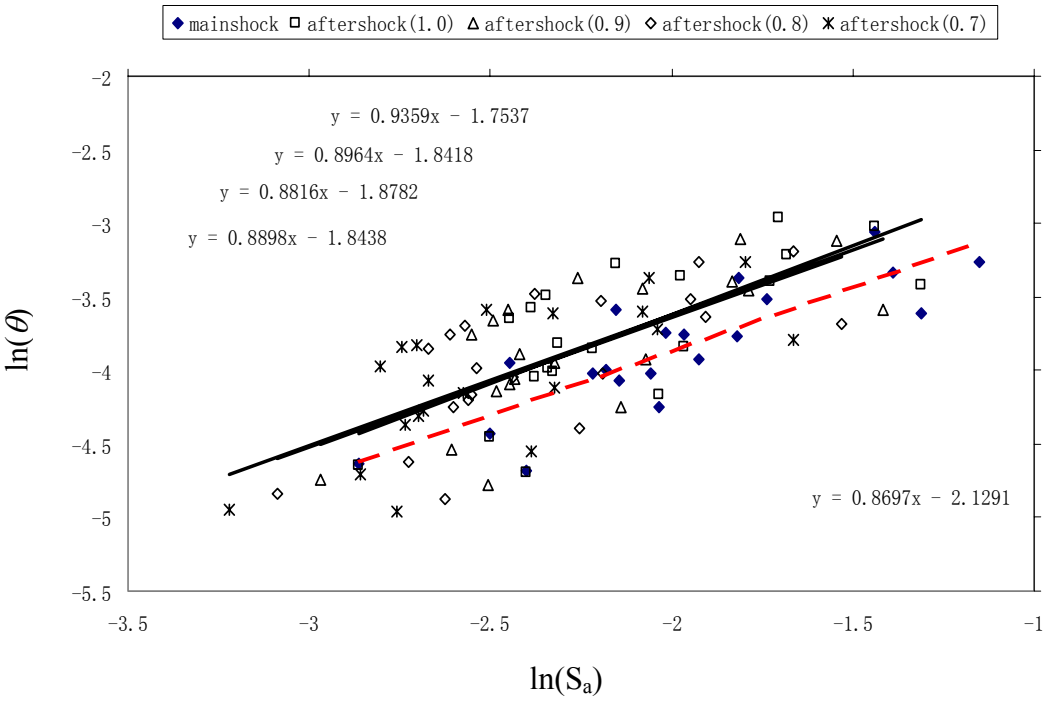

Figure 5.18. The relationship between the maximum inter-story drift ratio during aftershock and the aftershock's spectral acceleration at the damaged building's fundamental period

Table 5.9 Fundamental period of vibration of 20-story building prior to and following ground excitations for 10%/50yr and 2%/50yr seismic hazard levels.

T (undamaged)	T (damaged)			
	Main shock	T	Main shock	T
3.89	la01	3.89	la11	3.97
	la02	3.89	la12	3.89
	la03	3.99	la13	3.99
	la04	4.40	la14	3.89
	la05	4.12	la15	4.08
	la06	4.11	la16	4.03
	la07	3.93	la17	3.89
	la08	3.90	la18	4.04
	la09	3.99	la19	3.90
	la10	4.91	la20	3.91
	la21	4.03	la26	4.19
	la22	4.06	la27	5.27
	La23	4.61	la28	4.52
	La24	5.17	la29	4.38
	La25	4.01	la30	5.11

5.4 Probabilistic damage assessment of buildings subjected to main shock - aftershock sequences

Sections 5.2 and 5.3 compared the structural responses during the aftershock under two assumptions: “replicated” and “randomized” ground motion ensembles. In this section, the damage assessment will be based on the more realistic “randomized” case.

The relationship between the maximum inter-story drift ratio, θ, and the spectral acceleration S_a at the fundamental period of the structure was summarized in Table 5.7. The structural response during the aftershock can be evaluated by:

$$P[\theta_a > x \mid M_m = m] = \sum_{S_{a,a}} P\left[\theta_a > x \mid S_{a,a} = z\right] P\left[S_{a,a} = z \mid M_m = m\right] \quad (5.9)$$

in which θ_a is the maximum inter-story drift ratio during the aftershock, M_m is the magnitude of the main shock , and $S_{a,a}$ is the spectral acceleration of the aftershock at the fundamental period of the damaged structure. For the 9-story building, the first term on the right-hand side of Eq (5.9) can be evaluated from:

$$P[\theta_a > x \mid S_{a,a} = z] = 1 - \Phi\left(\frac{\ln(x) - \ln(0.0534 z^{0.572})}{0.225}\right) \quad (5.10)$$

The second term on the right-hand side of Eq (5.9), $P[S_{a,a} = z \mid M_m = m]$, describes the relationship between the earthquake intensities of the main shock and aftershock. This conditional probability can be evaluated by Monte Carlo simulation, as described in Section 5.2.

Based on Eqs (5.9) and (5.10), $P[\theta_a > x \mid M_m = 6.8]$ and $P[\theta_a > x \mid M_m = 7.0]$ for the 9-story building can be evaluated numerically, as shown in Figures 5.19(a) and 5.19(b). Similar results are presented for the 20-story building in Figure 5.20(a) and 5.20(b).

The probability of specific damage levels following the aftershock can be evaluated by:

$$P[D_a > x \mid D_m = y, M_m = m] = \sum_{S_{a,a}} P[D_a > x \mid D_m = y, S_{a,a} = z] P[S_{a,a} = z \mid M_m = m] \quad (5.11)$$

in which $x > y$. Suppose that following a main shock, an inspection reveals that some beam-to-column connections were damaged. Equation (5.11) might be used to estimate the probability of additional damage if an aftershock were to occur prior to repair. Such information might be useful in deciding whether to permit the building to remain occupied prior to repair. $P[D_a > x \mid D_m = y, S_{a,a} = t]$ can be evaluated using the

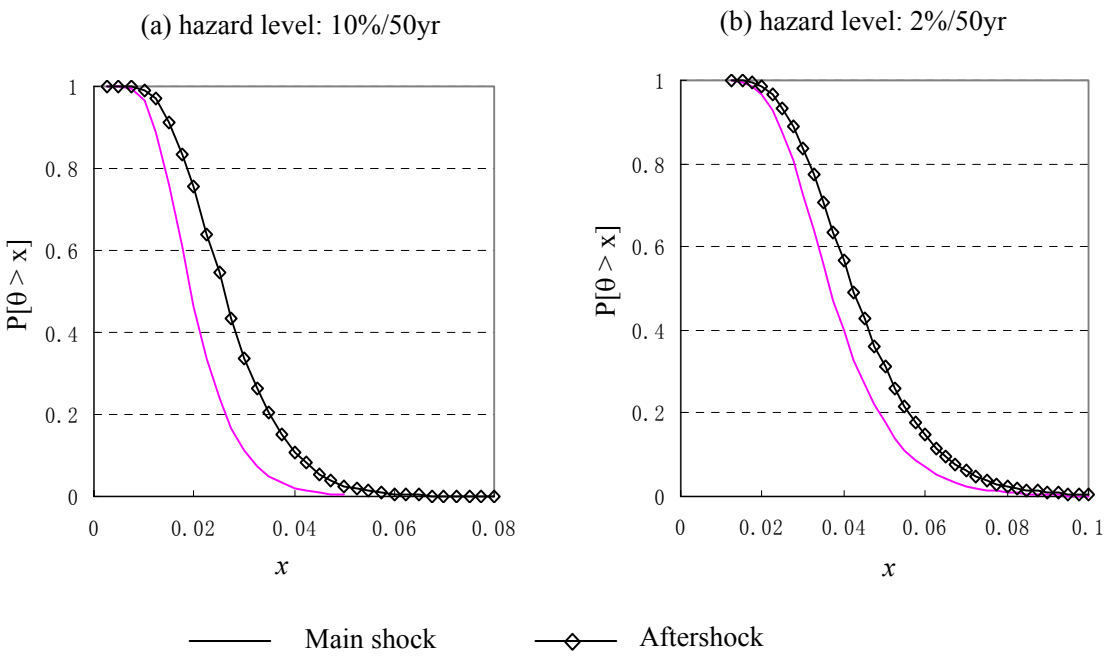

Figure 5.19 Exceedence probability for maximum inter-story drift ratio of 9-story building

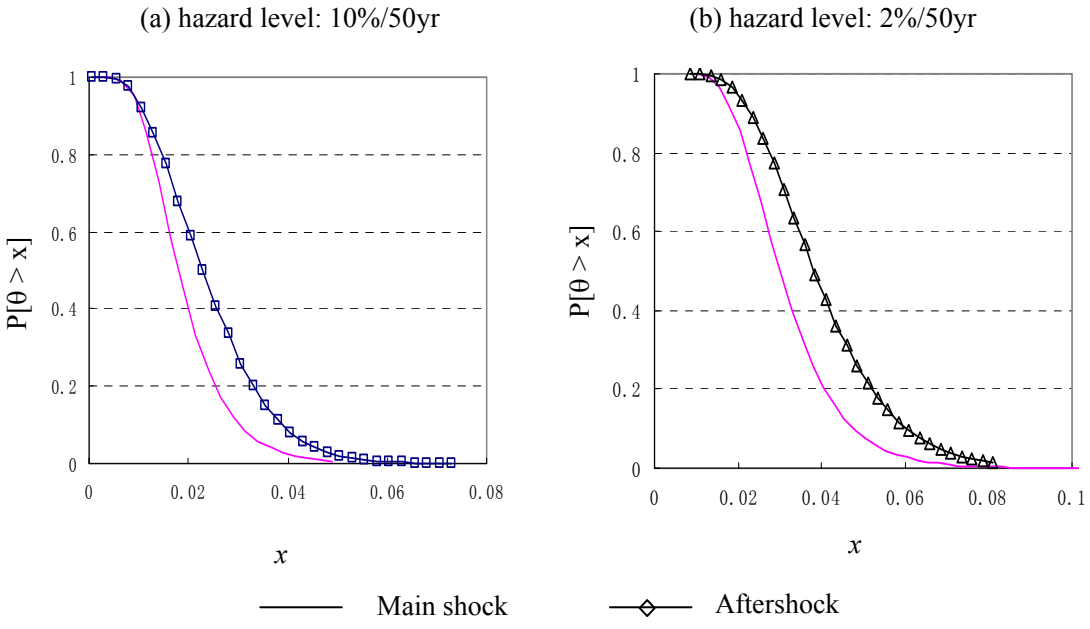

Figure 5.20 Exceedence probability for maximum inter-story drift ratio of 20-story building

equations presented in Table 5.6 for the 9-story building and Table 5.8 for the 20-story building. As an example for the 9-story building, if the aftershock has the same intensity as the main shock:

$$P[D_a > x \mid D_m = y, S_{a,a} = S_{a,m}] = 1 - \Phi\left(\frac{\ln(x-y) - \ln(-0.396y + 0.270)}{0.772}\right) \quad (5.12)$$

As mentioned above, $P[S_{a,a} = z \mid M_m = m]$ in Eq (5.11) can be evaluated by simulation. However, $P[D_a > x \mid D_m = y, S_{a,a} = z]$ is evaluated only at 4 discrete $S_{a,a}$ samples: $S_{a,a} = 1.0S_{a,m}$, $0.9S_{a,m}$, $0.8S_{a,m}$ and $0.7S_{a,m}$, and thus Eq (5.11) must be evaluated from these 4 samples. The point estimate (PE) method (Rosenblueth 1975), described in Chapter 3.3, has been shown to be an efficient technique for calculating the statistical moments of a function of random variables with only a few samples. Using the PE method, $P[S_{a,a} = z \mid M_m = m]$ is calculated from a set of algebraic equations that ensure that the statistical moments of the CDF in Figure 5.1 are matched. For the main shock with seismic hazard of 10%/50 years, the interval $[(M_m - M_a) \leqslant 0.6]$ is of interest because no additional damage was found to occur unless the difference between the magnitudes of the aftershock and main shock was relatively small. To apply the PE method to this situation, the moments of the random aftershock, conditioned on $[(M_m - M_a) \leqslant 0.6]$, first must be derived from the aftershock magnitude distribution shown in Figure 5.1. The first four moments are 0.337, 0.107, 0.0465 and 0.0222. Next, the probability concentrations $p_1 = P[M_a = 6.2 \mid M_m = 6.8]$, $p_2 = P[M_a = 6.4 \mid M_m = 6.8]$, $p_3 = P[M_a = 6.6 \mid M_m = 6.8]$, $p_4 = P[M_a = 6.8 \mid M_m = 6.8]$ are derived from:

$$\begin{cases} p_1 + p_2 + p_3 + p_4 = 0.337 \\ 0.6p_1 + 0.4p_2 + 0.2p_3 = 0.107 \\ 0.6^2 p_1 + 0.4^2 p_2 + 0.2^2 p_3 = 0.0465 \\ 0.6^3 p_1 + 0.4^3 p_2 + 0.2^3 p_3 = 0.0222 \end{cases} \tag{5.13}$$

Using Eq (5.13), the probability concentrations of aftershocks with different magnitudes are obtained as, p_1 = 0.0593, p_2 = 0.135, p_3 = 0.0884, p_4 = 0.0543. In a similar fashion, for the main shock with seismic hazard of 2%/50 years, the aftershock probability concentrations are: $P[M_a = 6.3 \mid M_m = 7.0] = 0.0596$, $P[M_a = 6.5 \mid M_m = 7.0] = 0.137$, $P[M_a = 6.8 \mid M_m = 7.0] = 0.0887$, $P[M_a = 7.0 \mid M_m = 7.0] = 0.0548$. Using the main shock-aftershock relations in Table 5.2,

$$\begin{cases} P[S_{a,a} = 0.7S_{a,m} \mid M_m = 6.8] = P[M_a = 6.2 \mid M_m = 6.8] = 0.0593 \\ P[S_{a,a} = 0.8S_{a,m} \mid M_m = 6.8] = P[M_a = 6.4 \mid M_m = 6.8] = 0.135 \\ P[S_{a,a} = 0.9S_{a,m} \mid M_m = 6.8] = P[M_a = 6.6 \mid M_m = 6.8] = 0.0884 \\ P[S_{a,a} = S_{a,m} \mid M_m = 6.8] = P[M_a = 6.8 \mid M_m = 6.8] = 0.0543 \end{cases} \tag{5.14}$$

$$\begin{cases} P[S_{a,a} = 0.7S_{a,m} \mid M_m = 7.0] = P[M_a = 6.3 \mid M_m = 7.0] = 0.0596 \\ P[S_{a,a} = 0.8S_{a,m} \mid M_m = 7.0] = P[M_a = 6.5 \mid M_m = 7.0] = 0.137 \\ P[S_{a,a} = 0.9S_{a,m} \mid M_m = 7.0] = P[M_a = 6.8 \mid M_m = 7.0] = 0.0887 \\ P[S_{a,a} = S_{a,m} \mid M_m = 7.0] = P[M_a = 7.0 \mid M_m = 7.0] = 0.0548 \end{cases} \tag{5.15}$$

Finally, the probabilities, p_i, determined from the PE method and Eqs (5.14) and (5.15) are used in Eq (5.11) to determine the probability that the damage ratio following the aftershock exceeds specified values.

The probabilities of exceeding specific damage ratios following the aftershock are presented in Figure 5.21 for the 9-story steel frame , under the assumptions that the main shock induces damage ratios of 20%, 30% and 40% to the beam-to-column connections. Similar results are presented for the 20-story building in Figure 5.22

under the assumption that the main shock causes damage ratios of 10%, 20% and 30%. If the inspection following the main shock reveals that the damage ratio is smaller than 40%, then the probability that any aftershock will cause a severe damage increment, for example $D_a > 70\%$, is very small. Moreover, for a severe damage state following main shock – aftershock sequence ($D_a > 70\%$ for example), the initial damage ratio has little impact on the estimated probability, e.g., $P[D_a > 0.70 \mid D_m = d]$ is less than 2% for d = 0.2 – 0.4.

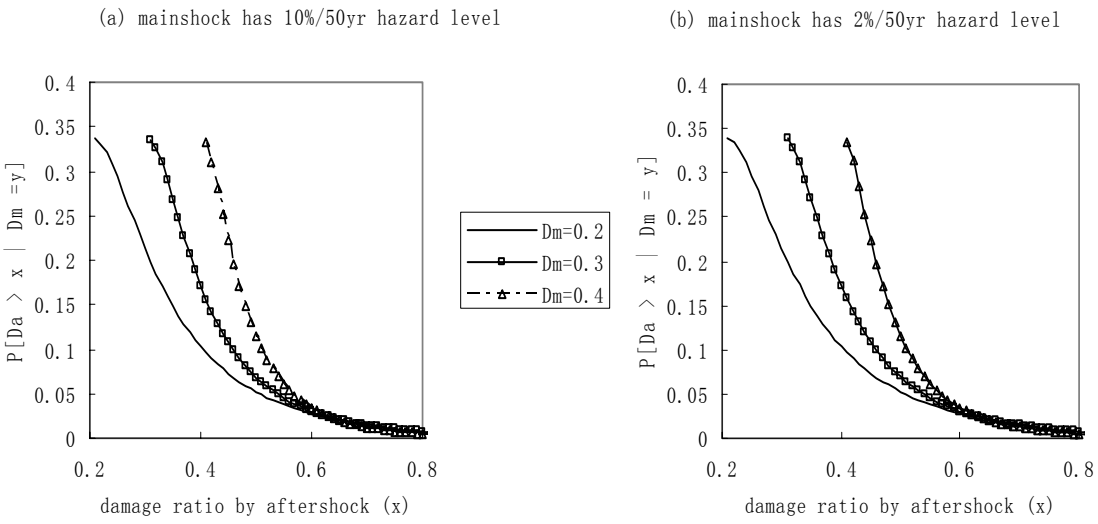

Figure 5.21. Probability distribution of the damage ratio of the 9-story building by aftershock

The main shock intensity has little influence on aftershock damage, as shown by comparing Figure 5.21(a) with 5.21(b) and Figure 5.22(a) with 5.22(b). The key factor to determine the damage state of the structure following the aftershock is the damage ratio following main shock rather than the intensity of the seismic excitation of the main shock.

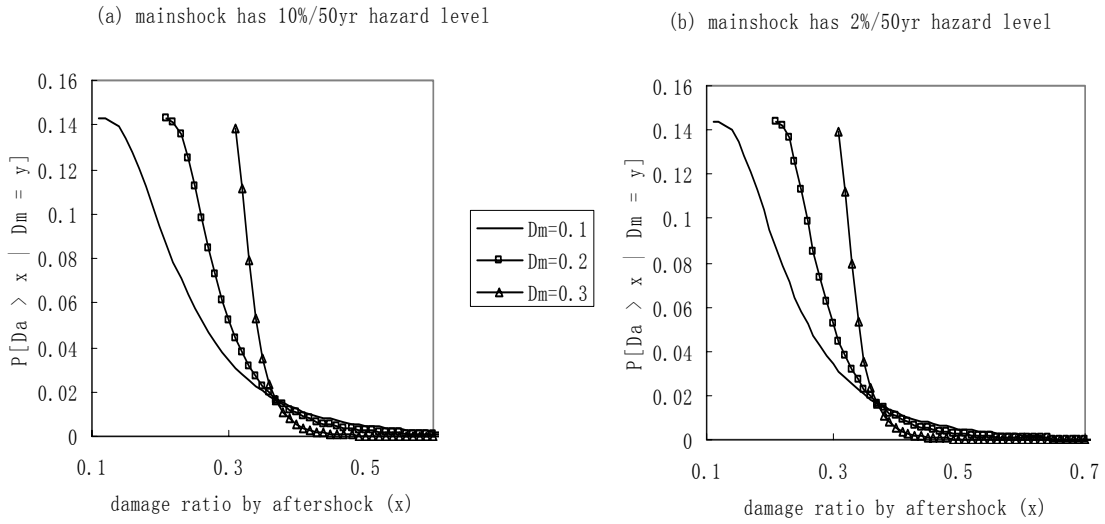

Figure 5.22. Probability distribution of the damage ratio of the 20-story building by aftershock

5.5 Summary

In this chapter, the performance of two steel moment-resisting building frames with welded moment-resistant connections that experience connection fractures during an earthquake main shock and are subjected to a subsequent aftershock was examined. The following conclusions can be made:

1. The EUMRHA method proposed in Chapter 4 was verified further. Comparing the seismic responses of the 9-story building determined by the EUMRHA and NLTHA methods, it was demonstrated that the EUMRHA method provides good estimates of not only story drifts, but also locations of damaged beam-to-column connections. Accordingly, the EUMRHA is a highly efficient analytical tool for analyzing the stochastic structural response of steel frames to sequences of earthquake ground motion.
2. The characteristics (amplitude and frequency content) of the aftershocks have a significant influence on the structural damage pattern that develops as a result of the aftershock. For the "replicate" assumption, the original damage pattern did not change as a result of the aftershock and the additional damage from the aftershocks did not depend on the initial damage from the main shock. On the other hand, under the "randomization" assumption the pattern of connection damage over the frame changed as a result of the aftershocks, to a degree depending on the characteristics of the aftershock ground motion. In this case, the additional damage from the aftershocks was related to the initial damage from the main shock.

3. If the damage ratio from the main shock is small (D_m < 30%), the "randomization" assumption led to a conservative estimate of damage from the aftershock relative to the "replicate" assumption. However, as the initial damage ratio caused by the main shock increased, the aftershock damage estimates under the two assumptions became closer. Regardless of which assumption was used, the probability that the aftershock causes large additional damage is small if the initial damage from the main shock is small.
4. A comparison of maximum inter-story drift ratios developed by the main shock-aftershock sequence found that the "replicate" assumption tended to overestimate the structural response because the characteristics of the principal ground motion that account for large structural deformations are reinforced by a replicate aftershock with the same frequency characteristics. Thus, the "replicate" assumption would lead to a conservative estimate of steel frame performance during main shock-aftershock sequences.

CHAPTER 6: POST-EARTHQUAKE EVALUATION CONSIDERING UNCERTAINTY IN DAMAGE INSPECTION

6.1 Introduction

Following an earthquake, an assessment of a steel moment-frame building might be performed to determine the likelihood that significant structural damage has occurred. A three-step process for this purpose was recommended in FEMA-352:

Screening: Estimate the probable ground motion experienced at the building site. If this estimated ground motion falls below a certain threshold, further evaluation is not required. Screening is intended to identify those buildings that experienced sufficient ground shaking to have sustained significant damage.

Preliminary Evaluation: A site visit is made to the building and the condition of the building is observed to determine if there are obvious indications of structural or nonstructural damage. If no damage is observed, occupancy may continue pending completion of detailed evaluation.

Detailed Evaluation: Detailed inspections of the building frame and connections are performed to determine the condition of the structure. If structural damage is detected in the course of these inspections, further evaluations are performed to determine the significance of this damage.

The condition assessment is hampered by the cost of inspecting beam-to-column connections for fractures, which may render inspection of all the moment-resisting connections in a building uneconomical, and by the inaccessibility of certain connections to inspection. As a result, the damage state of a building must be judged by partial inspection, and the true damage state is uncertain. Therefore, deciding how many connections to inspect and how best to select these connections become an important consideration.

Because of the uncertainties associated with structural materials found in connections, especially the workmanship in weld joints, damaged connections tend to be widely distributed throughout building frames and may occur at locations that might not be predicted by analysis (FEMA-352). The scatter in the locations of damaged connections throughout a steel frame building will be examined in Section 6.2 to determine whether or not the structural analysis is useful in guiding the inspection. Based on the observations in Section 6.2, an analysis-based method for selecting connections to be inspected is proposed, and a probability model of this selection scheme is developed in Section 6.3. Finally, the proposed selection method is illustrated by performing partial damage inspections of the 9-story and 20-story buildings considered in the previous Chapters. A post-earthquake evaluation of the damaged building is also performed to determine the frequency distribution of damaged connections following an earthquake as a basis for evaluating repair costs.

6.2 Structural fragilities and damage patterns in steel frames

The development of a plan for inspecting connections in earthquake-damaged building logically would begin with a structural analysis of the building frame. It was noted in FEMA-352 (p. 4-17) that "there has been a poor correlation of the location of damage and the locations of highest demand predicted by analysis" and it was recommended that the connections to be inspected be selected randomly. However, Song and Ellingwood (1999) noted some consistency in predicted damage patterns when a series of four frames were subjected to ensembles of ground motion. In this section, patterns of damage in connections throughout a structural frame will be investigated using the 9-story and 20-story SAC/Los Angeles steel frames described previously to determine the extent to which inspection can be guided by structural analysis. Uncertainties associated workmanship are considered as well as those associated with the structural material.

The quality of workmanship is reflected in the behavior of the beam-to-column connections. A well-trained welder generally produces high-quality weldments, while a poorly-trained welder produces connections with lower strength and larger variance in the welding quality. Among the 6 parameters in the beam-to-column connection model (Figure 2.1, Gross, 1998), β_1 and β_5 are the most significant in terms of inter-story drift response of the frame (Song and Ellingwood 1999). To model the impact of workmanship, parameters β_1 and β_5 are treated as random variables to reflect the uncertainties associated with workmanship. Due to a lack of data, β_1 and β_5 are assumed in this study to be uniformly distributed (the distribution of maximum

uncertainty) and statistically independent from one connection to another. For acceptable workmanship, the means and coefficients of variation are: $\mu_{\beta_1} = 0.4$, $\mu_{\beta_5} = 1.1$, COV(β_1) = 0.29 and COV(β_5) = 0.09. For marginal workmanship, the means and coefficients of variation are: $\mu_{\beta_1} = 0.3$, $\mu_{\beta_5} = 0.95$, COV(β_1) = 0.4 and COV(β_5) = 0.2. The uncertainties associated with workmanship are propagated in the reliability analysis using Latin Hypercube (LHC) sampling (Imam and Conover, 1980); Since there are 20 earthquake accelerations for hazard levels of 10%/50yr, the ranges of β_1 and β_5 are divided into 20 intervals of equal probability based on CDFs, leading to the Latin Hypercube connection parameters shown in Table 6.1.

Table 6.1 LHC samples for connection model of different workers.

Acceptable		**1**	**2**	**3**	**4**	**5**	**6**	**7**	**8**	**9**	**10**
	β_1	0.21	0.23	0.25	0.27	0.29	0.31	0.33	0.35	0.0.37	0.39
	β_5	0.9385	0.9555	0.9725	0.9895	1.0065	1.0235	1.0405	1.0575	1.0745	1.0915
		11	**12**	**13**	**14**	**15**	**16**	**17**	**18**	**19**	**20**
	β_1	0.41	0.43	0.45	0.47	0.49	0.51	0.53	0.55	0.57	0.59
	β_5	1.1085	1.1255	1.1425	1.1595	1.1765	1.1935	1.2105	1.2275	1.2445	1.2615
Marginal		**1**	**2**	**3**	**4**	**5**	**6**	**7**	**8**	**9**	**10**
	β_1	0.1005	0.1215	0.1425	0.1635	0.1845	0.2055	0.2265	0.2475	0.2685	0.2895
	β_5	0.6365	0.6695	0.7025	0.7355	0.7685	0.8015	0.8345	0.8675	0.9005	0.9335
		11	**12**	**13**	**14**	**15**	**16**	**17**	**18**	**19**	**20**
	β_1	0.3105	0.3315	0.3525	0.3735	0.3945	0.4155	0.4365	0.4575	0.4785	0.4995
	β_5	0.9665	0.9995	1.0325	1.0655	1.0985	1.1315	1.1645	1.1975	1.2305	1.2635

In addition, the uncertainties associated with the structural framing material - Young's modulus (E), yield strength of column $F_{y,col}$ and yield strength of beam $F_{y,beam}$ - are also considered. Column strengths and stiffnesses are assumed to be perfectly correlated over the height of the building; beam strengths and stiffnesses also are perfectly correlated over the bays. However, the column and beam properties are statistically independent and their probability distributions, means and coefficients of variation (C.O.V.) are presented in Table 6.2.

Table 6.2 Random material strength parameters

Parameter	Mean (ksi)	COV	CDF
E	29000	0.06	Uniform
$F_{y,col}$	57.6	0.12	Lognormal
$F_{y,beam}$	49.2	0.12	Lognormal

The ground motion ensembles corresponding to a hazard level of 10% / 50yr (la01-la20) are applied to the 9-story and 20-story steel frames using a nonlinear time history analysis and OpenSees, as described previously. Figures 6.1 and 6.2 show the relationship between the maximum inter-story drift ratio (θ_{max}) and spectral acceleration (S_a) for the 9-story and 20-story buildings. The relationships for three cases are compared: (1) deterministic buildings (using the mean of each random

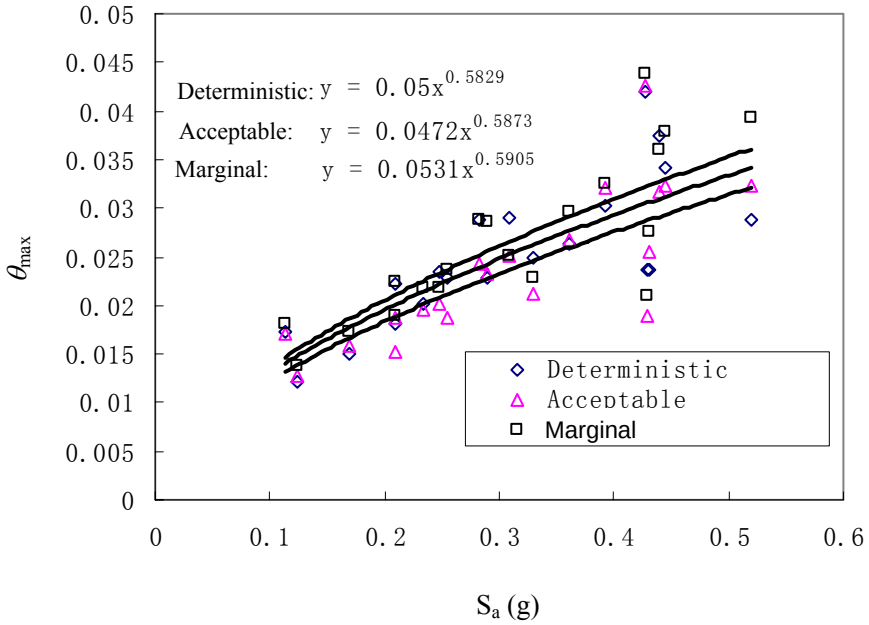

Figure 6.1 The relationship between θ_{max} and S_a for 9-story frame

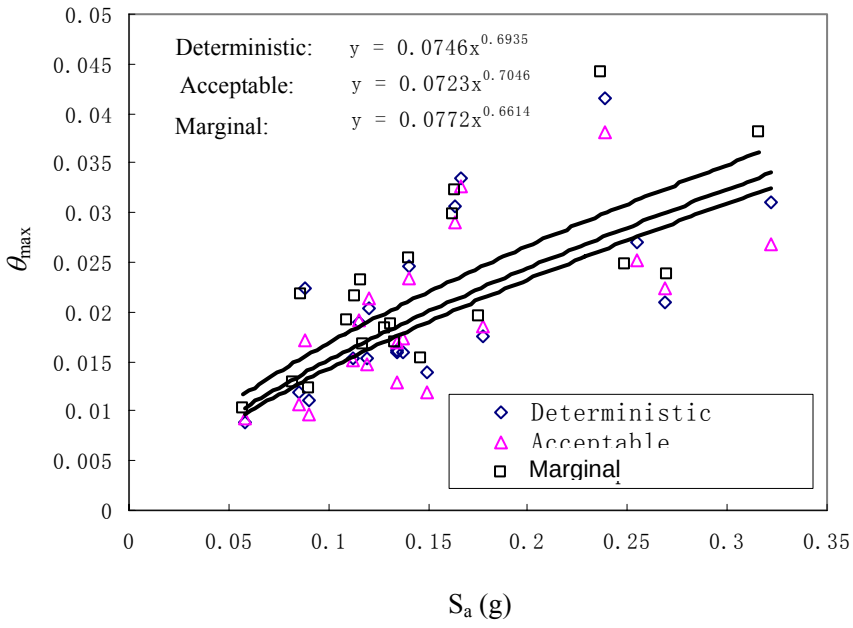

Figure 6.2 The relationship between θ_{max} and S_a for 20-story frame

variable), or buildings with uncertain properties, assuming the building is constructed by (2) acceptable or (3) marginal workmanship. The logarithmic standard deviation $\sigma_{\ln(\theta)|S_a}$ in $\theta_{\max}$ of the 9-story building is 0.163, 0.172 and 0.178 for the deterministic model and structural models with acceptable workmanship and marginal workmanship respectively. For the 20-story building, $\sigma_{\ln(\theta)|S_a}$ is 0.231, 0.240 and 0.249 respectively. These results show that the variance of structural response is dominated by the uncertainties associated with earthquake ground motions, rather than the uncertainties associated with structural model, a result that has been suggested by other investigators (Song and Ellingwood 1998, Maison and Bonowitz 1999).

According to FEMA 273, the performance levels of steel moment frames are categorized into Collapse Prevention (CP) ($2.5\% \le \theta_{\max} \le 5\%$), Life Safety (LS) ($0.7\% \le \theta_{\max} \le 2.5\%$) and Immediate Occupancy (IO) ($0 \le \theta_{\max} \le 0.7\%$). Using these definitions, the structural fragility curves of the 9-story and 20-story buildings are presented in Figure 6.3 and 6.4. If the quality of workmanship is acceptable, neglecting the uncertainties associated with structural modeling makes the fragility analysis conservative. On the other hand, if the quality of workmanship is marginal the structural fragility increases, especially at the CP performance level.

Next, the predictability of the patterns of seismic damage in these frames is investigated. To this end, 3 out of 20 building samples are subjected to the same ground motion (la03). The damage patterns for the 9-story and 20-story buildings are shown in Figures 6.5 and 6.6 for cases of acceptable or marginal workmanship. It can

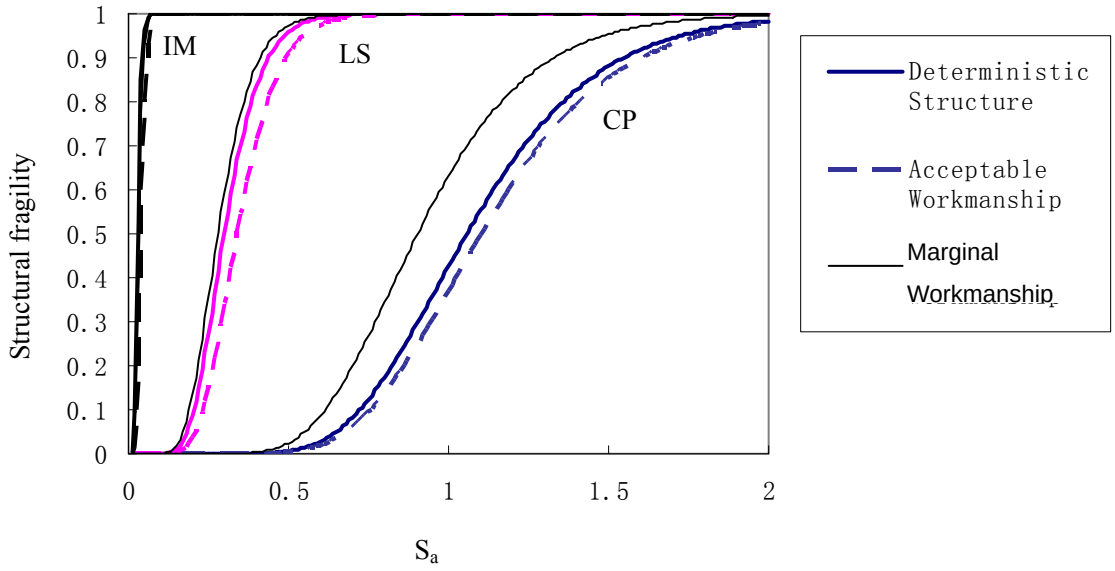

Figure 6.3 Structural fragility curves for the 9-story building

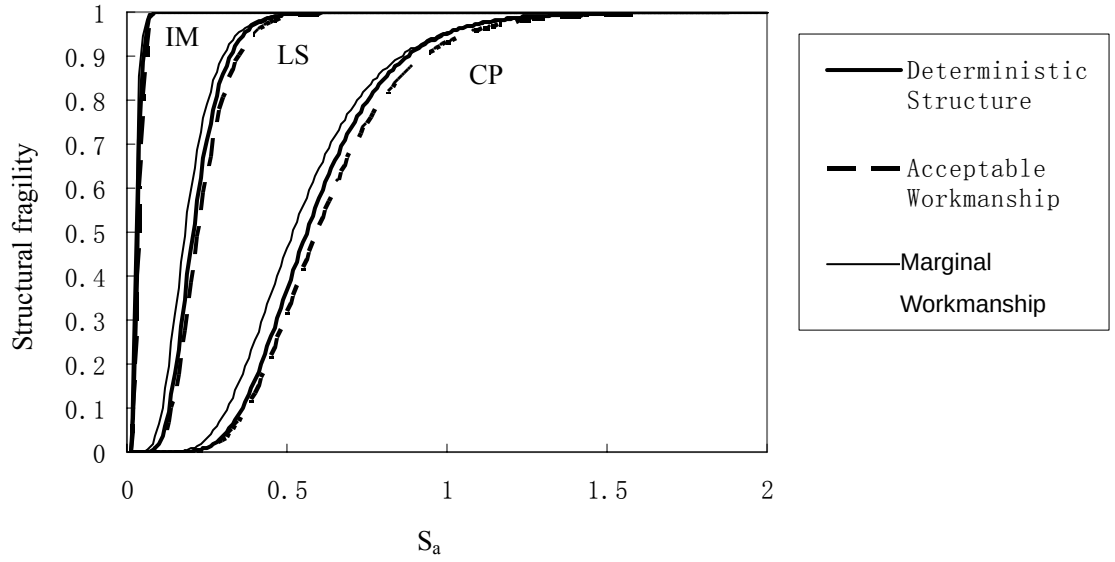

Figure 6.4 Structural fragility curves for the 20-story building

be observed that for all frame samples representing both acceptable and marginal workmanship, the damage patterns remain virtually unchanged: most of the structural damage accumulates in the lower stories, while a small amount of damage is scattered in the upper stories. If the quality of workmanship drops from the acceptable to the marginal level, the damage ratio (defined as the number of damaged connections divided by total number of connections, as in Chapter 5) increases from approximately 45% to 60% for 9-story building and from 30% to 40% for the 20-story building. It might be recalled that the analysis results of the deterministic 9-story and 20-story building by the proposed EUMRHA presented in Chapter 4 also showed that the lower stories are more likely to be damaged than the upper stories.

(a) sample realizations of damage pattern - acceptable workmanship

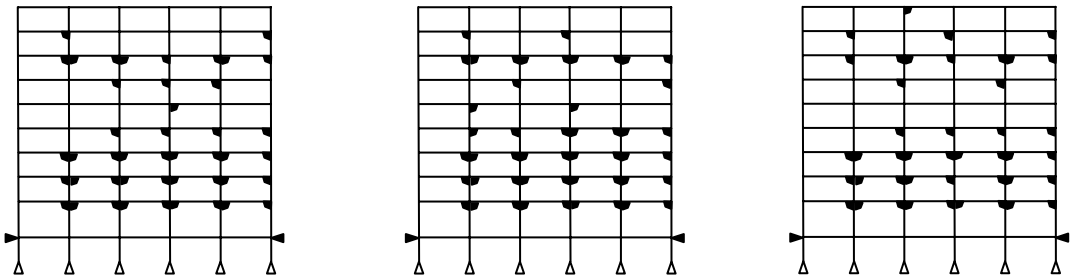

(b) sample realizations of damage pattern - marginal workmanship

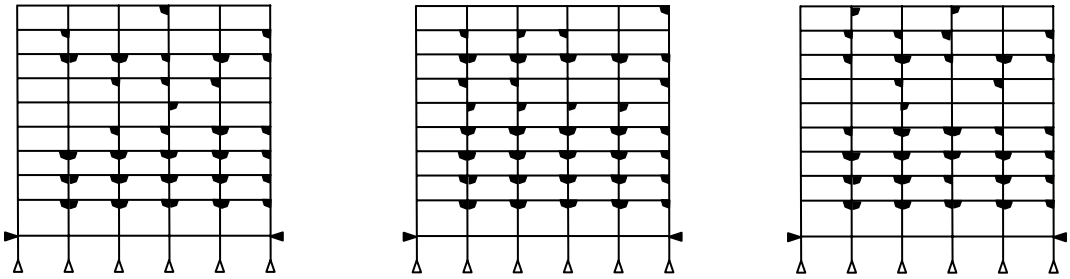

Figure 6.5 Sample damage patterns in 9-story building – la03 record

(a) Sample realizations of damage pattern - acceptable workmanship

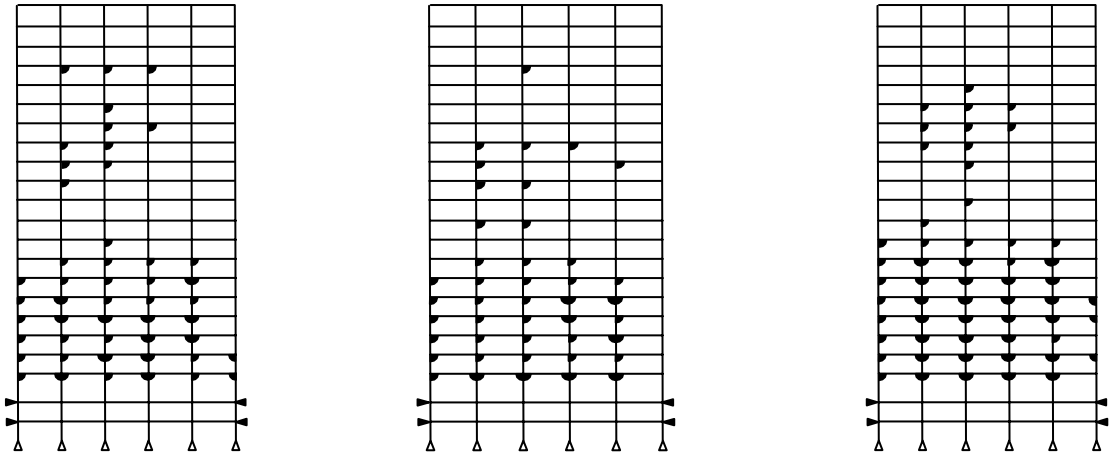

(b) Sample realizations of damage pattern - marginal workmanship

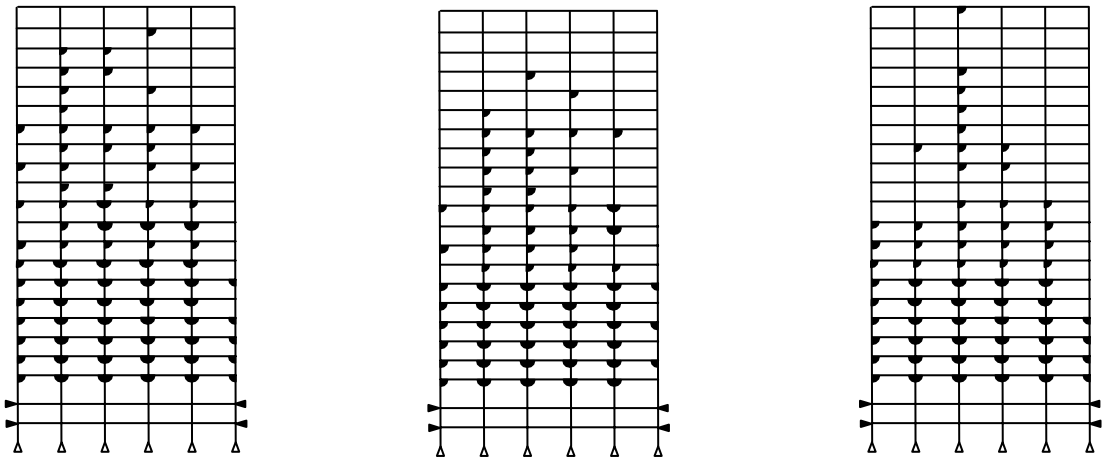

Figure 6.6 Sample damage patterns in 20-story building – la03 record

6.3 Probability Model of Connection Inspection

While the uncertainties in workmanship cause the damaged connections to be scattered over more stories, the basic damage patterns in all cases are governed by building type and frequency characteristics of earthquake ground motions. Therefore, the floors most vulnerable to connection damage in the 9-story or 20-story building under a specific earthquake can be identified with the help of the EUMRHA. For example, the distribution of the maximum inter-story drifts over the height of the 9-story and 20-story frames when they are excited by la03 and la14 is shown in Figure 6.7 (calculated by EUMRHA). Under the excitation of la03, connection damage appears to concentrate in the lower stories, while connection damage occurs at both lower and upper stories when the buildings are subjected to la14. The above information can guide the engineer in identifying those areas where the most seriously damaged connections are likely to be found. Those areas should be inspected first for the primary evaluation of the building damage state.

In a statistical sense, the building damage state estimated by inspecting only the most vulnerable floors is biased, because the damage states at floors identified as being less vulnerable, and thus not inspected, remains unknown. To eliminate this bias, some connections in the less vulnerable floors should be selected randomly for inspection, so as to have an un-biased estimate of the damage state at those floors. Therefore, the inspection scheme proposed in this chapter includes two parts: analysis-based selection of connections and floors to be inspected and random selection of connections at the un-inspected floors. The number of estimated damaged

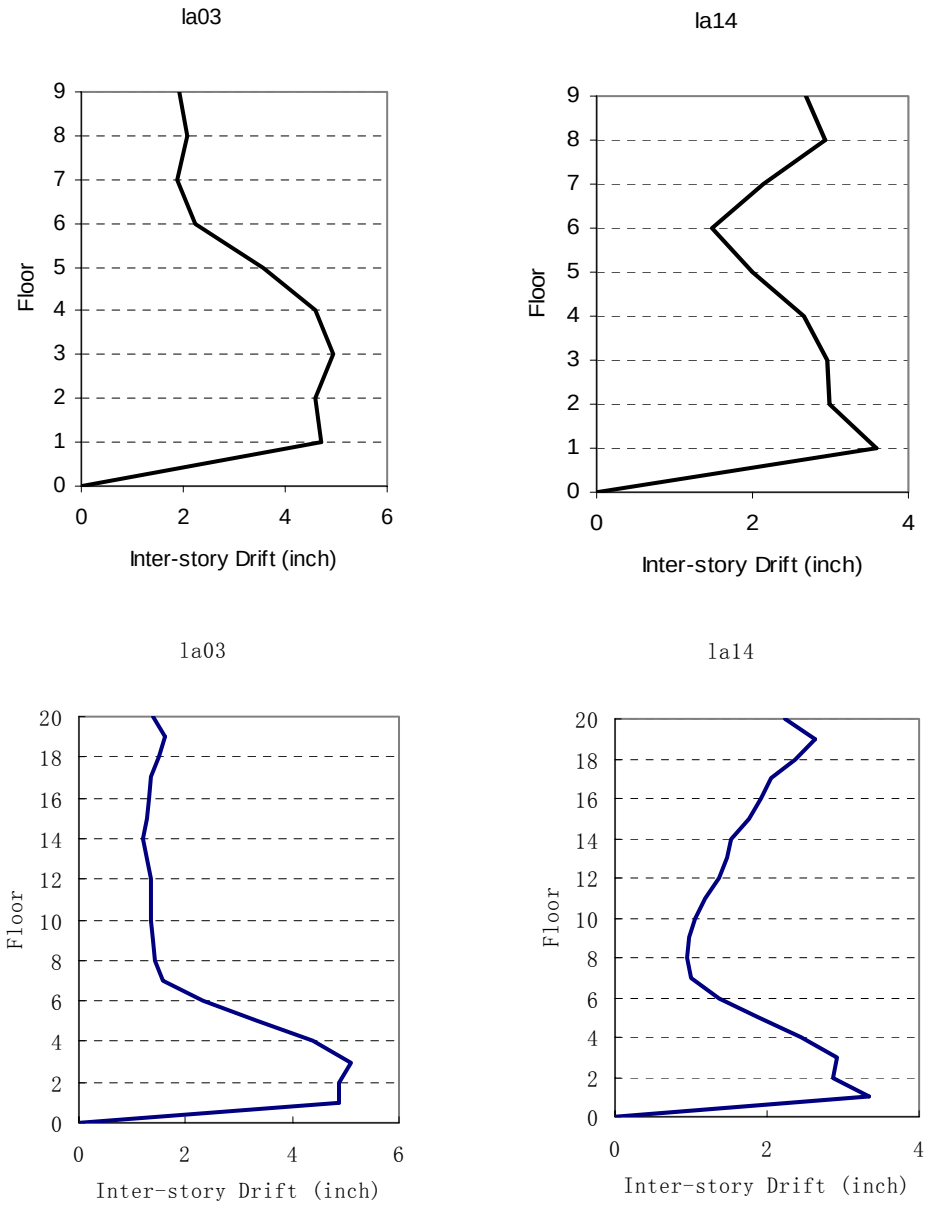

Figure 6.7 Maximum inter-story drift of 9-story and 20-story building subjected to la03 and la14 (EUMRHA)

connections within these two groups constitutes the total number of damaged connections $n_{d,est}$. In FEMA 352 (2000), the building damage index is the average of all member damage indices, in which the member damage index is assigned different values 0 (undamaged), 1, 2, 3 and 4 denoting different types of damage. In the present study, beam bottom flange fracture is assumed to be the only damage type (consistent with the connection model in Figure 2.1). For each beam-column connection, its damage index is either 0 (undamaged) or 1 (damaged). Therefore, the total number of estimated damaged connections ($n_{d,est}$) is chosen as a damage measure; its value is:

$$n_{d,est} = n_{d,a} + n_{d,r} \tag{6.1}$$

where $n_{d,a}$ is the estimated number of damaged connections within floors selected from analysis and $n_{d,r}$ is the estimated number of damaged connections from random selection within the un-inspected floors.

To estimate the first term $n_{d,a}$ in Equation 6.1, we observe from Figures 6.5 and 6.6 that once connection damage occurs at a particular level, most connections at the left (or right) ends of each beam at that level are damaged, implying that only a fraction of the connections at vulnerable floors needs to be inspected to estimate the damage degree at that floor. Simple heuristic "rules" can be devised from such observations. For example, in this study, only 4 out of 9 (9-story building) or 4 out of 10 (20-story building) connections are inspected: 2 outer connections and 2 middle connections, as shown in Figure 6.8. If the outer connection (connection 1 and 4 in Figure 6.8) is found to be damaged, its adjacent inner connection is also assumed to be damaged. If the inner connection (connection 2 and 3 in Figure 6.8) is found to be

damaged, the two inner connections adjacent to it are also assumed to be damaged. In addition, it is observed that when one specific floor is damaged, its adjacent floors are also likely to be damaged. Therefore, if 50% or more of the inspected connections at a particular floor level are damaged, the inspection should continue to the adjacent floors until a floor is inspected at which fewer than 50% of the connections are found to be damaged. Of course, these inspection "rules" introduce uncertainty (variance) to $n_{\mathrm{d,est}}$ in equation (6.1), which must be investigated.

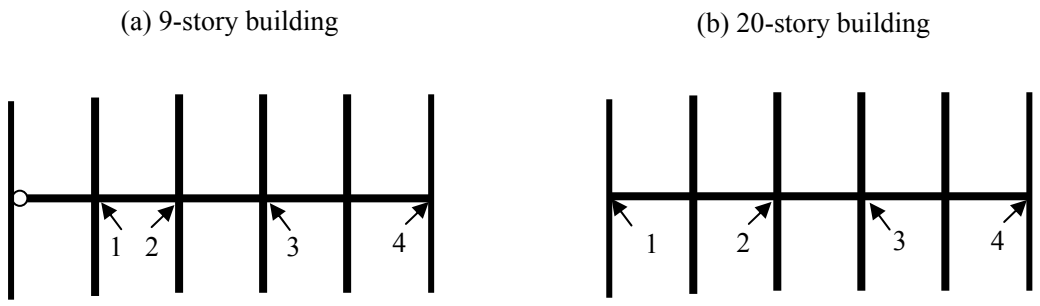

Figure 6.8 Inspection of connections at expected vulnerable floors in 9-story and 20-story buildings

Next, the variance introduced by $n_{\mathrm{d,a}}$ is investigated. Suppose that the actual number of damaged connections in the inspected floors is known to be $\overline{n}_{\mathrm{d,a}}$. Given the inspection results [i.e. $m^{a}_{\mathrm{d,i}}$ among m^{a}_{i} inspected connections are damaged], then $n_{\mathrm{d,a}}$ is described by a hypergeometric distribution with variance:

$$\mathrm{Var}(n_{\mathrm{d,a}}) = \left(\frac{m^a - m^a{}_{\mathrm{i}}}{m^a - 1}\right) \times \overline{n}_{\mathrm{d,a}} \times \frac{m^a{}_{\mathrm{d,i}}}{m^a{}_{\mathrm{i}}} \times \left(1 - \frac{m^a{}_{\mathrm{d,i}}}{m^a{}_i}\right) \times \left(\frac{m^a}{m^a{}_i}\right)^2 \tag{6.2}$$

where m^a is the total number of connections in the vulnerable floors. In a real inspection, the actual number of damaged connections in the inspected floors ($\overline{n}_{\mathrm{d,a}}$) is not known, and $\overline{n}_{\mathrm{d,a}}$ has to be replaced by the estimated number of damaged connections ($n_{\mathrm{d,a}}$) in Eq. (6.2). In addition, the selection of 2 inner and 2 outer connections at each floor to be inspected is not a purely random procedure because the selection utilizes prior knowledge of damage obtained from the analysis and the variance calculated by Equation. (6.2) is overestimated.

The second term in the right side of equation (6.1) $n_{\mathrm{d,r}}$ is estimated by inspecting connections selected at random in the un-inspected floors. With the inspection results [i.e. $m^r{}_{\mathrm{d,i}}$ among $m^r{}_{\mathrm{i}}$ inspected connections are damaged], a continuous probability function $f_F(z)$ for the true but unknown proportion of damaged connections among the un-inspected (F) can be derived (Luco and Cornell 2002):

$$f_F(z) = \frac{(m^r{}_{\mathrm{d,i}} + 1)!}{m^r{}_{\mathrm{d,i}}!(m^r{}_{\mathrm{i}} - m^r{}_{\mathrm{d,i}})!} z^{m\ \mathrm{d,i}} (1-z)^{m^r{}_{\mathrm{i}} - m^r{}_{\mathrm{d,i}}} \tag{6.3}$$

The probability density function in Equation (6.3) is a beta distribution with mean μ_{F} and variance $\sigma_{\mathrm{F}}{}^2$:

$$\mu_F = \frac{m^r{}_{\mathrm{d,i}} + 1}{m^r{}_{\mathrm{i}} + 2} \quad ; \quad \sigma_F{}^2 = \frac{\mu_F(1-\mu_F)}{m^r{}_{\mathrm{i}} + 3} \tag{6.4}$$

The derivation of Equation (6.3) assumes that the procedure of inspecting connections randomly represents Bernoulli trails with replacement. In reality, inspection is done without replacement, but the assumption is adequate if the number of inspected connections is less than 30% of the total (Luco and Cornell 2002).

According to Eq. (6.4), the mean and variance of $n_{d,r}$ are:

$$\text{Mean}(n_{d,r}) = \frac{m^r{}_{d,i} + 1}{m^r{}_i + 2}(m^r - m^r{}_i) + m^r{}_{d,i} \tag{6.5a}$$

$$\text{Var}(n_{d,r}) = \frac{\mu_F(1-\mu_F)}{m^r{}_i + 3}(m^r - m^r{}_i)^2 \tag{6.5b}$$

in which m^r is the total number of connections in the un-inspected floors.

The inspection rule of adaptively separating floors where damage accumulates from floors where it does not guarantees that the $n_{d,a}$ and $n_{d,r}$ are weakly correlated, so the total variance can be written as,

$$\text{Var}\ (n_{d,est}) = \text{Var}\ (n_{d,a}) + \text{Var}\ (n_{d,r}) \tag{6.6}$$

To investigate the efficiency of the proposed inspection scheme, it is applied to inspect the 9-story and 20-story frames damaged by an ensemble of ground motions with hazard level of 10%/50yr (la01-la20). Inspection based on purely random selection of the same number of connections is also considered for comparison. Tables 6.3 and 6.4 summarize the analysis-based inspection results assuming acceptable and marginal levels of workmanship. The comparison of actual and estimated number of damaged connection for both 9-story and 20-story frames is presented in Figure 6.9. The accuracy of the estimation based on analysis-based inspection is verified, especially when the workmanship quality is good. Figure 6.10 compares the analysis-based inspection and random inspection. The reduction in variance for analysis-based inspection is obvious, regardless of whether the quality of workmanship is acceptable or marginal.

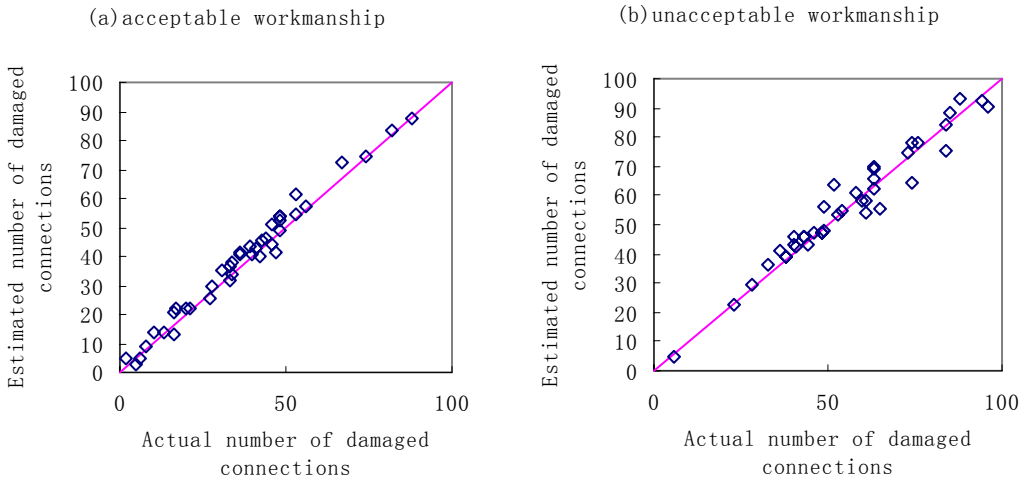

Figure 6.9 Comparison of expected and actual number of damaged connections

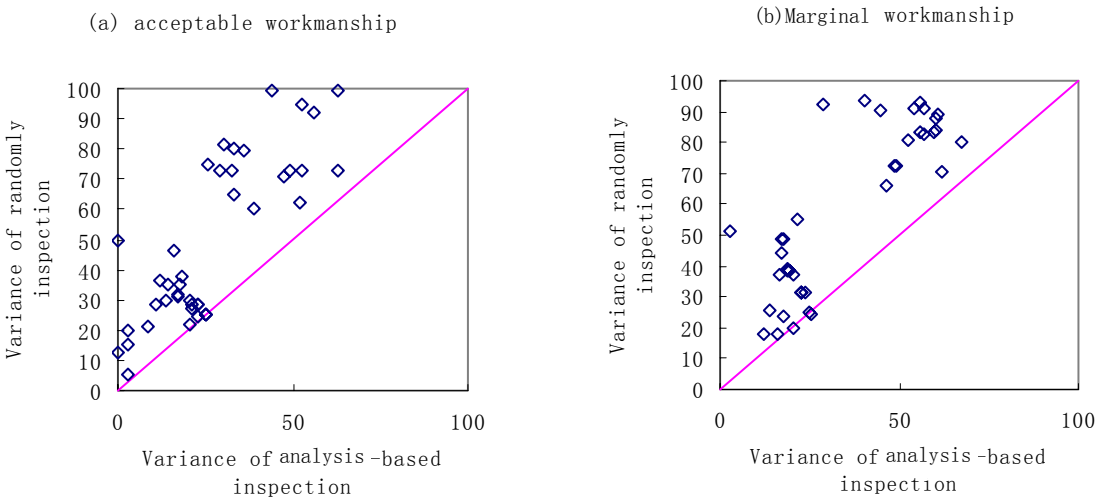

Figure 6.10 Comparisons of variances from analysis-based inspection and from random inspection

Table 6.3 Comparison between analysis-based inspection and random inspection (acceptable workmanship)

Building	Ground Motions	Analyze-based Inspection			Random Inspection			n_d		Variance	
		m_i	$m_{d,r}$	$n_{d,a}$	m_i	$m_{d,r}$	$n_{d,r}$	Estimatated	Actual	Proposed	Purely random
9-story	la01	28	14	33	4	0	2.333	35.33	31	20.407	29.668
	la02	32	19	42	2	0	1.75	43.75	39	22.774	28.304
	la03	36	26	57	0	0	0	57	56	20.566	21.875
	la04	24	11	23	6	0	2.625	25.63	27	17.496	30.983
	la05	24	17	38	6	0	2.625	40.63	40	14.455	34.85
	la06	12	5	11	12	0	3	14	10	8.6082	21.078
	la07	16	6	15	10	1	6.833	21.83	17	10.967	28.769
	la08	8	1	2	14	1	7.125	9.125	8	2.736	19.577
	la09	36	24	54	0	0	0	54	48	22.781	24.75
	la10	8	0	0	14	0	3.063	3.063	5	0.0698	12.739
	la11	32	21	49	2	0	1.75	50.75	41	21.348	28.338
	la12	8	1	2	14	0	3.063	5.063	2	2.6755	5.2966
	la13	24	13	29	6	3	13.5	42.5	41	17.636	34.85
	la14	36	15	34	0	0	0	34	34	24.917	24.969
	la15	20	8	19	8	0	2.8	21.8	21	13.973	29.813
	la16	36	21	46	0	0	0	46	44	24.917	25.438
	la17	32	21	47	2	0	1.75	48.75	48	21.348	27.371
	la18	32	19	44	2	0	1.75	45.75	43	22.774	28.235
	la19	8	1	2	14	0	3.063	5.063	6	2.6755	15.085
	la20	24	11	27	6	0	2.625	29.63	28	17.32	31.535
20-story	la01	36	12	32	22	1	8.333	40.33	42	30.413	81.642
	la02	32	5	14	24	1	8.385	22.38	20	16.086	46.518
	la03	72	26	70	4	0	2.667	72.67	67	63.136	73.06
	la04	56	19	49	12	0	3.429	52.43	48	47.525	71.17
	la05	48	28	71	16	0	3.556	74.56	74	44.187	99.565
	la06	60	19	51	10	0	3.333	54.33	53	49.161	72.709
	la07	36	14	37	22	0	3.667	40.67	36	32.484	72.636
	la08	28	11	28	26	0	3.714	31.71	33	25.465	74.875
	la09	60	33	84	10	0	3.333	87.33	88	56.208	91.98
	la10	56	31	80	12	0	3.429	83.43	82	52.381	94.386
	la11	44	12	33	18	1	8.2	41.2	47	33.179	80.431
	la12	32	6	17	24	0	3.692	20.69	16	18.547	38.042
	la13	60	22	58	10	0	3.333	61.33	53	52.748	72.709
	la14	52	14	38	14	0	3.5	41.5	36	38.749	60.236
	la15	32	13	34	24	0	3.692	37.69	34	29.346	72.93
	la16	44	14	36	18	1	8.2	44.2	46	36.276	79.234
	la17	12	0	0	34	2	13.33	13.33	16	0.0667	49.528
	la18	68	19	51	6	0	3	54	48	51.95	62.427

Table 6.4 Comparison between analysis-based inspection and random inspection (marginal workmanship)

Building	Ground Motions	Analyze-based Inspection			Random Inspection			n_d		Variance	
		m_i	$m_{d,r}$	$n_{d,a}$	m_i	$m_{d,r}$	$n_{d,r}$	Estimatated	Actual	Proposed	Purely random
9-story	la01	28	18	41	4	0	2.333	43.33	44	18.774	38.52
	la02	36	28	64	0	0	0	64	52	17.719	23.563
	la03	32	26	59	2	0	1.75	60.75	58	13.904	25.534
	la04	28	18	41	4	0	2.333	43.33	40	18.774	38.804
	la05	28	20	45	4	0	2.333	47.33	48	16.732	37.479
	la06	32	17	37	2	0	1.75	38.75	38	23.487	31.276
	la07	28	15	34	4	0	2.333	36.33	33	20.305	37.479
	la08	32	19	44	2	0	1.75	45.75	40	22.774	31.391
	la09	36	19	43	0	5	5	48	49	25.55	24.5
	la10	24	13	29	6	3	13.5	42.5	41	17.636	48.688
	la11	36	21	46	0	1	1	47	48	24.917	24.75
	la12	28	17	39	4	0	2.333	41.33	36	19.488	38.33
	la13	36	29	66	0	0	0	66	63	16.058	17.719
	la14	24	13	29	6	2	9.875	38.88	38	17.074	48.509
	la15	36	26	58	0	0	0	58	60	20.566	19.688
	la16	36	31	69	0	0	0	69	63	12.261	17.719
	la17	32	19	44	2	0	1.75	45.75	43	22.774	31.276
	la18	8	1	2	14	0	3.063	5.063	6	2.6755	51.328
	la19	24	11	27	6	0	2.625	29.63	28	17.32	44.056
	la20	32	19	44	2	0	1.75	45.75	43	22.774	31.276
20-story	la01	64	28	75	8	0	3.2	78.2	74	59.639	83.296
	la02	40	10	28	20	5	26.82	54.82	54	28.625	92.442
	la03	64	29	75	8	0	3.2	78.2	76	60.051	84.19
	la04	60	31	81	10	0	3.333	84.33	84	56.711	90.935
	la05	64	35	90	8	0	3.2	93.2	88	60.051	88.049
	la06	72	32	86	4	0	2.667	88.67	85	67.535	80.144
	la07	64	23	61	8	0	3.2	64.2	74	55.806	83.296
	la08	36	18	46	22	1	8.333	54.33	61	34.206	104.32
	la09	64	33	85	8	1	7.4	92.4	94	60.682	89.014
	la10	60	34	87	10	0	3.333	90.33	96	55.768	93.174
	la11	60	23	59	10	3	16.33	75.33	84	53.972	90.935
	la12	48	21	55	16	0	3.556	58.56	61	44.738	90.542
	la13	64	24	63	8	2	11.6	74.6	73	57.081	82.823
	la14	60	19	50	10	0	3.333	53.33	53	49.161	72.709
	la15	56	20	53	12	0	3.429	56.43	49	48.672	72.175
	la16	60	22	59	10	0	3.333	62.33	63	52.748	80.548
	la17	48	16	43	16	2	12.67	55.67	65	40.519	93.703
	la18	72	25	67	4	0	2.667	69.67	63	62.036	70.765

6.4 Selection of damage measures

6.4.1 Maximum inter-story drift ratio

In the previous chapters, the maximum inter-story drift ratio was used as the structural response measure under earthquake ground motions. For an existing building which may suffer additional damage from an earthquake, the structural response measure should indicate not only the additional damage caused by that earthquake but also should be related to the damage state (if any) of the building prior to the earthquake. In other words, a damaged building would be expected to suffer a larger maximum inter-story drift than a building without damage when both are subjected to the same earthquake ground motion. In a welded steel moment frame, damage may occur in either top or bottom beam flange-to-column flange welds. It has been found that "the maximum inter-story drift ratio for a building model with existing bottom flange fractures, but no top flange fractures, might not be dramatically different than that for the undamaged building model" (Luco, 2002). However, according to a damage survey following the Northridge earthquake of 1994 (Mahin 1998), top flange fractures were relatively rare and bottom flange fractures were the most commonly observed type of damage in the beam-column connections of welded steel moment-resisting frame (WSMF) buildings. Moreover, top flanges often are difficult to access and inspect. Therefore, the damage assessment in this study will focus on the bottom flange fractures. Specifically, the effect of existing (undetected and un-repaired following a prior earthquake) bottom flange fractures on the seismic response of a steel frame in term of maximum inter-story drift ratio is investigated

next.

Consider first, for simplicity, that the 3-story SAC building at Los Angeles has 3 and 6 bottom flange fractures respectively, as shown in Figure 6.11, assumed to be distributed randomly in the building. As discussed in Chapter 2, the yield strength of a damaged connection decreases to 40% of the original strength, and the stiffness decreases to 20% of its original stiffness (Refer to Figure 2.1). The backbone curve for the connection is presented in Figure 6.12. Next, undamaged and damaged 3 story frames in Figure 6.11 are excited by an ensemble of 30 earthquake ground motions (la01-la20 and la21-la30). The maximum inter-story drift ratios (θ) under all ground motion are recorded, and their relationships with the spectral acceleration (S_a) are presented in Figure 6.13. The maximum inter-story drift ratio is only weakly related to the number of existing beam bottom fractures of the building.

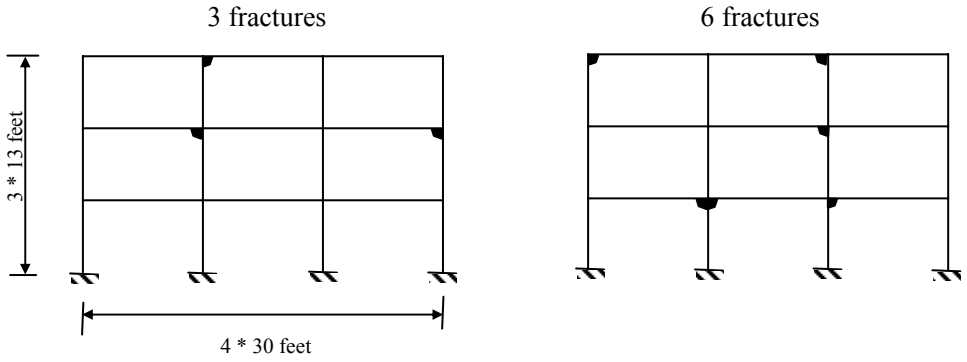

Figure 6.11 Example of damage in 3-story LA frame

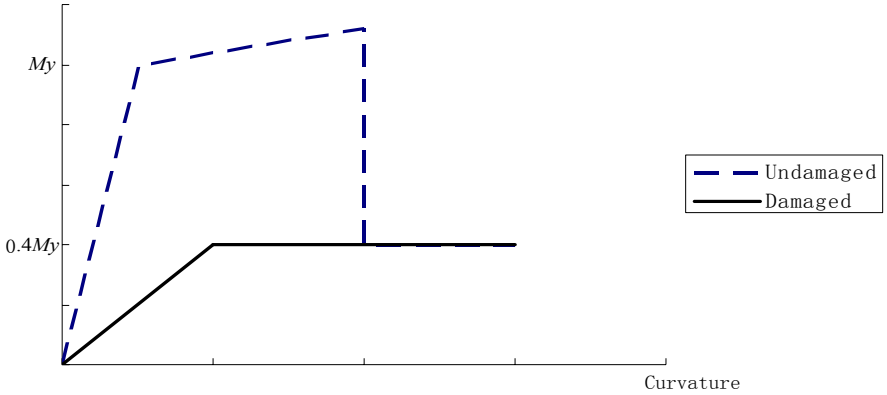

Figure 6.12 Moment-curvature relationship of damaged beam-column connections

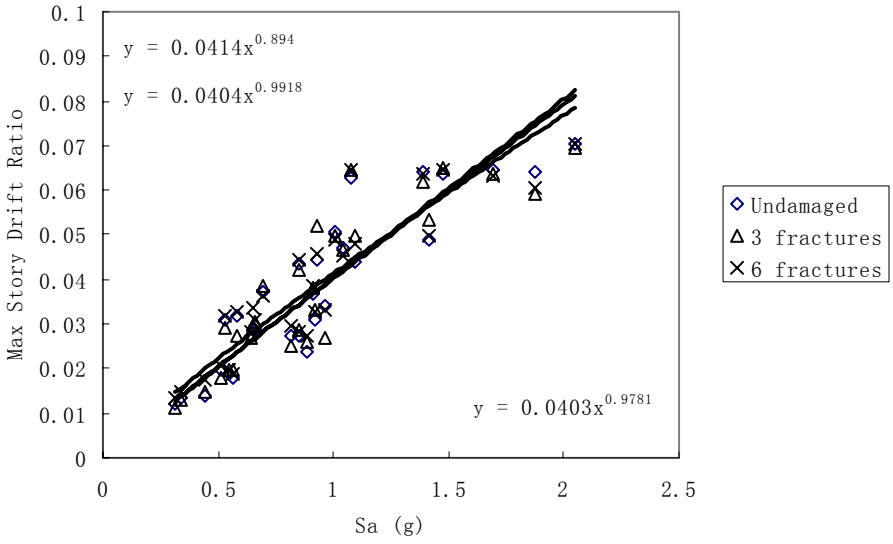

Figure 6.13 θ vs S_a for undamaged and damaged LA 3-story frames

Similar observations can be made for the 9-story building frame. The maximum inter-story drift ratios of the undamaged, light damaged, moderate damaged and major damaged building subjected to la01-la30 earthquake ground motions are presented in Figure 6.14. (Detailed information regarding the definition of damage states will be presented in the next section). The four relationships are so close that the seismic demands (and, by inference, the estimated seismic risk) on an undamaged frame and damaged frames with increasingly severe states of damage are virtually the same. This suggests that the maximum inter-story drift ratio may not be informative as a damage measure for an existing building because it cannot discriminate the performance of undamaged and damaged frames. A more informative damage measure would reflect the effect of initial (or existing) structural damage, and correlate well with the seismic intensity measure.

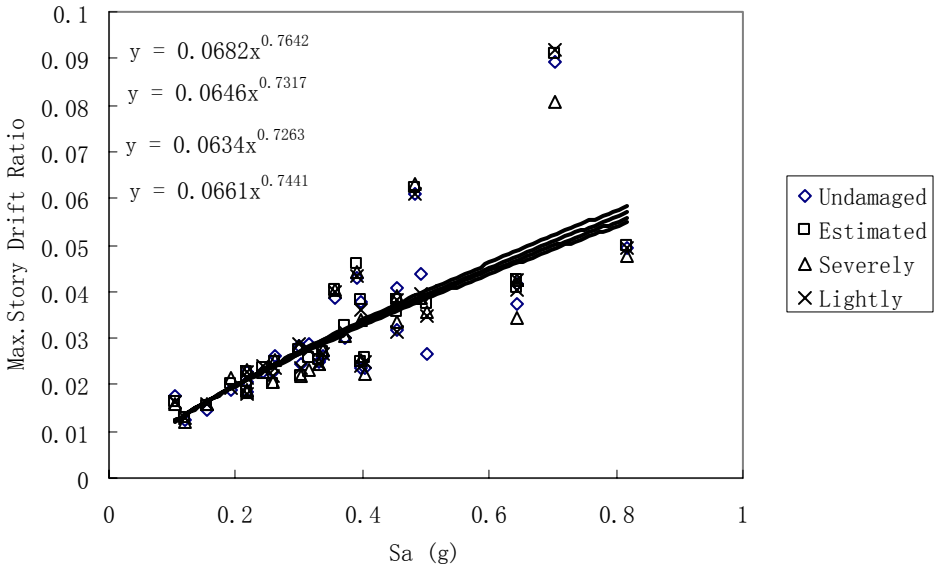

Figure 6.14 θ vs S_a for undamaged and damaged LA 9-story frames

6.4.2 Maximum floor acceleration and dissipated energy

In this section, two additional structural response parameters are investigated: maximum floor acceleration and dissipated energy.

The maximum floor acceleration ($A_{\max}$) is related to the maximum seismic force applied at any level in the structure. The dissipated energy (E_{dis}) is related to the hysteretic behavior of the structure, which is defined in the following:

$$E_{dis} = \sum_{i=1}^{n} \sum_{t} F_{i,t} \Delta D_{i,t} \tag{6.7}$$

in which n is the total number of floors, $F_{\text{i,t}}$ is the equivalent seismic force applied to floor i at time t, and $\Delta D_{\text{i,t}}$ denotes the floor i's displacement increase under floor force $F_{\text{i,t}}$. In equation (6.7), it is assumed that the energy is dissipated solely in the beam-to-column connections.

These two structural response parameters are investigated using the 9-story frame. Two different damage states are considered: (1) all the connections at floors 1 and 2 fracture, and (2) all the connections at floors 1, 2, 7 and 8 fracture. The relationship between maximum floor acceleration and spectral acceleration is presented in Figure 6.15. The relationship between dissipated energy and earthquake spectral acceleration is presented in Figure 6.16. The maximum floor acceleration decreases when structural damage becomes severe because of the softening effect caused by structural damage. The ability to dissipate seismic energy is also decreased when the structural damage becomes severe, as shown in Figure 6.16. However, neither maximum floor acceleration nor dissipated energy appears to correlate particularly well with spectral acceleration. Thus, it will be assumed that damage can

be measured simply by the total number of damaged beam-column connections.

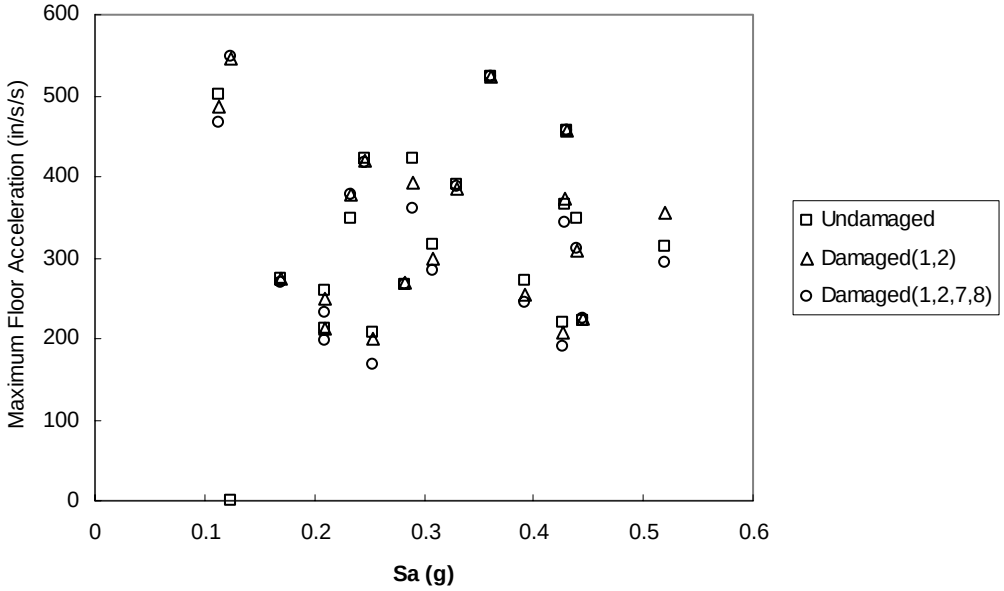

Figure 6.15 Maximum floor acceleration vs earthquake spectral acceleration

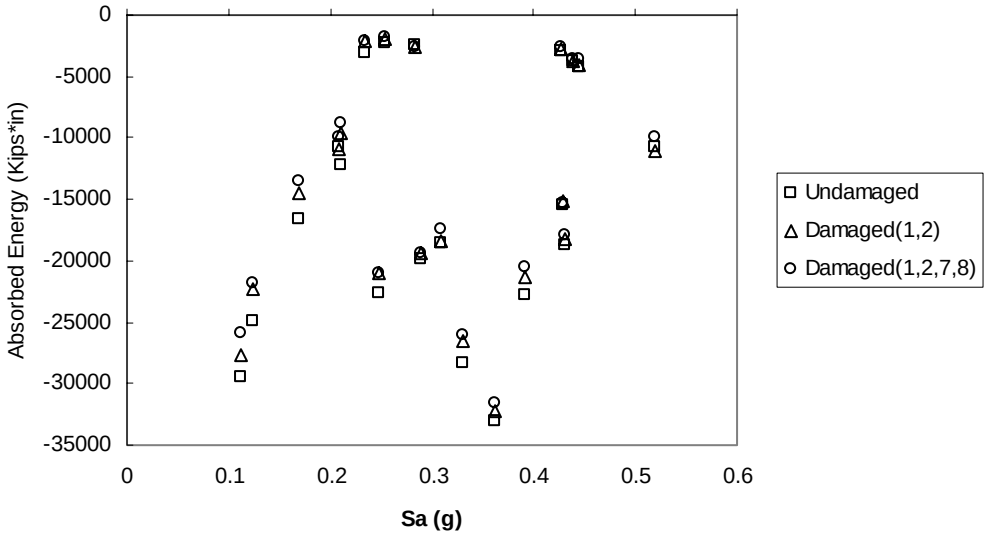

Figure 6.16 Dissipated energy vs earthquake spectral acceleration

6.4.3 Mapping between the damage ratio and damage state

One advantage of the maximum inter-story drift ratio (θ_{max}) as a damage measure is that the mapping between θ_{max} and the damage state of the structure has been studied and established (FEMA-273). In this Chapter, the damage ratio of beam-column connections is used as damage measure. The mapping between connection damage ratio (D) and damage states is investigated further in the following paragraphs.

The damage ratio of beam-column connections is closely related to the repair cost of the damaged building. For example, if the repair cost for a damaged building exceeds the cost to replace it, the building can be viewed as "severely damaged". Generally, owners do not like to divulge information on the structural repair cost, and available information is limited. In this study, the following information is used. (1) According to SAC damage inspection and repair evaluation of SMRF buildings following the Northridge Earthquake[3], repair costs for damaged connections range from \$3,000 to \$20,000 per connection, but are typically in the \$5,000 to \$8,000 range. In addition, the owner's hidden costs associated with tenant expenses and lost rent may range from \$0 to \$45,000 per connection. From the newest Sweet's Catalog[4], the cost to fabricate a welded moment-resisting connection ranges from \$2,000 to \$5,000. Therefore, the repair cost is approximately 2 to 20 times the fabrication cost per connection if the indirect costs such as business interruption are taken into account. (2) It is also recommended that, for steel construction, approximately 50% of

[3] SAC Document from http: //www.sacsteel.org / background / gates1-p1.html (assessed on 01/07/2006)

[4] The author is grateful to Professor Schmeckpeper for guiding him to this source of data.

the costs are used in fabricating the beam-column connections (including material cost, production cost, coating cost and erection cost)[5] (3) The ratio of the number of moment connections to gravity connections in a steel building ranges from 1: 2 to 1: 4. (4) The cost of a moment connection is 2 to 4 times the cost of a gravity connection. (5) The survey of frame damage following the Northridge earthquake shows that the ratio of the number of damaged moment connections to damaged gravity connections ranged from 3:2 to 20: 1.[6] According to the above information, the mapping between connection damage ratio and damage state will be established.

Assuming that the total number of moment connections of a steel building is n, then the number of gravity connections ranges from $2n$ to $4n$ according to (3). This number is assumed to be uniformly distributed for simplicity. If c is the average cost to fabricate a moment connection, then the average cost to fabricate a gravity connection is $0.25c$ to $0.5c$ according to (4). This average cost also is assumed to be uniformly distributed. The repair cost per connection is 2 to 20 times the fabrication cost according to (1) and the range becomes narrower as the connection damage ratio increases. A summary in the SAC document noted above[4] provides some information on the range of repair costs as well as their likely values. This information is encoded by a triangular relative frequency, as shown in Figure 6.17: Finally, the ratio of damaged connections in a gravity frame is assumed to be 1/20 to 2/3 of the ratio for a moment frame and is assumed to be uniformly distributed according to information

[5] AISC document from http://www.aisc.org/Content/ContentGroups/ Documents / Connections_IV_Proceedings/14.pdf (assessed on 01/07/2006)

[6] SAC Document from http: //www.sacsteel.org / background / gates1-p1.html. (assessed on 01/07/2006)

(5).

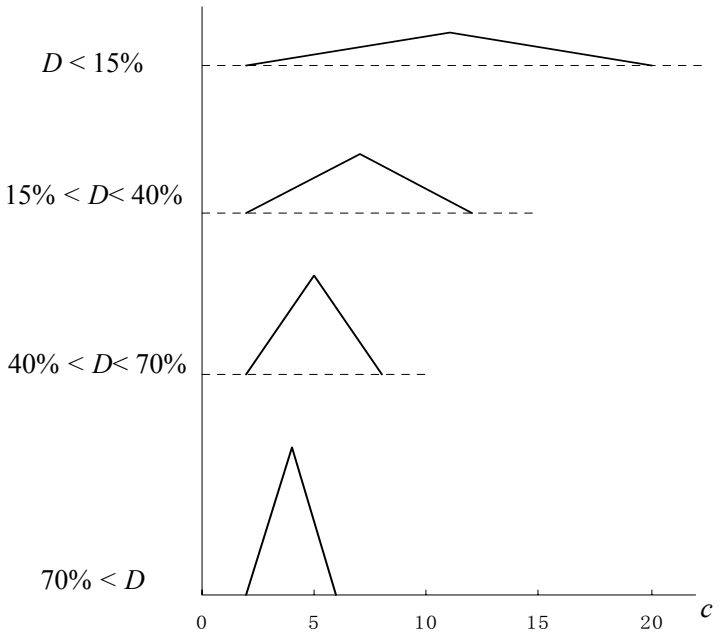

Figure 6.17 The probability distribution of repair cost for different connection damage ratio

The damage states (light, moderate, major and severe damage) are defined in term of connection damage ratio, as shown in Table 6.5. The probability distribution of repair cost (expressed as a percentage of replacement cost) for different moment connection damage ratios is calculated, and also is summarized in Table 6.5. Light damage seldom causes repair costs exceeding 50% of replacement cost; for moderate damage, the repair cost ranges between 20% to 70% of replacement cost. When damage is major, the repair cost is frequently more than 50% of the replacement cost,

and in fact exceeds replacement cost with probability of 23%. For "severe" damage, the probability that repair cost exceeds replacement cost is 55%, indicating that the building probably should be replaced rather than repaired. The expected repair costs for different damage states, presented in the last line of Table 6.5, will be used to assess damage in terms of repair cost in the next section.

Table 6.5 Relative frequency of repair cost for different moment connection damage ratios

D / $C_{repaire}$	0 – 15% (light)	15% - 40% (moderate)	40% - 70% (major)	70% - 100% (severe)
0 - 10%	0.2254			
10% - 20%	0.2069	0.0224		
20% - 30%	0.173	0.1117	0.0028	
30% - 40%	0.1456	0.1623	0.0223	
40% - 50%	0.1085	0.1955	0.0684	0.0035
50% - 60%	0.0695	0.1608	0.1167	0.0228
60% - 70%	0.0405	0.129	0.1502	0.062
70% - 80%	0.0182	0.0942	0.1549	0.0917
80% - 90%	0.0093	0.0639	0.1426	0.1243
90% - 100%	0.0031	0.0398	0.1136	0.1423
> 100%		0.0204	0.2285	0.5534
E [C_{repair}]*	0.274	0.532	0.775	0.917

*If the repair cost exceeds the replacing cost, it is assumed to equal the replacing cost in calculating E [C_{repair}].

6. 5 Conditional assessment of damaged structure

Damage assessment combines the existing damage state with the probabilistic seismic hazard for a given structure at a designated site. The probability of exceeding a particular damage state (measured by the total number of damaged connections n_d) is expressed as:

$$P[n_d > x] = \iint P[n_d > x \mid DM = y, IM = z] \cdot f_{DM}(y)dy \cdot f_{IM}(z)dz \tag{6.8}$$

where DM denotes damage state, whose definition and distribution are obtained by damage inspection, as described in Section 6.3 and IM denotes earthquake intensity measure.

In practice, Equation (6.8) can be evaluated with the following formula:

$$P[n_d > x \mid n_{d,est} = y] = \sum_{IM} \sum_{n_{d,act}} P[n_d > x \mid n_{d,ini} = p, IM = z] \cdot P[n_{d,ini} = p \mid n_{d,est} = y] \cdot P[IM = z] \tag{6.9}$$

where $n_{d,\mathrm{est}}$ is the estimated number of damaged connections and $n_{d,\mathrm{ini}}$ is the probable initial number of damaged connections provided the estimated $n_{\mathrm{d,est}}$. The first term on the right side of Equation (6.9) should be evaluated by simulating the damage state and performing a probabilistic seismic demand analysis, while the second term is evaluated from the probability distribution of $n_{\mathrm{d,act}}$ when $n_{\mathrm{d,est}}$ is given. The calculation of this conditional probability will be illustrated in the following examples.

Parameter $n_{\mathrm{d,est}}$ is non-negative, and is assumed to be described by a lognormal distribution for simplicity (the 9 and 20-story buildings have a sufficient number of connections that the discrete distribution can be replaced with a continuous one.). Two sources of uncertainty must be considered: the variability produced by the

earthquake itself, expressed as $\sigma_{n_t|IM}$, and the variability produced by the estimated number of damaged connections, expressed as $\sigma_{n_t|n_{est}}$ .The source of $\sigma_{n_t|n_{est}}$ includes two parts: (1) variability associated with the estimated damage, and; (2) variability introduced by different damage patterns that may be associated with an identical damage ratio. The first part can be evaluated with Equation (6.3). The second part will be investigated in the following.

Consider, as an illustration, damage assessment of the 9-story frame. Assuming that the frame suffers damage to 36 beam-column connections, two different damage patterns are considered. In the first, damage to connections occurs at floors 1, 2, 3 and 4, while in the second, the damaged connections are found at floors 6, 7, 8 and 9. The damaged building now is subjected to an ensemble of earthquake ground motions (la01 to la20). The number of damaged connections following the earthquakes is presented in Figure 6.18. The number of damaged connections following the second earthquake is affected by the initial distribution of damage within the system. In this example, if the structural damage from the first earthquake had accumulated in the upper stories, a significant amount of additional structural damage would occur in the lower stories if a second earthquake were to occur. On the other hand, if the structural damage accumulate in the lower stories, the additional structural damage occurring at upper stories is not significant. The reason is that the frequency characteristics of ground motions la01-la20 make the lower stories more vulnerable to connection damage than the upper stories.

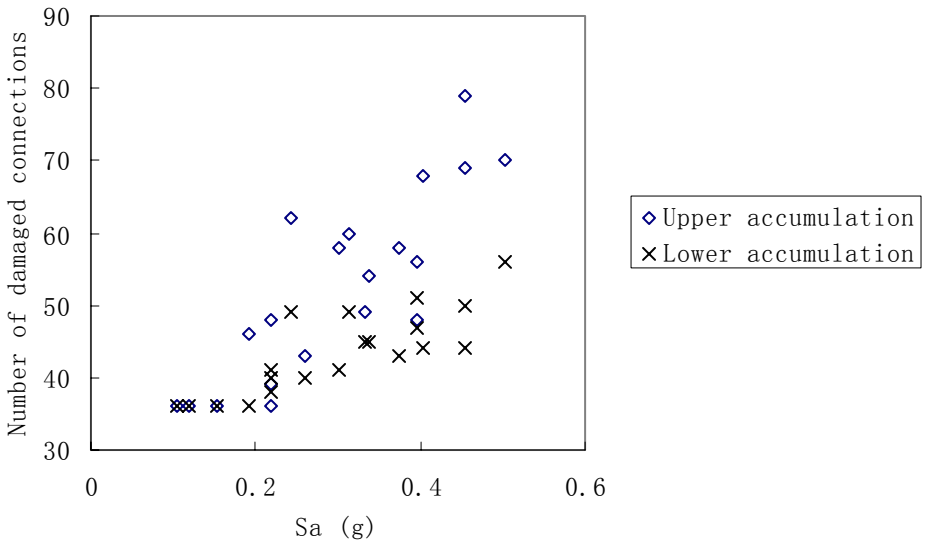

Figure 6.18 Influence of initial damage pattern on structural damage from subsequent earthquake

Considering the significant influence of the pattern of pre-existing damage (by story) on subsequent damage caused by strong ground motion, it is important to identify the most vulnerable floors of the existing building correctly. With the aid of the Enhanced Uncoupled Modal Response History Analysis (EUMRHA) described previously, the vulnerable floors can be identified quickly. Furthermore, the analysis-based inspection method described earlier identifies the damage pattern correctly, as illustrated in Section 6.3, providing an important advantage over random inspection. Therefore the variance caused by different damage patterns is neglected in the following analysis.

Next, the damage assessment of existing buildings will be illustrated using two examples: the 9-story and 20-story steel building frames considered previously.

(1) 9-story steel building frame

The structural analysis using EUMRHA indicates that floors 1 and 7 are most vulnerable to connection damage, so the damage inspection begins at those floors. If damaged beam-column connections are found, the neighboring floors are inspected next. Floors 4, 5 and 9 are un-inspected floors, and 6 connections at those floors are selected randomly for inspection. The results of the analysis-based inspection are shown in Figure 6.19 (a), where the semi-circles denote the beam-column connections that were inspected, and the squares denote randomly inspected connections. The open circles and squares indicate undamaged connections, while the black ones indicate damaged connections. The estimated damage state of the 9-story building is shown in Figure 6.19 (b). However, as mentioned above, the variance in the analysis-based inspection method and the possibility of more severe or lighter structural damage must be taken into account. The most severe damage state (all un-inspected connections are assumed to be damaged in the damaged floors, r_d = 40%, "Major damage") and lightest damaged state (all un-inspected connections are assumed to undamaged in the damaged floors, r_d = 12%, "Light damage") are presented in Figures 6.19 (c) and (d). It should be noted that some damaged connections are scattered around the un-inspected floors. According to Equation (6.3), on average, there are $\frac{1}{8} \times (27 - 6) = 2.625$ damaged connections scattered among the un-inspected floors. These scattered damaged connections have little influence on structural behavior, so their locations are positioned randomly in modeling the damaged structure.

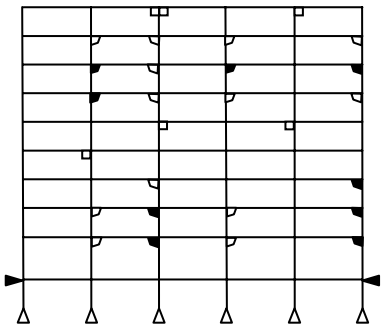

(a) Inspection result
(9 of 22 connections are damaged)

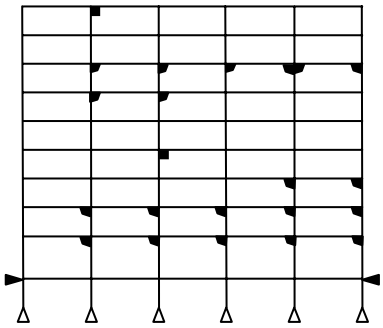

(b) Estimated damage state
(damage ratio = 22/ 90)

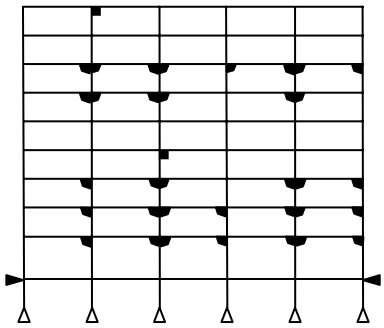

(c) Most severe damage state
(damage ratio = 36/ 90)

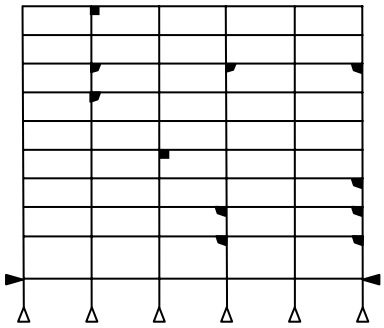

(d) Lightest damage state
(damage ratio = 11/ 90)

Figure 6.19 Damage inspection and estimated locations of damaged connections

An ensemble of ground motions (la01-la30) then was applied to the damaged buildings and the number of connections found to be damaged after the earthquake was counted for the entire structure. This number is related to the spectral acceleration, as summarized in Figure 6.20.

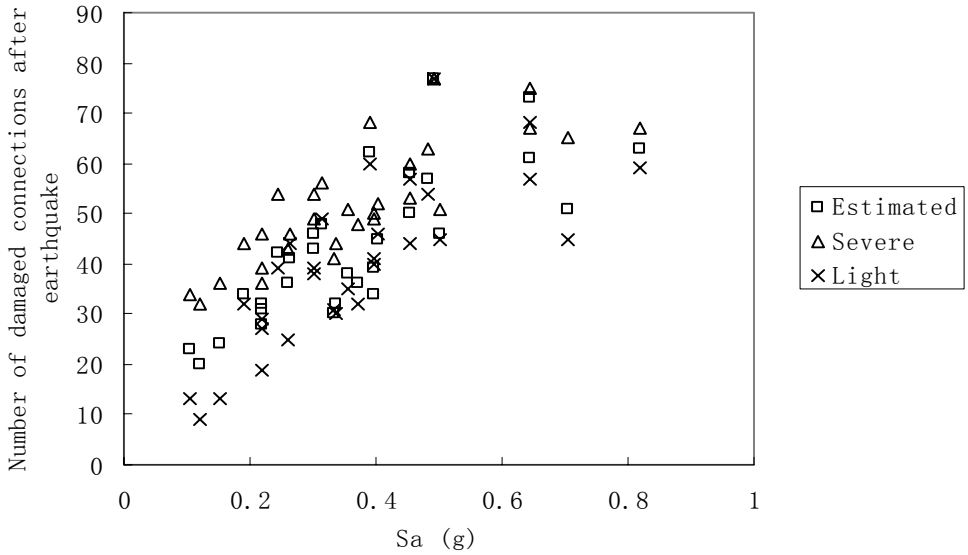

Figure 6.20 Number of damaged connections after earthquake vs spectral acceleration for damaged 9-story structure

The influence of the initial number of damaged connections on the final number weakens as the earthquake intensity becomes stronger. To illustrate the additional damage caused by an earthquake to a building that was damaged previously, the additional number of damaged connections $n_{\mathrm{d,add}}$ is presented in Figure 6.21. The mean relationship between $n_{\mathrm{d,add}}$ and S_a can be approximated by:

$$n_{d,add}(S_a) = a_0 + a_1 S_a + a_2 S_a^{\,2} + a_3 S_a^{\,3} \tag{6.10}$$

This relationship should have the following properties:

(1) be non-negative and intersect the origin; thus, $a_0 = 0$;

(2) $n_{d,add}$ equals the total number of undamaged connections when S_a is sufficiently large. For the 9-story building, all connections are assumed to be

damaged when S_a = 1.0g. This trend can be seen in Figure 6.19.

(3) $\frac{dn_{d,add}}{dS_a} > 0$

(4) $\frac{dn_{d,add}}{dS_a} = 0$ when S_a is sufficiently large; in this case, when S_a = 1.0g.

Properties (1), (2) and (4) provide 3 equations; a fourth equation is provided by assuming the relationship includes the point (Mean (S_a), Mean (n_{add})). Therefore, the parameters are solved for different number of initial damaged connections. If the number of initial damaged connections equals 11 (light damage):

$$n_{d,add}(S_a) = 32.4S_a + 151.3S_a^{\,2} - 111.6S_a^{\,3} \tag{6.11a}$$

If the number of initial damaged connections equals 22 (estimated moderate damage)

$$n_{d,add}(S_a) = 5.6S_a + 171.8S_a^{\,2} - 116.4S_a^{\,3} \tag{6.11b}$$

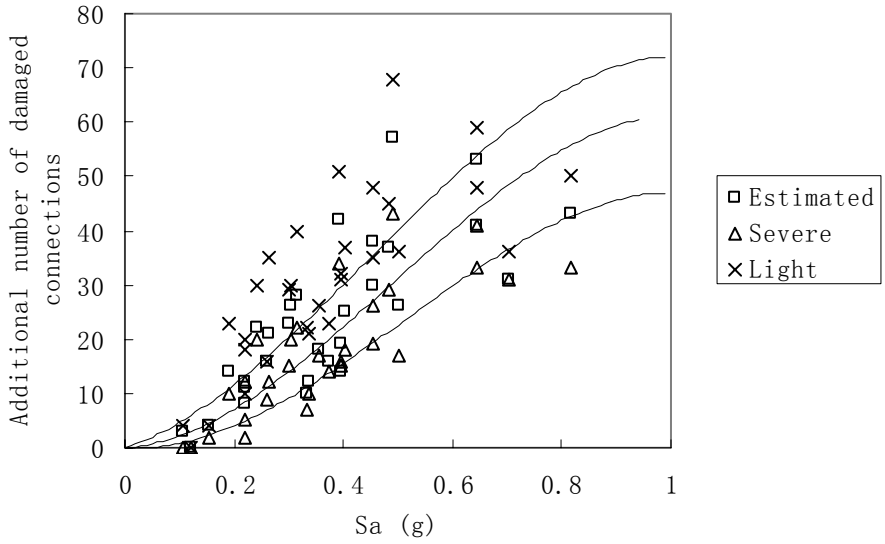

Figure 6.21 Number of additional damaged connections after earthquake vs spectral acceleration for damaged 9-story frame

Finally, if the number of initial damaged connections is 36 (major damage)

$$n_{d,add}(S_a) = -7.0S_a + 154.9S_a^{\,2} - 100.9S_a^{\,3} \tag{6.11c}$$

These curves are also presented in figure 6.20. For comparison, the n_{add} for non-damaged ($n_{\text{ini}} = 0$) building is:

$$n_{d,add}(S_a) = 55.8S_a + 158.4S_a^{\,2} - 124.2S_a^{\,3} \tag{6.11d}$$

The standard deviations $\sigma_{n_{add}|S_a}$ calculated for initial damage states of "major", "moderate", "light" and "non-damaged" are 6.7, 8.1, 9.4 and 11.6, respectively.

Therefore, given that the number of initial damaged connections is z, the probability that more than *x* beam-column connections are damaged in the subsequent earthquake is:

$$P[n_d > x \mid S_a = y, n_{d,ini} = z] = 1 - \Phi\left(\frac{\ln(x) - \ln(n_{d,add}(y) + z)}{\xi}\right) \tag{6.12}$$

The first term in Equation (6.9) is solved for $n_{\text{d,ini}} = 11$, 22 and 36. From Eq. (6.1) and (6.4), $\mu_{n_{d,ini}} = 22$ and $\sigma_{n_{d,nii}}^{\,2} = 22.95$. The second term in Equation (6.9), $P[n_{\text{d,ini}} = p \mid n_{\text{d,est}} = 22]$ for $p = 11$, 22 and 36, will be calculated according to PE rules described in Chapter3. Solving the equations:

$$\begin{bmatrix} 1 & 1 & 1 \\ 11 & 22 & 36 \\ 11^2 & 22^2 & 36^2 \end{bmatrix} \cdot \begin{bmatrix} P[n_{d,ini} = 11 \mid n_{d,est} = 22] \\ P[n_{d,ini} = 22 \mid n_{d,est} = 22] \\ P[n_{d,ini} = 36 \mid n_{d,est} = 22] \end{bmatrix} = \begin{bmatrix} 1 \\ 22 \\ 22^2 + 22.95 \end{bmatrix} \tag{6.13}$$

one obtains $P[n_{d,ini} = 11 \mid n_{d,est} = 22] = 0.083$; $P[n_{d,ini} = 22 \mid n_{d,est} = 22] = 0.851$; $P[n_{d,ini} = 36 \mid n_{d,est} = 22] = 0.066$.

If this damaged and un-repaired structure were to be excited by an earthquake with spectral acceleration of 0.4g in the future, the probabilities of resulted damage states can be calculated, as presented in Table 6.6.

Table 6.6 Damage state probabilities estimated for future earthquake (S_a = 0.4g)

Damage State	n_{ini}	P[n_d < x | $n_{d,ini}$]	P[$n_{d,ini}$ | $n_{d,est}$]	P [Damage State]
Light	11	0.000196	0.083	0
(0, 13.5)	22	0	0.851	
x = 13.5	36	0	0.066	
Moderate	11	0.34039	0.083	0.279
[13.5, 36)	22	0.294973	0.851	
x = 36	36	0	0.066	
Major	11	0.92009	0.083	0.574
[36, 63)	22	0.853988	0.851	
x = 63	36	0.753314	0.066	
Severe	11	1.0	0.083	0.147
[63, 90)	22	1.0	0.851	
x = 90	36	1.0	0.066	

The probability distributions of repair cost C_{repair} and its expected values for different damage states were summarized in Table 6.5. The expected repair cost is calculated by:

$$E[C_{repair}] = \sum_{i=1}^{4} E[C_{repair} \mid \text{Damage state } i] \cdot P[\text{Damage state } i] \tag{6.14}$$

For this case, $E[C_{repair}]$ is $0.728C_{replace}$, which means if the building is un-repaired following the first earthquake, a future earthquake with S_a = 0.4g will cause the expected repair cost to increase from 0.532 $C_{replace}$ to $0.728C_{replace}$ (the estimated initial damage state is "moderate"). Figure 6.22 shows the results from repeating the calculation of $E[C_{repair}]$ for different S_a. The expected repair cost increases with the increase of the future earthquake's intensity.

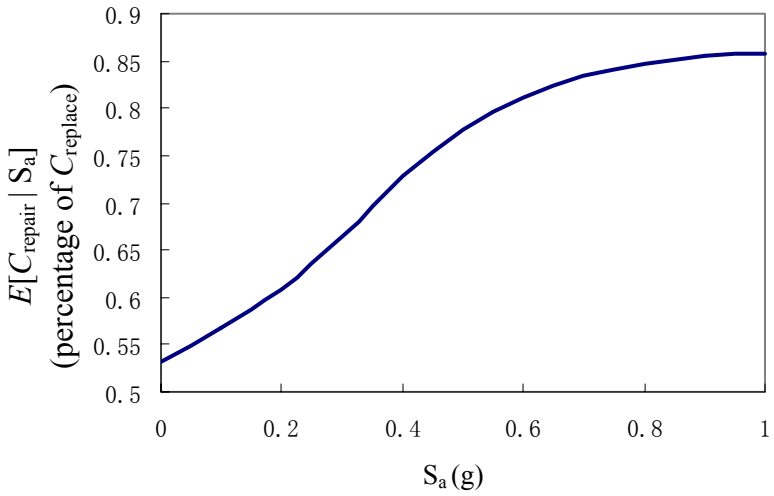

Figure 6.22 Expected repair cost for 9-story frame caused by a future earthquake

The probability distribution of C_{repair} for a damaged building is evaluated by:

$$P[C_{repair} > C_{limit}] = \sum_{i=1}^{4} P[C_{repair} > C_{limit} \mid \text{Damage state } i] \cdot P[\text{Damage state } i] \qquad (6.15)$$

If S_a = 0.4g, $P[C_{repair} > C_{replace}]$ is calculated to be 0.218. In other words, a future earthquake with S_a = 0.4g would increase $P[C_{repair} > C_{replace}]$ from 0.0204 (the estimated initial damage state is "moderate") to 0.218. Repeating these calculations of $P[C_{repair} > C_{replace}]$ for different S_a, one obtains the vulnerability curve in Figure 6.23. If the building is repaired immediately after the damage occurs, the probability of $[C_{repair} > C_{replace}]$ is 0.21. This probability increases to 0.45 if the repair work is postponed and is performed only after an earthquake with S_a = 0.8g.

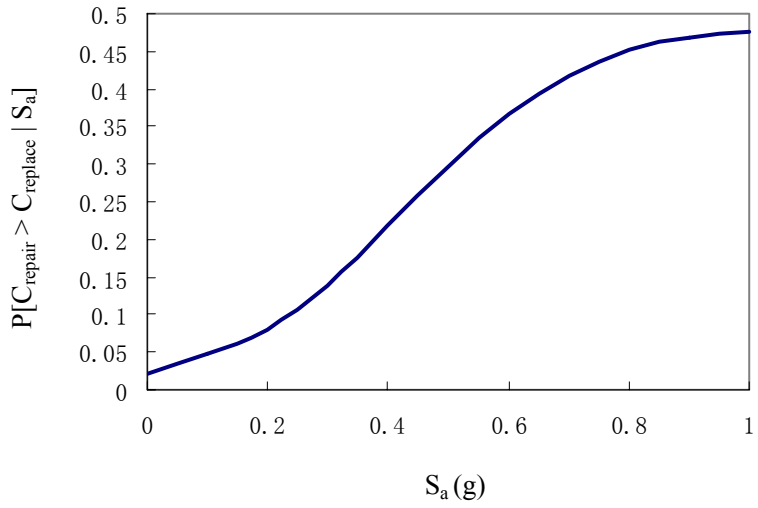

Figure 6.23 Vulnerability curves for $P[C_{repair} > C_{replace} \mid n_{d,est} = 22]$ (9-story building)

The above analysis provides useful information on the possible future consequences if the damaged structure is not repaired following the first earthquake. Such information could help the owner to decide whether or not to repair the damaged building immediately. This sort of analysis would be most useful if the damage state following the first earthquake is "light". If the damage is severe, most owners would simply replace the building, rather than perform this sort of evaluation.

(2) 20-story steel building frame

A similar damage inspection and fragility analysis are performed for the 20-story building frame. The results of the analysis-based inspection are shown in Figure 6.24(a), where the semi-circles denote the beam-column connections that were inspected based on the structural analysis, while the squares denote randomly inspected connections. The open circles and squares indicate connections that were

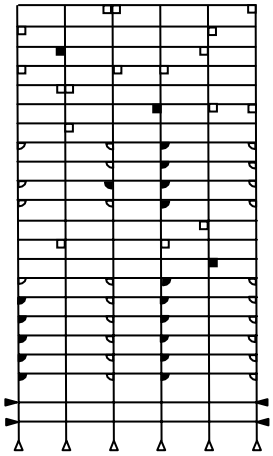

(a) Inspection result
(20 of 60 connections are damaged)

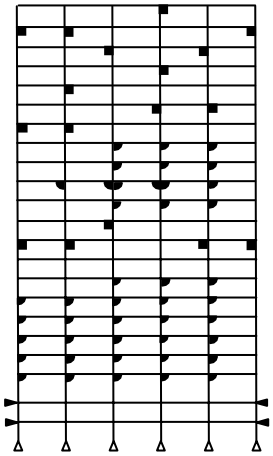

(b) Estimated damage state
(damage ratio = 60/ 200)

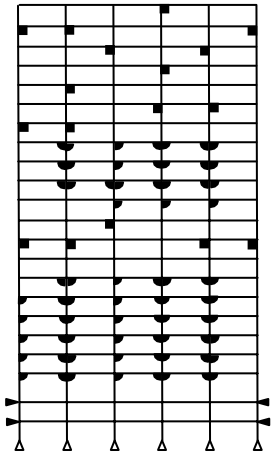

(c) Most severe damage state
(damage ratio = 88/ 200)

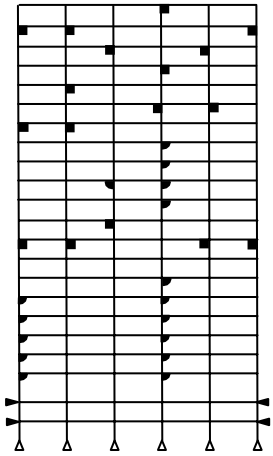

(d) Lightest damage state
(damage ratio = 30/ 200)

Figure 6.24 Inspection and estimated locations of damaged connections in 20-story frame

found to be undamaged, while the black ones indicate connections found to be damaged. The estimated damaged state of the 20-story frame is shown in Figure 6.24 (b). Possible severe damage and light damaged states are shown in Figures 6.24 (c) and (d). The damaged connections (on average, $3+\frac{4}{22}*80=17.55$) estimated by random inspection are sampled randomly in the damaged structure modeling.

Next, an ensemble of ground motions (la01-la30) was applied to the damaged 20-story frame and the number of damaged connections following the earthquake was calculated by NLTHA. The relationship between the number of additional damaged connections (n_{add}) and the spectral acceleration is presented in Figure 6.25.

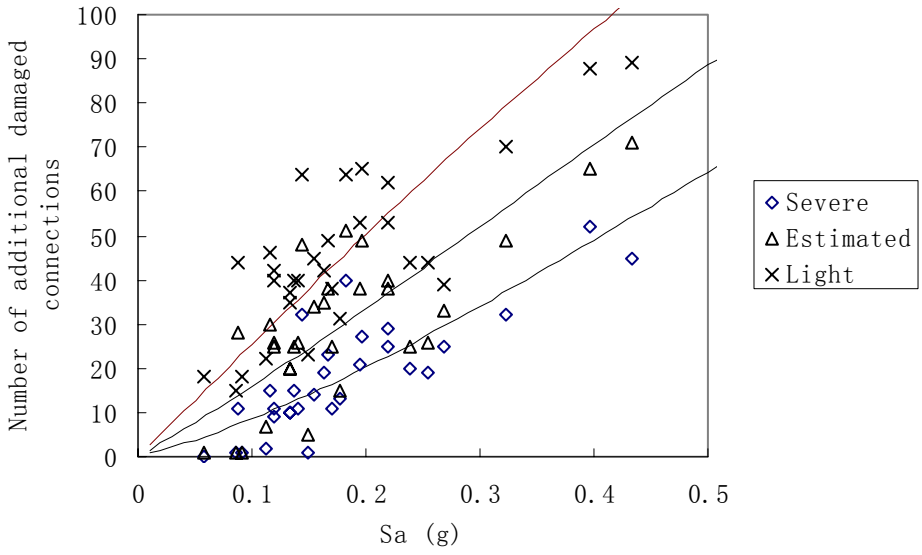

Figure 6.25 Number of additional damaged connections following earthquake vs spectral acceleration for previously damaged structure

Using the procedure described for the 9-story frame, the parameters in Equation (6.10) for the 20-story frame are determined, yielding the following relationships between number of additional damaged connections and S_a:

Number of initial damaged connections = 30 (light damage)

$$n_{add}(S_a) = 255.4S_a - 0.813S_a^{\,2} - 84.6S_a^{\,3} \tag{6.16a}$$

Number of initial damaged connections = 60 (estimated moderate damaged)

$$n_{add}(S_a) = 148.3S_a + 123.5S_a^{\,2} - 131.7S_a^{\,3} \tag{6.16b}$$

Number of initial damaged connections = 88 (major damage)

$$n_{add}(S_a) = 67.0S_a + 201.9S_a^{\,2} - 157.0S_a^{\,3} \tag{6.16c}$$

These curves are also presented in figure 6.25. If $n_{ini} = 0$ (undamaged building):

$$n_{add}(S_a) = 306.1S_a - 12.1S_a^{\,2} - 94.0S_a^{\,3} \tag{6.16d}$$

Table 6.7 Damage state probabilities estimated for future earthquake ($S_a = 0.3g$)

Damage State	n_{ini}	P[n_d < x | $n_{d,ini}$]	P[$n_{d,ini}$ | $n_{d,est}$]	P [Damage State]
Light	30	0	0.083	
(0, 30)	60	0	0.851	0
x = 30	88	0	0.066	
Moderate	30	0.062844	0.083	
[30, 80)	60	0.039603	0.851	0.039
x = 80	88	0	0.066	
Major	30	0.95588	0.083	
[80, 140)	60	0.786425	0.851	0.753
x = 140	88	0.738682	0.066	
Severe	30	1.0	0.083	
[140, 200)	60	1.0	0.851	0.208
x = 200	88	1.0	0.066	

The standard deviations calculated for initial damage states "major", "estim ated moderate", "light" and "undamaged" are 7.7, 11.5, 12.8 and 14.4, respecti vely.

According to Equations (6.1), (6.4), (6.5) and (6.6), $\mu_{n_{ini}}$ =60.55; $\sigma_{n_{ini}}^{2}$ = 81.197. Using the PE method, $P[n_{d,ini} = p \mid n_{d,est} = 60]$ is calculated for p = 30, 60 and 88, similarly Eq. (6.13), yielding the probability concentrations:

$P[n_{d,ini} = 30 \mid n_{d,est} = 60] = 0.047$; $P[n_{d,ini} = 60 \mid n_{d,est} = 60] = 0.903$;

$P[n_{d,ini} = 88 \mid n_{d,est} = 60] = 0.05$.

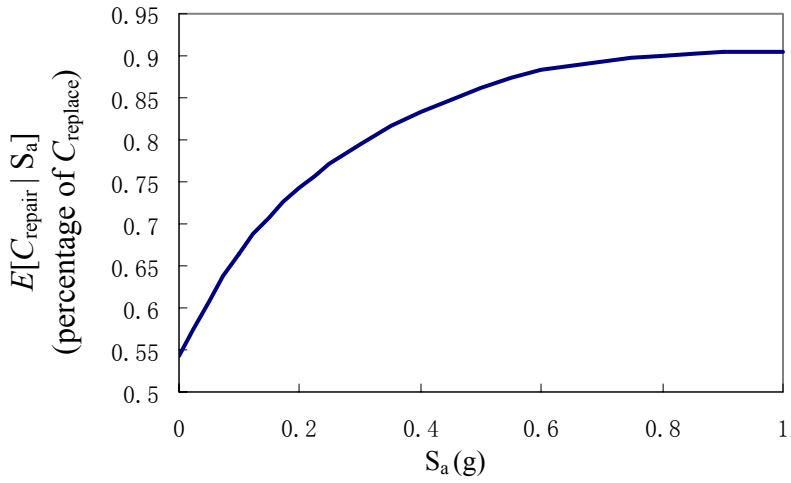

Figure 6.26 Expected repair cost to 20-story frame caused by a future earthquake

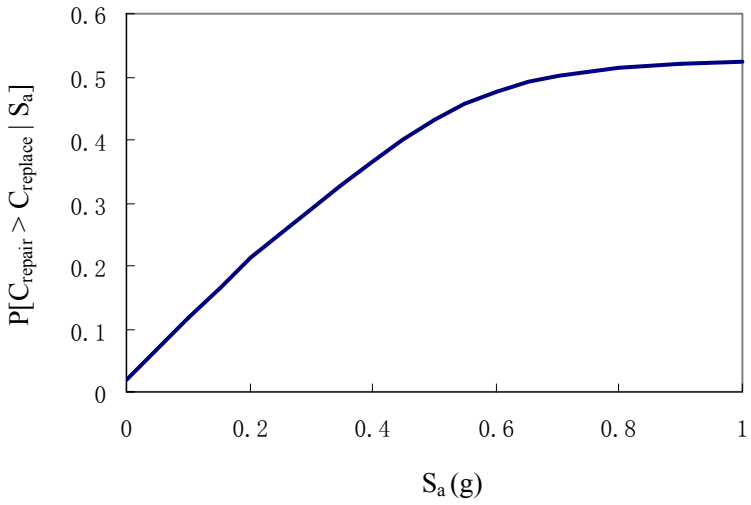

Figure 6.27 Vulnerability curves for $P[C_{repair} > C_{replace} \mid n_{d,est} = 60]$ (20-story building)

6.6 Summary

This chapter investigated patterns of connection damage in steel moment-resisting frames subjected to an earthquake, considering the uncertainties associated with workmanship quality. These damage patterns appear to be governed mainly by the structural properties of the buildings and frequency characteristics of earthquakes, even when the quality of workmanship is poor and significant uncertainties are introduced in the beam-column connection behavior.

Based on this observation, an analysis-based inspection scheme was proposed and its probability model was developed. When compared to method suggested by FEMA-352, where the connections to be inspected are selected randomly, the analysis-based inspection scheme reduces the variance associated with estimated

damage to the frame. Moreover, the connection damage patterns can be identified accurately by analysis-based inspection, which is important for post-earthquake analysis and damage assessment of a damaged building.

Post-Northridge earthquake surveys of building damage suggested that damage to welded connections occurred mainly in the bottom beam flange-to-column flange weld. If only these bottom-flange fractures are considered, the seismic response of a damaged frame in terms of the maximum inter-story drift ratio is not significantly different from the response of the comparable undamaged frame. Thus, inter-story drift (or changes in inter-story drift) does not appear to be a good indication of connection damage. Therefore, the number of damaged connections is used as structural damage parameter in this chapter. As illustrated by the examples, the proposed procedure can provide information that can be used to decide whether or not to repair a damaged frame immediately after an earthquake and as a basis for estimating the cost of connection repair in a damaged frame.

CHAPTER 7: CONCLUSIONS AND RECOMMENDATIONS

7.1 Conclusions

Structural performance evaluations and seismic reliability analyses of complex structural systems are required to develop and implement performance-based and consequence-based earthquake engineering methods. This dissertation developed and validated several computational procedures that are aimed at relieving the significant computational burdens that involved in PBE and CBE. Specific advances were made in (1) Interval Point Estimate Sampling (IPES), which is an efficient sampling technique to reduce the effort required to perform reliability analysis of structural frames subjected to earthquake ground motions; (2) Enhanced Uncoupled Modal Response History Analysis (EUMRHA), an efficient structural seismic response analysis procedures to make time history dynamic analysis of structural response in the nonlinear range less time-consuming; and (3) probabilistic modeling of inspection of connections to assess damage. These techniques were used to investigate the structural behavior of steel buildings subjected to main shock – aftershock sequences and to assess the performance of an existing building in a future earthquake.

The IPES and EUMRHA accomplished the following research objectives:

1. The IPES technique is more efficient in covering the probability space than

Latin Hypercube Sampling and provides relatively stable and accurate estimates of response moments and probabilities for highly nonlinear performance functions and low-probability events. The Point Estimate method is especially convenient for those situations where, for reasons of efficiency, the samples for nonlinear finite element analysis are not selected purely at random (e.g. the magnitude of aftershocks in chapter 5 and the number of damaged beam-column connections in chapter 6). It is as accurate as regression analysis for this purpose, and more convenient to use.

2. The EUMRHA method yields reasonably accurate estimates of structural response (not only story drifts, but also locations of damaged beam-to-column connections) of both 9-story and 20-story steel frames. Statistically, the standard deviation in the ratio of inter-story drifts computed by the NLTHA and EUMRHA is less than 20% for the ensemble of 10%/50yr ground motions and less than 30% for the ensemble of 2%/50yr ground motions.
3. The estimated variation of inter-story drift response over the height of these frames agrees reasonably well with estimates obtained from NLTHA, suggesting that this method can provide a rapid estimate of the stories most likely to be damaged from an earthquake. This would be helpful for damage inspection.
4. The advantage of the EUMRHA over NLTHA with regard to computational efficiency is at least a one order of magnitude reduction, which is attractive for performing rapid assessments immediately following an earthquake, where a

decision must be made quickly whether or not to permit a damaged building to be re-occupied prior to completion of repairs. It also is useful in simulation-based reliability assessment and in performing parametric studies required to support the development of PBE and CBE.

Both NLTHA and EUMRHA methods are applied to investigate the performance of steel buildings during an earthquake main shock and subsequent aftershocks, and the main shock-aftershock sequences are modeled according to "replicate" and "randomization" assumptions respectively. Based on the analysis results, several conclusions are drawn:

5. The characteristics (amplitude and frequency content) of the aftershocks have a significant influence on the structural damage patterns that develop as a result of the aftershock. For the "replicate" assumption, the original damage pattern did not change as a result of the aftershock and the additional damage from the aftershocks did not depend on the initial damage from the main shock. On the other hand, under the "randomization" assumption the pattern of connection damage over the frame changed as a result of the aftershocks, to a degree depending on the characteristics of the aftershock ground motion. In this case, the additional damage from the aftershocks was related to the initial damage from the main shock.
6. If the damage ratio from the main shock is small (D_m < 30%), the "randomization" assumption led to a conservative estimate of damage from the aftershock relative to the "replicate" assumption. However, as the initial

damage ratio caused by the main shock increased, the estimates of aftershock damage under the two assumptions became closer. Regardless of which assumption was used, the probability that the aftershock causes large additional damage is small if the initial damage from the main shock is small.

7. A comparison of maximum inter-story drift ratios developed during sequences of main shock and aftershock revealed that the "replicate" assumption tended to overestimate the structural response because the characteristics of the principal ground motion that account for large structural deformations are reinforced by a replicate aftershock with the same frequency characteristics. Thus, such an assumption would lead to a conservative estimate of steel frame performance and damage accumulation during a main shock-aftershock sequence.

Finally, to assess the safety condition of existing buildings, an analysis-based inspection scheme based on an associated probability model of connection damage is proposed, and a procedure to assess the performance of un-repaired building in future earthquake is developed. Implementation of this model for the 9-story and 20-story steel frames showed that:

8. Compared with the purely random selection of inspected connections recommended in FEMA-352, the analysis-based inspection scheme reduces the variance in the number of damaged connections identified through the inspection process. Moreover, the connection damage patterns can be identified accurately by analysis-based inspection, which is very important for

post-earthquake analysis and damage assessment of a damaged building, where it may not be possible to inspect all the connections in the building frame.

9. The inter-story drift (or changes in inter-story drift) does not appear to be a good structural response parameter for assessing performance or for seismic reliability analysis of existing buildings. Instead, the beam-to-column connection damage ratio is a more informative performance parameter.
10. A procedure to assess the damage state of an existing building in terms of repair cost is introduced. This procedure can provide information that can be used to decide whether or not to repair a damaged building immediately after an earthquake and can be used as a basis for estimating the connection repair cost for a damaged building. This procedure is illustrated by an example.

7.2 Recommendations for Further Studies

Results from the analyses performed in this dissertation identified several topics worthy of further investigation.

1. The proposed EUMRHA achieved good estimates of structural responses of regular buildings where the building is symmetric in floor plan and regular in elevation, a situation in which the centers of structural rigidity and seismic mass coincide and the modes are effectively uncoupled. If the building is non-symmetric, its behavior is different under seismic load in different directions. Whether the accuracy of EUMRHA is impacted by the non-symmetry in building

plan or elevation needs to be investigated further. Moreover, all buildings analyzed in this dissertation have strong columns and weak beams. As a result, the beam-to-column connections at a given floor tend to fracture simultaneously, causing the structure's load capacity to decrease abruptly. On the other hand, if the building has weak columns and strong beams, yielding generally will occur in the panel zone rather than in the elements of the beam-to-column connection, and the sudden drop in loading capacity will not occur. The accuracy of the EUMRHA in predicting such structural behavior requires further investigation.

2. The relationship between the magnitudes of earthquake main shock and aftershocks proposed by Sunasaka and Kiremidjian was adopted in this dissertation to investigate the impact of main shock-aftershock sequences on damage accumulation. To model the aftershock ground motions, the Gutenberg-Richter law was assumed to determine appropriate scaling factors to derive the average intensities of aftershock ground motion ensembles. Moreover, the aftershocks were modeled using both "randomized" and "replicate" assumptions. The above assumptions may result in the modeled main shock – aftershock sequences having frequency contents that differ significantly from the actual sequences. The development of more realistic main shock – aftershock sequences is most important for further study on the structural behavior under main shock – aftershock sequences.

3. The maximum inter-story drift ratio (θ_{max}) is widely used as a damage measure, and the categorization of damage states (e.g. IO, LS, CP) in terms of θ_{max} has been

studied and established in FEMA-273/356. However, for the seismic reliability analysis of an existing building, θ_{max} is not entirely satisfactory as a structural response parameter, because it fails to reflect the influence of initial damage properly. In this dissertation, to evaluate the structural damage of an existing building, the damage states are categorized as “light”, “moderate”, “major” and “severe” in terms of beam-to-column connection damage ratio, which in turn can be related to the connection repair cost. Available cost information is limited because building owners generally do not like to divulge information on the structural repair costs. Moreover, the fracture of beam bottom flange at the column is the only damage type considered in this thesis, and each connection is classified as damage or undamaged, neglecting the classification of damage degree for each connection. As a result, this categorization should be modified when more information becomes available.

4. According to the proposed analysis-based inspection scheme, additional connections will be inspected if new connection damage is identified in the course of inspection. In other words, finding damaged connections serves as an incentive to inspect adjacent connections. The significant cost of conducting additional inspections, however, also needs to be taken into account. Practically, the additional amount of inspection is a function of what is found in the previous inspection by comparing the further inspection cost and the benefits of more inspection. The engineer must decide on an optimal amount of inspection, or to decide (in a sequential manner) whether to inspect further as new results are

discovered. A study should be performed to consider this optimization, in view of the constraints imposed by PBE.

BIBLIOGRAPHY

1. Abrams, D.P., Elnashai A.E. and Beavers J.E. (2002) "A new engineering paradigm: Consequence-based engineering", paper submitted to *Earthquake Spectra*, Earthquake Engineering Research Institute.

2. Amadio C., Fragiacomo M., Rajgelj S. (2003) "The effects of repeated earthquake ground motions on the non-linear response of SDOF systems" *Earthquake Engrg. & Struct. Dyn.* 2003; **32**: 291-308.

3. Antoniou, S., Pinho, R.(2004) "Advantages and limitation of adaptive and non-adaptive force-based pushover procedures" *Journal of Earthquake Engineering* 8(4) 497-522.

4. Bath, M. (1965) "Lateral inhomogeneities in the upper mantle" *Tectono-physics*, 2, 483-514, 1965.

5. Bazzurro, P. and Cornell, C.A. (1994a) "Seismic Hazard Analysis of Nonlinear Structures, **I**: Methodology", *Journal of Structural Engineering ASCE*, Vol. 120, No. 11, Nov, 1994

6. Bazzurro, P. and Cornell, C.A. (1994b) "Seismic Hazard Analysis of Nonlinear Structures, **II**: Application", *Journal of Structural Engineering ASCE*, Vol. 120, No. 11, Nov, 1994

7. Bonowitz, D. and Youssef, N. (1995) "SAC Survey of Steel Moment Frames Affected by the 1994 Northridge Earthquake" *Surveys and Assessment of Damage to Buildings Affected by the Northridge Earthquake of January 17, 1994*. Sacramento, CA, SAC Joint Venture (SAC 95-06), December 1995。

8. Bracci, J. M., Kunnath, S. K., Reinhorn, A. M. (1997) "Seismic performance and retrofit evaluation of reinforced concrete structures" *Journal of Structural Engineering* 123(1) 3-10.

9. Chatpan, C., Chopra, A. K. (2002) "Evaluation of modal pushover analysis using generic frames" *Earthquake Engineering and Structural Dynamics* 32, 417 – 442.

10. Chatpan, C., Chopra, A. K. (2004) “Seismic Response of vertically irregular frames: response history and modal pushover analysis” *Journal of Structural Engineering ASCE* Vol. 130, No. 8, 1177 – 1185.

11. Charles, W. and Roeder, M. (2002) “Connection Performance for Seismic Design of Steel Moment Frames”, *Journal of Structural Engineering ASCE*, Vol. 128, No. 4, 517-525.

12. Chopra, A. K. (2001) *Dynamics of Structures: Theory and Applications to Earthquake Engineering*, Prentice-Hall: Englewood Cliffs, NJ.

13. Chopra, A. K., Goel, R. K. (2002) “A modal pushover analysis procedure for estimating seismic demands for buildings” *Earthquake Engineering and Structural Dynamics* 31, 561-582.

14. Cornell, C.A. (1994) “Risk Based Structural Design” *Proceedings of Symposium on Risk Analysis*, Nowak Editor, Dept. of Civil Engineering, University of Michigan, 1994

15. Cornell, C.A.(1996) “Calculating Building Seismic Performance reliability: a Basis for Multi-Level Design Norms” *Proc. Of 11 World Conference on Earthquake Engineering*, Paper No. 2122, Acapulco, Mexico, June 1996

16. Cornell C.A., Fatemeh Jalayer, Ronald Hamburger, Douglas A. Foutch (2002) Probabilistic Basis for 2000 SAC Federal Emergency Management Agency Steel Moment Frame Guidelines, *Journal of Structural Engineering, ASCE*, Vol. 128, No. 4, 526-533

17. Dispasquale E, Cakmak AS (1989) “On the relation between local and global damage indices”, *Technical Report NCEER-89-0034*, State University of New York at Buffalo, 1989

18. Ditlevsen, O. Melchers, R.E., Gluver, N. (1990) “General multidimensional probability integration by directional simulation”, *Computers and Structures* 36 (1990) 355-373.

19. Drakopoulos (1971) “A statistical modal on the occurrence of aftershocks in the area of Greece” *Bull. Seism. Soc. of Am*., Vol. 67 1173-1194.

20. Ellingwood B. (1998) “Reliability-based performance concept for building construction”, *Structural Engineering Worldwide* 1998, Paper T178-4 (CD-Room), Elsevier, New York.

21. Elnashai AS., Bommer JJ., Martinez-Pereira A.(1998) "Engineering implications of strong-motion records from recent earthquake" *Proceedings of the 11th European Conference on Earthquake Engineering*, Paris, 1998 [CD-ROM].

22. Engelund S. and Rackwitz R. (1993) "A benchmark study on importance sampling techniques in structural reliability", *Structural Safety*, 12 (1993): 255-276.

23. Esteva, L. (1970) "Seismic risk and seismic design decisions" *Seismic Design of Nuclear Power Plants*, MIT Press, Cambridge, Massachusetts.

24. FEMA-273 (1997) "*NEHRP Guidelines for the Seismic Rehabilitation of Buildings*", prepared by the Applied Technology council for the Building Seismic Safety Council, published by the Federal Emergency Management Agency, Washington, DC.

25. FEMA-351 (2000), "*Recommended Seismic Evaluation and Upgrade Criteria for Existing Welded Steel Moment-Frame Buildings*", prepared by the SAC Joint Venture for the Federal Emergency Management Agency, Washington, DC.

26. FEMA-352 (2000), "*Recommenced Post-earthquake Evaluation and Repair Criteria for Welded Steel Moment-Frame Buildings*" prepared by the SAC Joint Venture for the Federal Emergency Management Agency, Washington, DC.

27. FEMA-355 (2000) *State of the Art Report on Systems Performance of Steel Moment Frames Subjected to Earthquake Ground Shaking*, prepared by the SAC Joint Venture for the Federal Emergency Management Agency, Washington, DC.

28. Fragiacomo M., Amadio C., Macorini L. (2004) "Seismic response of steel frames under repeated earthquake ground motions" *Engineering Structures* 26 (2004) 2021-2035.

29. Gross J.L. (1998), "A connection model of the seismic analysis of welded steel moment frames", *Engineering Structures*, Vol. 20, No. 4-6, 390-397

30. Gunturi S.K.V. and Shah H.C. (1992) "Building specific damage evaluation", *Proc. 10th World Conference on Earthquake Engineering*, Madrid 1992: 10: 6000-6006.

31. Gupta, A. and H. Krawinkler (2000). "Behavior of ductile SMRFs at various seismic hazard levels." *J. Struct. Engrg. ASCE* 126(1):98-107.

32. Gupta, A. and Krawinkler, H. (2000) "Estimation of seismic drift demand for frame structures" *Earthquake Eng. Struct. Dyn*., 29(9), 1287 – 1305.

33. Helmstetter A. and Sornette D. (2003) “Bath’s law Derived from the Gutenberg-Richter law and from Aftershock Properties” *Physics*, Vol. 2 Sep. 23 2003

34. International Code Council (2003) *International Building Code*, Falls Church VA.

35. Iman, R. L. and Conover, W.J. (1980) “Small sample sensitivity analysis techniques for computer models, with an application to risk assessment”, *Commun. Statist. Theor. Meth*. A9(17): 1749-1842

36. Krawinkler, H. and Seneviratna, G.D.P.K. (1998) “Pros and cons of a pushover analysis of seismic performance evaluation”, *Engineering Structures* 20(4-6), 452-464

37. Krawinkler H. (2002) “A general approach to seismic performance assessment”, *International Conference on Advances and New Challenges in Earthquake Engineering Research*, ICANCEER 2002, Hong Kong, August 19-20

38. Kunnath S.K. Reinhorn A.M., Park Y.J. (1990) Analytical modeling of inelastic seismic response of R/C structures, *Journal of Structural Engineering, ASCE*, Vol. 116, No. 4, 996-1017.

39. Lee K. and Foutch D. A. (2002) “Seismic performance evaluation of pre-Northridge steel frame buildings with brittle connections” *J. Struct. Eng*. 128(4), 546-555.

40. Lee K. and Foutch D. A. (2004) “Performance Evaluation of Damaged Steel Frame Buildings Subjected to Seismic Loads” *Journal of Structural Engineering*, Vol. 130, No. 4: 588-599.

41. Li Q. and Ellingwood B.R. (2005) “Structural Response and Damage Assessment by Enhanced Uncoupled Modal Response History Analysis” *Journal of Earthquake Engineering*, Vol. 9, No. 5 (2005) 1-19

42. Luco, N. and Cornell, C. A. (2000) “Effects of connection fractures on SMRF seismic drift demands” *Journal of Structural Engineering ASCE* 126(1): 127-136

43. Luco N. and Cornell, C. A.(2002) “Probabilistic Seismic Demand Analysis, SMRF Connection, Fractures, and Near-Source Effects” *Ph.D. dissertation* ,Department of Civil and Environmental Engineering of Stanford University.

44. Luco N., Cornell C. A. and Yeo G.L. (2002) "Annual limit-state frequencies for partially-inspected earthquake-damaged buildings", *Structural Safety* Vol. 24 (2002), 281-296

45. Luco N., Bazzurro P. and Cornell, C.A. (2004) "Dynamic versus static computation of the residual capacity of a mainshock-damaged building to withstand an aftershock", *Proceedings of the 13th World Conference on Earthquake Engineering*, Paper No. 2405, Vancouver, B.C., Canada.

46. Madsen H., Krenk S. and Lind N. (1986) *Methods of Structural Safety*, Prentice-Hall, Englewood Cliffs, N.J.

47. Mahin S.A. (1998) "Lessons from Steel Buildings Damaged by the Northridge Earthquake". National Information Service for Earthquake Engineering, University of California, Berkeley. Available online at http://nisee.berkeley.edu/northridge/mahin.html (accessed on 01/04/2006)

48. Maison, B.F., Bonowitz, D. (1999) "How safe are pre-Northridge WSMFs ? A case study of the SAC Los Angeles nine-story building" *Earthquake Spectra*, 15(4): 765-789

49. Mazzoni, S. et.al. (2003) "Open System for Earthquake Engineering Simulation (OpenSees) Command Language Manual" downloaded from http://opensees.ce.berkeley.gatech.edu (accessed on 12/16/2005)

50. Melchers R.E. (1989) "Importance sampling in structural systems", *Structural Safety*, 6 (1989): 3-10

51. NFPA (2002) *Life safety code: code for safety to life from fire in buildings and structures*, Quincy, MA: National Fire Protection Association.

52. Park Y.J., Ang A.H-S. (1985a) "Mechanistic seismic damage model for reinforced concrete", *Journal of Structural Engineering, ASCE*, Vol. 111, No. ST4, 722-739

53. Park Y.J., Ang A. H-S. (198b) "Seismic damage analysis of reinforced concrete buildings", *Journal of Structural Engineering, ASCE*, Vol. 111, No. ST4, 740-757

54. Park Y.J., Ang A. H-S. (1987) "Damage-limiting aseismic design of buildings", *Earthquake Spectra, EERI*, Vol. 3, No. 1, 1-32

55. Rosenblueth E. (1975) "Point estimates for probability moments", *Proc. Nat. Acad. Sci. USA*, Vol. 72, No. 10, 3812-3814

56. Rosenblueth E. (1981) “Two-point estimates in probabilities”, *Appl. Math. Modeling*, Vol. 5, October 1981,329-335

57. SAC 95-07 (1995), Technical Report: “Case Studies of Steel Moment-Frame Building Performance in the Northridge Earthquake of January 17, 1994”, prepared by the SAC Joint Venture for the Federal Emergency Management Agency, Washington, DC.

58. Shome N., Cornell C.A. (1999), Probabilistic seismic demand analysis of nonlinear structures, *Report No. RMS-35, Dept. of Civil and Environmental Engineering*, Stanford Univ., Calif.

59. Singhal A., Kiremidjian A.S. (1996), “Method for probabilistic evaluation of seismic structural damage”, *Journal of Structural Engineering, ASCE*, Vol. 122, No. 12, 1459-1467.

60. Somerville P., Smith N., Puntamurthula S., Sun J. (1997) “Development of ground motion time histories for phase 2 of the FEMA/SAC steel project.” *SAC background Document No. SAC/BD-97/04*, SAC Joint Venture, Richmond, Calif.

61. Song, J., Ellingwood, B. R. (1998) “Seismic reliability evaluation of steel frames with damaged welded connections” *Ph.D. Dissertation*, Department of Civil Engineering, Johns Hopkins University, Baltimore, Maryland.

62. Song J, Ellingwood B. R. (1999a), “Seismic reliability of special moment steel frames with welded connection: **I**”, *Journal of Structural Engineering, ASCE*, Vol. 125, No. 4, 357-371

63. Song J, Ellingwood B. R. (1999b), “Seismic reliability of special moment steel frames with welded connection: **II**”, *Journal of Structural Engineering, ASCE*, Vol. 125, No. 4, 372-384.

64. Sunasaka Y. and Kiremidjian A. S. (1993) “A method for structural safety evaluation under mainshock-aftershock earthquake sequences,” The John A. Blume Earthquake Engineering Center, Report No. 105.

65. Turner R. (1991) Monte Carlo simulation methods of structural system reliability analysis, Brite Project P1271, Task III.3, 1991.

66. U tsu T. (1961) “A statistical study on the occurrence of aftershocks” *Geophys. Magazine*, Vol. 30, No. 1, 521-616

VITA

Quanwang LI was born in Tianjin, PRC. After graduating from Baodi the First Middle School, Tianjin in 1994, he went to Tsinghua University in Beijing to have his college education, where he was awarded the Bachelor in Civil Engineering Degree in 1999 and the Master in Civil Engineering Degree in 2001. He entered the School of Civil and Environmental Engineering at the Georgia Institute of Technology in August, 2001 as a candidate for the Ph.D. degree.